



University of Twente
Enschede - The Netherlands



University of Twente
Enschede - The Netherlands

MOLECULAR ENGINEERING OF DESIGNER SURFACES BY CONTROLLED
RADICAL POLYMERIZATIONS: BRUSHES, HEDGES AND HYBRID GRAFTS

MOLECULAR ENGINEERING OF DESIGNER SURFACES BY CONTROLLED RADICAL POLYMERIZATIONS: BRUSHES, HEDGES AND HYBRID GRAFTS

Edmondo M. Benetti

Edmondo M. Benetti



• 2009

ISBN 978-9036528245



9 789036 528245



Molecular Engineering of Designer Surfaces by Controlled Radical Polymerizations: Brushes, Hedges and Hybrid Grafts

Molecular Engineering of Designer Surfaces by Controlled Radical Polymerizations: Brushes, Hedges and Hybrid Grafts

Edmondo M. Benetti

Thesis University of Twente, Enschede, The Netherlands

ISBN 978-90-365-2824-5

This research was financially supported by the European Commission through the Biopolysurf Marie Curie research network.

Publisher:

Ipskamp Drukkers B.V., Josink Maatweg 43, 7545 PS, Enschede,
The Netherlands, <http://www.ipskampdrukkers.nl>

© Edmondo M. Benetti, Enschede, 2009

Cover graphics by Monica Rocco @ Ologram Graphic Association (Padova, Italy)

Email: jam@ologram.org

Tel: (+39)3343585008

Skype: monica.rocco

Info: www.ologram.org

Cover Picture: Particular of “the battle of Lepanto” by Paolo Veronese (Verona 1528 – Venice 1588) placed in the Galleries of the Academy, Venice, Italy.

Molecular Engineering of Designer Surfaces by Controlled Radical Polymerizations: Brushes, Hedges and Hybrid Grafts

PROEFSCHRIFT

ter verkrijging van
de graad van doctor aan de Universiteit Twente,
op gezag van de rector magnificus,
prof. dr. H. Brinksma,
volgens besluit van het College voor Promoties
in het openbaar te verdedigen
op donderdag 23 april 2009 om 13:15 uur

door

Edmondo M. Benetti

geboren op 6 oktober 1980

te Trieste, Italië

Dit proefschrift is goedgekeurd door:

Promotor: Prof. dr. G. Julius Vancso

*Il lavoro riassunto in questo libro e' dedicato alle molte persone
che lavorano, lottano e si sacrificano per cercare di rendere il mio paese
migliore.*

A mio Padre.

*Ai giovani ricercatori dell'Universita' degli Studi di Padova che vanno avanti
nel nome del loro amore per la scienza.*

Dr. Alessandro Donoli

Dr. Diego Montagner

Dr. Stefano Voltolina

Dr.ssa Irene Duse

Dr. Valerio Causin

Dr. Dario Codogno

Dr. Alessio De Giusti

Dr. Carlo Sanavio

Dr.ssa Valeria Garbin

Dr. Andrea Frasson

Dr.ssa Sara Cadamuro

Dr. Milko Shiorlin

Dr. Fabio Volpin

collegi e amici, Grazie.

Table of Contents

Chapter 1	General Introduction	3
1.1	Introduction	3
1.2	Concept of This Thesis	5
1.3	References	8
Chapter 2	Polymer Brushes for Designing and Engineering of Functional Surfaces	11
2.1	Synthesis of Grafted Polymers	11
2.1.1	Atom Transfer Surface-Initiated Polymerization	13
2.1.2	Iniferter-Mediated Surface-Initiated Polymerization	14
2.2	Structuring Surfaces by Polymer Brushes	15
2.3	Nano-Lithographic Techniques and SIP: Towards Single Macromolecular Grafted Systems	20
2.4	Summary	25
2.5	References	25
Chapter 3	Effect of Initiator Surface Coverage on the Polymerization Kinetics, Morphology and Properties of Poly(methacrylic acid) Grafts	29
3.1	Introduction	30
3.2	Results and Discussion	32
3.2.1	Mixed Initiating SAMs	32
3.2.2	Photografting of PMAA	34
3.2.3	Surface Morphology of PMAA by AFM	38
3.2.4	Properties of PMAA Grafts	42
3.2.5	In-Situ QCM-D Measurements	44
3.3	Conclusions	49
3.4	Experimental	50
3.5	References	53

Chapter 4	Tunable Temperature-Responsive Polymer Brushes on Gold by Iniferter-Based Surface-Initiated Polymerization	57
4.1	Introduction	57
4.2	Results and Discussion	59
4.2.1	Iniferter-Based Photografting of NIPAM	59
4.2.2	Temperature Response by In-Situ AFM	60
4.2.3	Control over Chain Ends via Radical Exchange	63
4.3	Conclusions	64
4.4	Experimental	64
4.5	References	65
Chapter 5	RGD-Functionalized Poly(methacrylic acid) Brushes: Control Over Cell Adhesion via Chemical Structuring	69
5.1	Introduction	70
5.2	Results and Discussion	71
5.2.1	Surface Characterization	71
5.2.2	Cell Adhesion Studies	79
5.3	Conclusions	84
5.4	Experimental	84
5.5	References	88
Chapter 6	Poly(hydroxyethyl methacrylate)-Based Brush Gels: Synthesis, Characterization and Use for the Fabrication of Polymer/Metal Nano-Particles Hybrid Films	91
6.1	Introduction	92
6.2	Results and Discussion	95
6.2.1	PHEMA-Based Gels: Preparation and Characterization	95
6.2.2	pH-Responsive Behavior of PHEMA-Based Gels	102
6.2.3	Controlled Synthesis of Silver Nano-Particles Using PHEMA-Based Gels	104
6.3	Conclusions	108

6.4	Experimental	109
6.5	References	111
Chapter 7	Controlled Fabrication of Polymer “Hedge” and “Dot” Brushes by AFM-Assisted Lithography and Surface-Initiated Polymerization	115
7.1	Introduction	116
7.2	Results and Discussion	120
7.2.1	Preparation and Characterization of Polymer “Hedges” Grafted from Gold Nano-Wires	120
7.2.2	Preparation and Characterization of pH-Responsive “Hedge” and “Dot” Brushes by Scanning Probe Oxidation and Surface-Initiated Polymerization	123
7.3	Conclusions	130
7.4	Experimental	131
7.5	References	132
	Summary and Outlook	137
	Sammevatting	143
	Acknowledgments	151

Chapter 1

General Introduction

1.1 Introduction

Surface science and technology are to a large extent driven by the need for new functional surfaces. To this end, novel physical and chemical approaches have been introduced in the engineering of designer surfaces and interfaces, addressing the needs for numerous application areas, from biomaterials to electronics and devices.

The fundamental requirements for these application areas can now be treated by tuning the chemical properties of surface platforms and enhancing our capability of morphological structuring of modified surfaces across the length scales. Significant efforts aiming at developing new methods for the synthesis of novel coatings with fully controllable characteristics have been made. In addition, owing also to the technological advances brought about by emerging “nano-scale” techniques for surface modification, a wide range of new fabrication methods have been introduced.

Historically, a well-studied chemical tool for surface modification involves self-assembled monolayers (SAMs) on metallic surfaces¹⁻³. For instance, molecular monolayers of thiol-based adsorbates on gold have been widely employed in order to control the adsorption of proteins⁴⁻⁷ or to synthesize functional surfaces which can serve as highly specific chemical receptors.^{8,9} Another widely used tool for chemical surface modification is based on silane chemistry.¹⁰

An alternative approach for the functionalization of a wide range of surfaces and interfaces encompasses the chemical/physical attachment of synthetic polymers. This strategy offers additional system parameters that can be precisely adjusted,

including the possibility to simultaneously tune the chemical^{11,12} (e.g., composition) and the physical^{13,14} (e.g., thickness, morphology) properties of the modifying layers.

In order to tether polymer molecules to a surface, a relatively facile approach consists in synthesizing macromolecules bearing chemical moieties that have a sufficiently high reactivity towards the target substrate. This technique is generally named “grafting-to” of polymers and presents the attractive feature of ensuring the control over the mass and composition of the macromolecules of which the grafted layer is composed.

Swift progress in the synthesis of polymeric coatings has been stimulated by developments of novel synthetic methods where the polymerization was initiated from the surface.¹⁵ A typical surface-initiated polymerization (SIP) approach involves the immobilization of initiators prior to polymerization to the substrates’ surface. Subsequently, the macromolecules that constitute the film were grown in-situ in a manner similar to that of a solution or bulk process.^{16,17} These methods, generally defined as “grafting from” of polymers, have permitted the grafting density of chains to become markedly increased.^{18,19} Moreover, such processes promote the preparation of dense assemblies of surface-tethered macromolecules, known as polymer brushes (of which the concept was introduced already in the early nineties²⁰), which, due to chain crowding, stretch away from the surface.²¹

The development of controlled living polymerization techniques has preceded the widespread use of SIP methods. Hence controlled polymerizations have been intensively employed in SIP, thereby leading to good control over the chemical (e.g., end groups) and physical properties (e.g., chain length) of the films.²¹⁻²³

The intrinsic characteristic represented by the very high surface concentration of chemical functionalities has rendered brush films attractive alternatives for the preparation of well-defined polymeric coatings, which find numerous applications in biology as well as in materials science.^{24,25} A particular category among these surface-tethered systems is represented by brush layers where the constituting macromolecules respond to small physical (e.g., temperature) or a chemical (e.g., ionic strength) stimuli by a large response and variation of their characteristics.²⁶ This is the case of weak polyelectrolytes or various amphiphilic polymers that can be prepared in the form of stimuli-responsive polymer brushes.²⁷⁻³⁰ Such platforms have been widely used to tune the morphological and chemical properties of surfaces, thus leading to applications in the fabrication of bio-interfaces³¹⁻³³ or sensors.^{24,34-36}

The versatility offered by controlled SIP techniques renders it possible to fine-tune the properties of the layers. At the same time, the responsiveness ensures that the characteristics of the layers can be reversibly altered under determined conditions. In addition, the combination of stimuli-responsive polymers and controlled SIP with the most advanced lithographic techniques for surface nanopatterning would eventually enable structural control in three dimensions.^{37,38} As a result, designer materials with structure and function from the nanometer scale can eventually be synthesized through bottom-up methods.

The work described in this thesis has aimed at investigating novel aspects of combinations of all the above-mentioned approaches. SIP is shown to be an effective means of preparing chemically structured brush layers for which the properties can be varied in response to external stimuli such as temperature or pH. It is demonstrated that the prepared polymeric platforms represent suitable starting materials for the design of bio-hybrid or nano-composite systems. In addition, the development of robust nano-lithographic methods coupled with SIP are described. Following this strategy, functional polymer brushes are shown to be readily grown in determined positions down to the nano-scale. These polymeric nanostructures represent useful study-boards for understanding the behavior of macromolecular systems based on a limited number of isolated surface-tethered chains. The possible further development of the mentioned techniques is anticipated to eventually allow the controlled grafting of single macromolecules, which may play a key role in the design of novel sensing materials or bioassays at the single molecular level.

1.2 Concept of This Thesis

This thesis describes the use of functional polymer brushes as tools for the nano-structuring of designer surfaces. The kinetics aspects of controlled surface-initiated radical polymerization are first presented, with focus on the synthesis of brush layers based on weak polyacids and concentrating on the influence of the composition of the precursor-initiating SAMs on the final properties of the films. The introduced polymerization method is subsequently shown to be an effective tool for synthesizing stimulus-responsive brush systems with tunable chemical characteristics and physical properties that vary as a function of the temperature of

the medium in which they are immersed. Subsequently, functional brushes are shown to be easily fabricated following multiple-step synthesis/bio-functionalization in order to obtain 3-D structured platforms that act as test substrates for controlling the cell morphology.

The controlled fabrication of brush-gels is described, with the aim of synthesizing new hybrid-grafted films based on polymer brushes. These novel materials demonstrate pH-dependent swelling properties and serve as efficient reactors for the synthesis of metallic nano-particles of controlled size.

Finally, the combination of AFM-assisted nano-lithographic techniques for a local modification of surfaces and controlled SIP is discussed. These nano-fabrication methods can be employed for the synthesis of polymeric structures with typical dimensions ranging from hundreds to a few tens of nanometers. The so-formed brush-based nano-structures present peculiar chemical and physical properties and represent useful study-boards of the behavior of grafted macromolecular nano-objects immobilized in specified positions on a flat surface.

Chapter 2 introduces the general topics addressed in the present thesis. Surface-initiated controlled radical polymerization methods are discussed, and reports are given of the most relevant techniques that allow the synthesis of grafted films. This overview also highlights the fabrication routes for the synthesis of functional polymeric platforms and brush-based nano-structures as well as of single grafted macromolecules.

Chapter 3 introduces the SIP method based on initiator-transfer-terminator agents (iniferter) and presents a thorough study of its kinetics in films grafted from SAMs of photo-initiators on gold surfaces. Poly(methacrylic acid) (PMAA) was used as a model polymer in this investigation. The morphological and mechanical properties of the PMAA brush-films were characterized with AFM, with focus on the influence of the composition of the initiating SAMs on the characteristics of the polymer grafts. The photopolymerization experiments were also performed inside a quartz crystal microbalance with a dissipation (QCM-D) setup in order to monitor in-situ the advancement of the grafting process and to gain insights into the viscoelastic properties of the PMAA brushes as a function of their growth.

Chapter 4 deals with the application of iniferter-mediated SIP from SAMs on gold for the synthesis of tunable thermo-responsive poly-N(isopropylacrylamide) (PNIPAM) brushes. The controlled synthesis of PNIPAM brush-films is reported,

with emphasis on how to perform an in-situ monitoring with AFM of the properties of the brushes upon their temperature-driven transition.

Chapter 5 describes the fabrication of 3-D structured brush-peptide hybrid systems and their use as platforms for controlling cell adhesion. PMAA brushes were synthesized by iniferter SIP, subsequently functionalized with arginine-glycine-aspartic acid (RGD) peptides and finally extended via a further re-initiation-polymerization step. The surface exposure of cell-adhesive peptides could thus be varied, which induced relevant morphological changes for osteoblast cells incubated on the synthesized films.

Chapter 6 reports on the design of hydrogel-brush/silver nanocomposite films. The synthesis and the characterization of novel poly(hydroxyethyl methacrylate) (PHEMA)-based crosslinked brushes is first introduced. The influence of the preparation conditions is then demonstrated to play a relevant role on the morphology and the properties of the polymer layers. Finally, the use of these brush-gels as effective reactors for the synthesis of silver nano-particles of controlled size is illustrated.

Chapter 7 presents two examples of the coupling of AFM-assisted nonolithographic approaches with SIP methods. By exploiting these techniques, functional polymeric nanostructures with lateral sizes of a few tens of nanometers, denoted polymer “hedge” brushes, were successfully fabricated. Moreover, it was possible to easily accomplish a controlled grafting of a limited number of polymer chains in determined positions by varying the parameters that rule the nano-modification of the precursor surfaces. The properties of “hedge” brushes were thus demonstrated to be dependent on their size as well as on the preparation conditions used during the polymerization process.

1.3 References

- (1) Laibinis, P. E.; Hickman, J. J.; Wrighton, M. S.; Whitesides, G. M. *Science* **1989**, *245*, 845.
- (2) Prime, K. L.; Whitesides, G. M. *Science* **1991**, *252*, 1164.
- (3) Ulman, A.; Eilers, J. E.; Tillman, N. *Langmuir* **1989**, *5*, 1147.
- (4) Palegrosdemange, C.; Simon, E. S.; Prime, K. L.; Whitesides, G. M. *J. Am. Chem. Soc.* **1991**, *113*, 12.
- (5) Prime, K. L.; Whitesides, G. M. *J. Am. Chem. Soc.* **1993**, *115*, 10714.
- (6) Tokumitsu, S.; Liebich, A.; Herrwerth, S.; Eck, W.; Himmelhaus, M.; Grunze, M. *Langmuir* **2002**, *18*, 8862.
- (7) Herrwerth, S.; Eck, W.; Reinhardt, S.; Grunze, M. *J. Am. Chem. Soc.* **2003**, *125*, 9359.
- (8) Vanvelzen, E. U. T.; Engbersen, J. F. J.; Reinhoudt, D. N. *J. Am. Chem. Soc.* **1994**, *116*, 3597.
- (9) Schierbaum, K. D.; Weiss, T.; Vanvelzen, E. U. T.; Engbersen, J. F. J.; Reinhoudt, D. N.; Gopel, W. *Science* **1994**, *265*, 1413.
- (10) Ulman, A. *Chem. Rev.* **1996**, *96*, 1533.
- (11) Mansky, P.; Liu, Y.; Huang, E.; Russell, T. P.; Hawker, C. J. *Science* **1997**, *275*, 1458.
- (12) Kim, J. B.; Huang, W. X.; Bruening, M. L.; Baker, G. L. *Macromolecules* **2002**, *35*, 5410.
- (13) Laschitsch, A.; Bouchard, C.; Habicht, J.; Schimmel, M.; Rhe, J.; Johannsmann, D. *Macromolecules* **1999**, *32*, 1244.
- (14) Lemieux, M.; Usov, D.; Minko, S.; Stamm, M.; Shulha, H.; Tsukruk, V. V. *Macromolecules* **2003**, *36*, 7244.
- (15) Edmondson, S.; Osborne, V. L.; Huck, W. T. S. *Chem. Soc. Rev.* **2004**, *33*, 14.
- (16) Rhe, J. *Macromol. Symp.* **1998**, *126*, 215.
- (17) Prucker, O.; Rhe, J. *Langmuir* **1998**, *14*, 6893.
- (18) Tsujii, Y.; Ohno, K.; Yamamoto, S.; Goto, A.; Fukuda, T. *Adv. Polym. Sci.* **2006**, *197*, 1.
- (19) Bao, Z. Y.; Bruening, M. L.; Baker, G. L. *Macromolecules* **2006**, *39*, 5251.
- (20) Milner, S. T. *Science* **1991**, *251*, 905.
- (21) Advincula, R. C.; Brittain, W. J.; Caster, K. C.; Rhe, J. *Polymer Brushes: Synthesis, Characterization, Applications*; Wiley-VCH: Weinheim, **2004**.
- (22) Dyer, D. J. *Adv. Polym. Sci.* **2006**, *197*, 47.
- (23) Advincula, R. *Adv. Polym. Sci.* **2006**, *197*, 107.
- (24) Senaratne, W.; Andruzzi, L.; Ober, C. K. *Biomacromolecules* **2005**, *6*, 2427.

- (25) Zhao, B.; Brittain, W. J. *Prog. Polym. Sci.* **2000**, *25*, 677.
- (26) Brittain, W. J.; Boyes, S. G.; Granville, A. M.; Baum, M.; Mirous, B. K.; Akgun, B.; Zhao, B.; Blicke, C.; Foster, M. D. *Adv. Polym. Sci.* **2006**, *198*, 125.
- (27) Israels, R.; Leermakers, F. A. M.; Fleer, G. J. *Macromolecules* **1994**, *27*, 3087.
- (28) Israels, R.; Leermakers, F. A. M.; Fleer, G. J.; Zhulina, E. B. *Macromolecules* **1994**, *27*, 3249.
- (29) Minko, S. *Polymer Reviews* **2006**, *46*, 397.
- (30) Benetti, E. M.; Zapotoczny, S.; Vancso, J. *Adv. Mater.* **2007**, *19*, 268.
- (31) Ma, H. W.; Hyun, J. H.; Stiller, P.; Chilkoti, A. *Adv. Mater.* **2004**, *16*, 338.
- (32) Alarcon, C. D. H.; Farhan, T.; Osborne, V. L.; Huck, W. T. S.; Alexander, C. *J. Mater. Chem.* **2005**, *15*, 2089.
- (33) Matsuda, T.; Ohya, S. *Langmuir* **2005**, *21*, 9660.
- (34) Tugulu, S.; Silacci, P.; Stergiopoulos, N.; Klok, H. A. *Biomaterials* **2007**, *28*, 2536.
- (35) Pinto, J. C.; Whiting, G. L.; Khodabakhsh, S.; Torre, L.; Rodriguez, A. B.; Dalgliesh, R. M.; Higgins, A. M.; Andreasen, J. W.; Nielsen, M. M.; Geoghegan, M.; Huck, W. T. S.; Siringhaus, H. *Adv. Funct. Mater.* **2008**, *18*, 36.
- (36) Magoshi, T.; Ziani-Cherif, H.; Ohya, S.; Nakayama, Y.; Matsuda, T. *Langmuir* **2002**, *18*, 4862.
- (37) Kaholek, M.; Lee, W. K.; Ahn, S. J.; Ma, H. W.; Caster, K. C.; LaMattina, B.; Zauscher, S. *Chem. Mater.* **2004**, *16*, 3688.
- (38) Lee, W. K.; Patra, M.; Linse, P.; Zauscher, S. *Small* **2007**, *3*, 63.

Chapter 2

Polymer Brushes for Designing and Engineering of Functional Surfaces.

2.1 Synthesis of Grafted Polymer Layers

When macromolecules are attached by one end to a surface or an interface at relatively high coverage, they stretch away from the surface/interface in order to avoid overlapping forming a so-called polymer brush.¹ The theory necessary for describing the physical properties of polymer brushes has been developed by Alexander² and de Gennes.^{3,4} In their description polymer brushes present free chain ends as confined at the top of the grafted layer and they are characterized by vertical polymer concentration profile which follows a step function. Following further developments of this study new assumptions were made by Milner,^{5,6} predicting a parabolic concentration profile. Many properties of brush systems, nevertheless, are not sensitive to the profile assumed and they have generally the same functional dependence on the polymer chain length and on the density of grafted chains (i.e. grafting density).

A number of methods may be used to fabricate surface tethered macromolecules but only few of them are suitable for the synthesis of high-density polymer brushes. As it has been already mentioned in Chapter 1, following a “grafting to” approach preformed end-functional macromolecules are attached to a surface via physisorption or chemical reactions with a substrate.⁷ Due to steric hindrance (slow diffusion and limited access of the macromolecules through the already grafted chains to the surface) only relatively low grafting densities can be achieved. At most, “semi-dilute” brushes may be formed for low molecular weight polymers. “Grafting from” utilizes surface-tethered initiating sites from which polymeric chains can

grow.⁸ The active sites can be generated in situ via e.g. plasma or UV/ozone treatment of surfaces.⁹ As an alternative, polymerization initiators can be immobilized on surfaces, by embedding them in SAMs.¹⁰ This method does not only allow to precisely control the surface density of effective grafting sites¹¹ but also to subsequently tune the morphology of the grafted chains.

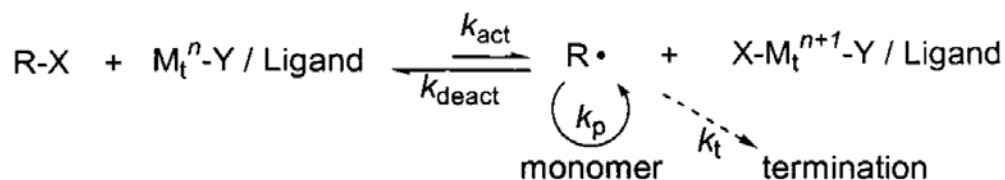
The general model platforms for the synthesis of polymer grafts from SAMs are mainly gold and silicon/glass surfaces. Thus, the initiators for polymerization should present thiol or silane functionalities which are capable to covalently react with the substrates' surfaces forming robust and covalently attached precursor layers.

Many different synthetic routes have been developed so far for the fabrication of polymer brushes from SAMs of initiators such as: conventional^{10,12} and controlled radical polymerization (CRP),^{7,13,14} cationic¹⁵ and anionic living polymerizations¹⁶ as well as ring-opening polymerizations.¹⁷⁻²⁰ CRP has proven to be the most versatile method for surface-initiated polymerization (SIP) on model surfaces. The most popular CRP techniques used include nitroxide-mediated and iniferter-based (INItiators-transFER-terminaTER agent) polymerizations,²¹ Atom Transfer Radical Polymerization (ATRP)²² and Reversible Addition–Fragmentation chain Transfer (RAFT) polymerization.²³ The mechanism involved in these polymerization methods is generally based on the reversible homolytic cleavage of (a) a dormant chain end group into the corresponding polymeric radical (which induces chain propagation) and (b) a stable, persistent radical that cannot undergo addition to monomer ²⁴ The radical-dormant adduct equilibrium can be established via the application of thermal energy, light or the addition of a catalyst as a function of the particular method considered.

This thesis focuses on the use of ATRP and iniferter-mediated polymerization for the synthesis of diverse brush architectures, thus these two general methods will be introduced in the following sections in more details.

2.1.1 Atom Transfer Surface-Initiated Radical Polymerization

Atom transfer radical polymerization (ATRP), introduced by Matyjaszewski in 1995,²² has become a widespread system to achieve controlled polymerization, mostly because of its tolerance to a wide range of functional monomers and accessible experimental conditions. During ATRP the growing polymer chains are predominantly in a dormant state (R-X in Scheme 1.2), occasionally transferring a halide (X) to a metal salt (M) to leave a radical (R•) which can propagate by addition of monomer units before returning to the dormant state. In Scheme 1.2 a general mechanism of ATRP initiated from halide-bearing species is depicted.



Scheme 2.1. General mechanism for atom transfer radical polymerization.²²

The metal catalyst has a number of different oxidation states which allow the addition of a halide as a ligand from an organo-halide adduct which functions first as initiator and later on as chain-propagator (equilibrium between M_tⁿ-Y / Ligand and X-M_tⁿ⁺¹-Y / Ligand depicted in Scheme 1.2). After initiation and propagation, the radical on the chain is reversibly terminated (donation of halide) by reacting with the catalyst in its higher oxidation state. Thus, the red-ox process produces an equilibrium between dormant (polymer-halide, R-X) and active (polymer-radical R•) chains. Due to this phenomenon the polymerization proceeds slowly and ideally no termination reactions take place during the process.

Considering the particular case of SIP, the atom transfer radical process operates from halide-bearing initiators immobilized on the flat surfaces (e.g. via self assembly).¹⁴ This technique is particularly attractive for the grafting of polymer chains in the confined environment of a surface since the low concentration of active radicals results in a minimal interaction between chain ends and thus the risk of termination (generation of “loops” and in-active chains) is markedly reduced. This method has been successfully applied in order to graft styrenes, acrylates, and

methacrylates via SIP.^{14,25-27} The latter two groups of monomers represent a particularly important category since the corresponding polymers are fundamental starting materials for the fabrication of functional platforms and their subsequent chemical modification.

2.1.2 Iniferter-Mediated Surface-Initiated Polymerization

Molecules which act as “*Iniferters*” (*initiator-transfer-terminator*) were originally introduced by Otsu et al.^{21,28} with the purpose of inducing a living radical polymerization, creating block copolymers and more mono-disperse polymers. Similar to ATRP also in the case of *iniferter*-based polymerization, the basic mechanism is characterized by a reversible termination reaction allowed by end functionalities, which can eventually reinitiate the polymerization upon further external stimulus.

Depending on the stimulus which induces the initiation reaction, basically heat or UV-light, chemically different iniferter molecules can be used. The chemistry of “thermal iniferters” is mainly based on the triphenylmethane derivatives (Figure 1.2a), while, in the case of photoiniferters, these are usually based on dithiocarbamate derivatives, which possess UV labile C-C or C-S bond in their chemical structure (Figure 1.2b).

In the particular case of SIP, dithiocarbamate bearing adsorbates are mainly used as starting modifiers. The photo-induced process is most popular technique also considering the reduced thermal stability of SAMs and the easy operational protocols for photopolymerization.^{29,30}

The UV photolysis of a photoiniferter yields a carbon radical and a dithiocarbamyl radical. The carbon radical, reacting with the monomer molecules, initiates the radical polymerization and propagates the process upon addition of monomer molecules. The more stable dithiocarbamyl radical reacts weakly or not at all with the monomer but, on the other hand, it can act as a transfer agent or reversible terminator, recombining with the growing macro-radicals. Also in the case of iniferter-based SIP the initiator-bearing functionalities can be easily immobilized on surfaces via self assembly³⁰ or by chemically modifying the precursor surfaces through the introduction of dithiocarbamate moieties.

This SIP technique allows the synthesis of thick brush layers in a relatively short reaction time, furthermore, the presence of functionalizable dithiocarbamyl groups at the chain ends contributes to the precise tuning of the chemistry at the brush-medium interface.³¹

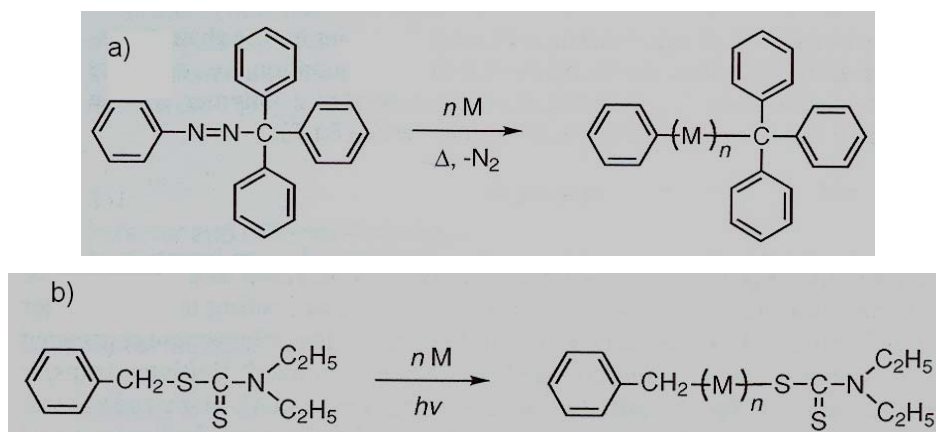


Figure 2.1. Example of molecular species which act as thermal (a) and photoinitiators (b).

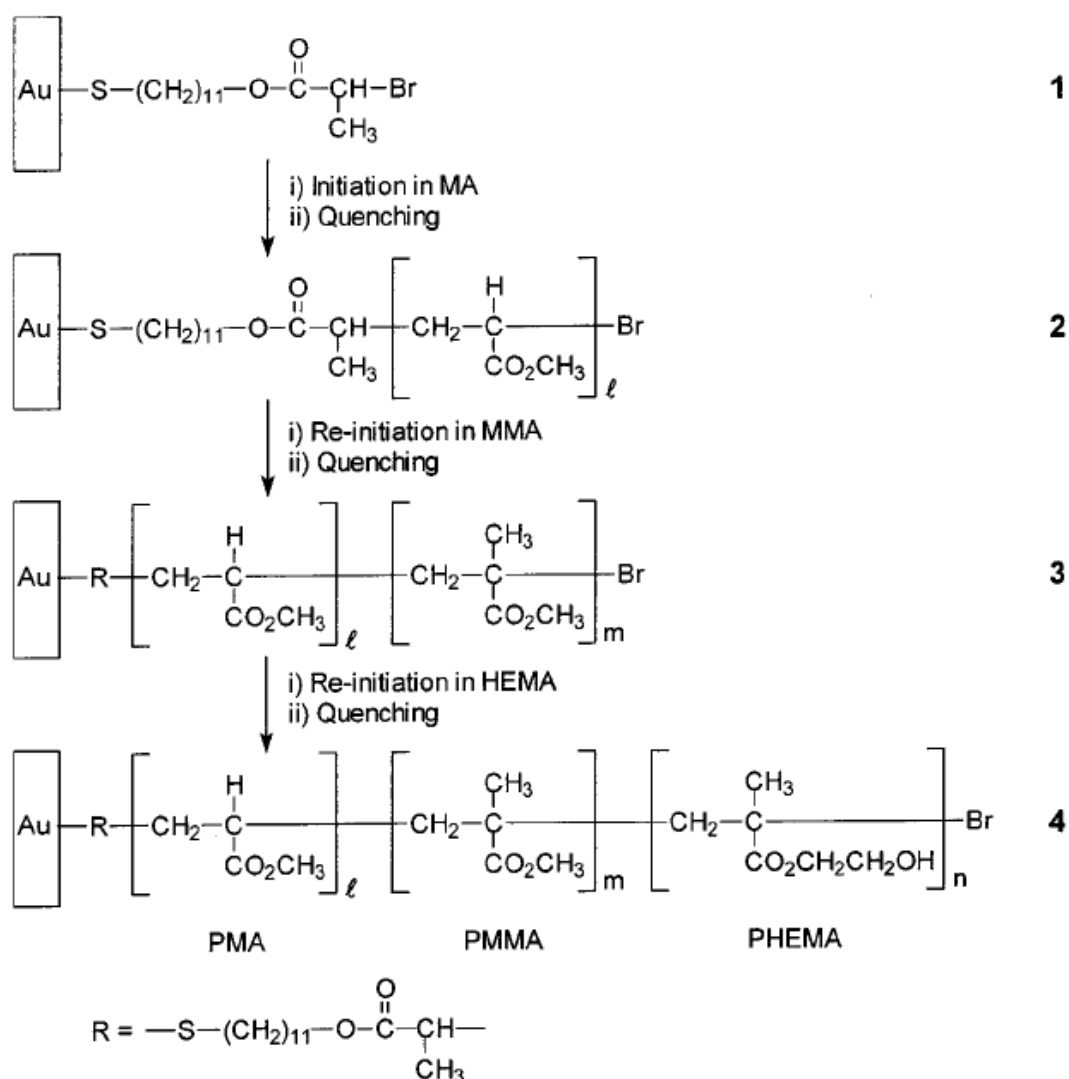
2.2 Structuring Surfaces by Polymer Brushes

As it has been mentioned, the structuring of surfaces using grafted macromolecules represents an extraordinarily versatile tool for the synthesis of tunable platforms which can be used in a wide range of applications. Control at the surface chemistry and to obtain reversible properties is often the main objective of modern surface engineering. In order to achieve this objective, controlled SIP and its inherent chemical characteristics could be exploited to introduce target functionalities or objects at predetermined positions in the brush architecture. A bright example of this kind of fabrication approaches was given by the modification of initiators for controlled radical SIP at the level of the initiating sites which, later on, will constitute the chain ends.

For example in iniferter-mediated SIP the initiator adsorbates themselves were shown to be easily functionalized with protein receptors.³² Following controlled grafting of polyacrylamides from the previously activated glass substrate the grafted polymer chains presented the bio-molecules of interest as chain ends.

As polyacrylamides constitute temperature-responsive polymers, which undergo a sharp hydrophilic-hydrophobic transition around their lower critical solution temperature (LCST), the surface properties of polyacrylamide brush films can be tuned by increasing-decreasing the temperature of the medium with respect to the LCST. Such transitions were already exploited to vary the bio-adhesive character of brush surfaces towards the adsorption of bacteria.³³ When the polymer chains furthermore bear attachment sites for binding of target proteins, the adsorption-release of bio-molecules from solutions could be made specific in addition to reversible. In this way the surface availability of protein receptors can be varied as a function of the swelling of the grafted chains.

The peculiar characteristic of controlled SIP, that is to maintain dormant initiating moieties at the chain ends following the grafting process, was also exploited to fabricate well defined block-copolymer brush systems. By carrying out multiple termination/re-initiation steps, under similar experimental conditions but using different monomer solutions, block-copolymerization efficiencies up to 95% for chain extension were obtained. Owing to these techniques, multiblock copolymer brushes were prepared keeping good control over the thickness of each block (Scheme 2.2).³⁴



Scheme 2.2. Schematic representation of the preparation of tri-block copolymer brushes from SAMs of ATRP initiators on Au (1) constituted by poly(methyl acrylate) (2), poly(methyl methacrylate) (3) and poly(hydroxyethyl methacrylate) (4).³⁴

Block-copolymer brush platforms could be tailored in order to respond to external stimuli such as the type of solvent in which they are immersed. In the case of diblock copolymer brushes, the subsequent exposure to selective solvents induced a clear morphological rearrangement in the grafts' architecture by turning the soluble segments to the interface and resulting in a collapse of the non-soluble ones. This effect was shown to precisely control the wettability properties of the synthesized films.³⁵

Not only solvent-responsive platforms could be fabricated by SIP but also brush films which can change their morphological/physical characteristics in response to a double stimulus. This was the case of double-responsive diblock-

copolymer brushes which were shown to be easily grafted with controlled SIP by subsequently growing a pH- and a temperature-sensitive segment. An example of this responsive brush architecture was given by poly-N-(isopropyl acrylamide) (PNIPAM) brushes copolymerized with weak polyacids.^{36,37} The so-formed film responded to an increase of temperature above the LCST of the PNIPAM block, undergoing aggregation of the corresponding segments. At the same time, the charge density of the polyacid blocks could be varied by changing the pH of the medium. In this way, not only the swelling properties of the ionizable segments could be tuned, but a change in the degree of protonation of the polyelectrolyte was also utilized to influence the temperature-induced transition of PNIPAM (Figure 2).³⁷

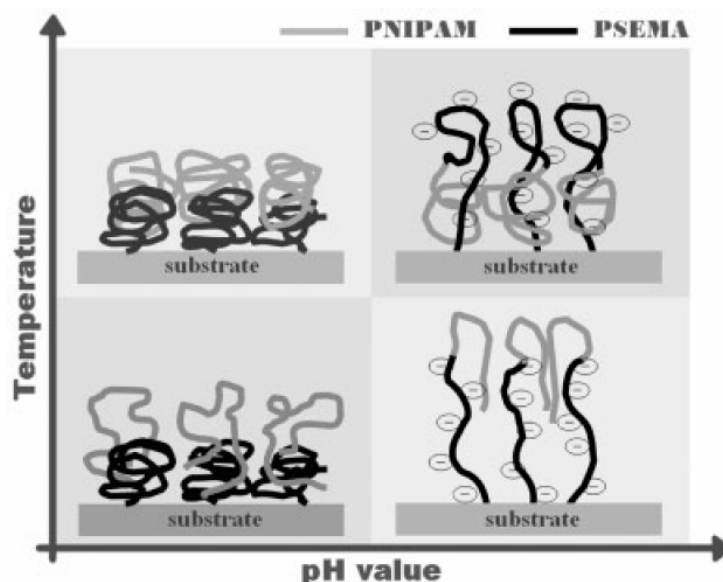


Figure 2.2. Responsive mechanism under temperature and pH stimuli by double responsive copolymer made by a polyacid (PSEMA) copolymerized with PNIPAM. Under low pH values the weak polyacid resulted in the protonated form thus influenced the PNIPAM Temperature-driven transition (up left section) by the formation of hydrogen bonding.³⁷

Responsive polymer brushes were also used to fabricate mixed polymeric platforms in which two different polymer species with complementary characteristics were grafted.³⁸⁻⁴⁰ An example of such responsive mixed brushes is given by surfaces where two different weak polyelectrolytes were grafted. In the case of polybases grafted together with polyacids the surface charge polarity and density could be precisely tuned by immersion in media presenting different pH values.³⁸ These tunable properties were, for instance, accomplished by mixing poly(vinyl pyridine)

and poly(acrylic acid) brushes onto the same support. The first brush presented net positive charges at $\text{pH} < 6.7$, increasing its charge density at lower pH values (Figure 2.3A). On the contrary, poly(acrylic acid) was negatively charged at $\text{pH} > 3.2$, following a similar increase of charge density upon exposure to higher pH values (Figure 2.3B). Thus, the absolute polarity of the whole brush film could be switched by simply treating the surface with aqueous solutions at determined pH. At a given pH value, the correspondingly charged polyelectrolytes extended out of the film interface while the uncharged ones assumed a collapsed conformation (see Figure 3.2).

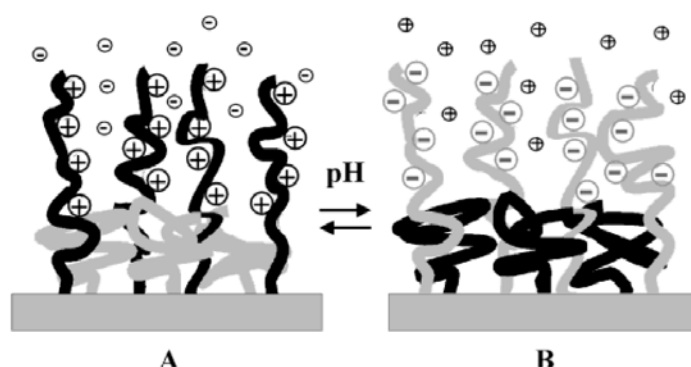


Figure 2.3. Schematic representation of switching behavior of mixed PE brush upon change of pH: at low pH values (A) at high pH values (B).³⁸

The pH-induced swelling/deswelling of grafted polyelectrolytes can also be exploited to fabricate hybrid films which can act as chemical sensors. In these platforms the matrix is represented by the brush structure itself which can be modified by loading inorganic nano-objects inside its structure. Following this approach, poly(vinyl pyridine) brushes were functionalized with silver nanoparticles.⁴¹ Through stabilization of the metal clusters by the pyridine moieties the nanoparticles could be easily incorporated inside the brush architecture keeping, at the same time, the properties of the polyelectrolytes unchanged. The pH-induced transition of the grafted chains influenced the inter-particle distance inside the composite film, thus affected the position of the UV adsorption band characteristic of the metal clusters. This effect turned into an effective analytical mean to indirectly monitor the pH of the medium in which the platform was immersed. Similar fabrication strategies were used to synthesize CdSeS nanocrystals-responsive brush

hybrid platforms which acted as fluorescence sensors^{42,43} or, alternatively, to design gold nanoparticles-based composite films which exploited localized surface plasmons to monitor changes in the pH of the incubation solutions.

The above-reported synthetic approaches demonstrated the wide range of possible routes for surface structuring using polymer brushes. Going from multifunctional platforms, with fine tuning of surface response, to hybrid systems, where the responsiveness turns into sensing, grafted polymers proved their effectiveness as versatile building blocks for such an aim.

The scaling-down to the nano-level of SIP-based fabrication was accomplished in combination with nano-lithographic techniques for surface modification. This capability indeed provided new gains for the precise tuning of surface properties and it is the main topic described in the following paragraph.

2.3 Nano-lithographic Techniques and SIP: Towards Single Macromolecular Grafted Systems

As it was reported in the previous section, functional polymer brushes were successfully used to tune the chemistry, the morphology and the physical properties of surface coatings. The coupling of top-down/bottom-up techniques for the confined modification of surfaces on the nano-scale provide with SIP further control over the shape, the dimension and the inter-feature spacing of brush architectures. All these capabilities, if fully achieved, would allow “SIP-based nano-lithography” to represent a robust mean for the fabrication of macromolecular sensors, single-protein platforms and novel nano-fluidic devices and would eventually serve as an enabling platform to obtain precisely engineered molecular architectures towards these dimensions.

The structuring of surfaces on the nano-scale using SIP is generally based on the localized delivery of precursors for polymerization (i.e. initiator adsorbates or molecular species which can be later on activated to initiators). This process requires on the one hand high patterning resolutions and, on the other hand, inertness of the surrounding surface towards contamination. These main objectives allow the subsequent SIP process to be selectively carried out on the activated positions and to avoid any undesired secondary effects by the surrounding substrate (either

physisorption of polymer from solution during SIP or polymerization initiated by defects on the surface).

Suitable methods to modify on the nano-scale precursor surfaces have been electron beam (EBL) and AFM-based lithography techniques,⁴⁴ which have been widely used in combination with SIP following single or multiple fabrication steps.

As an example, in a step-wise lithographic method, EBL was used to locally etch a polymeric resist layer on silicon surfaces and to subsequently allow the formation of well defined gold nano-islands. Thiol-based initiators for controlled SIP were selectively chemisorbed on the so-fabricated features and eventually resulted in the growth of PNIPAM nano-brushes with a lateral resolution of few hundreds nanometers (Figure 2.4). These grafted nano-structures were shown to respond to temperature variations of the medium by changing their morphology and alternatively collapsing and swelling across the LCST, provided that the appropriate stimulus-responsive macromolecules were used.

Following an approach similar to the one just mentioned, SAMs on gold surfaces could be chemically modified by EBL, introducing functionalizable moieties on specific positions.^{45,46} For example, NO₂-terminated SAMs could be locally reduced to NH₂-bearing molecular structures which were show to easily react with precursors for radical SIP. By optimizing the EBL-assisted initial modification of the SAMs, brush-line-widths down to 50 nm were obtained thus accomplishing the grafting of few tens of polymer chains on determined positions at the surface (Figure 2.5).

Similar line-width resolutions could also be obtained by applying AFM-based lithographic methods in combination with SIP. With this technique, precursor SAMs which acted as resist on the gold surface could be mechanically removed by scanning a localized area with an AFM-tip at high loaded force.^{47,48} This “nano-shaving” method allowed the formation of areas where the bare gold surface was exposed, and which could be backfilled by adsorbing thiol-based initiators with high spatial selectivity. Controlled SIP of NIPAM also in this case, resulted in the synthesis of PNIPAM nano-brushes reaching pattern diameters down to few hundred nm (Figure 2.6).

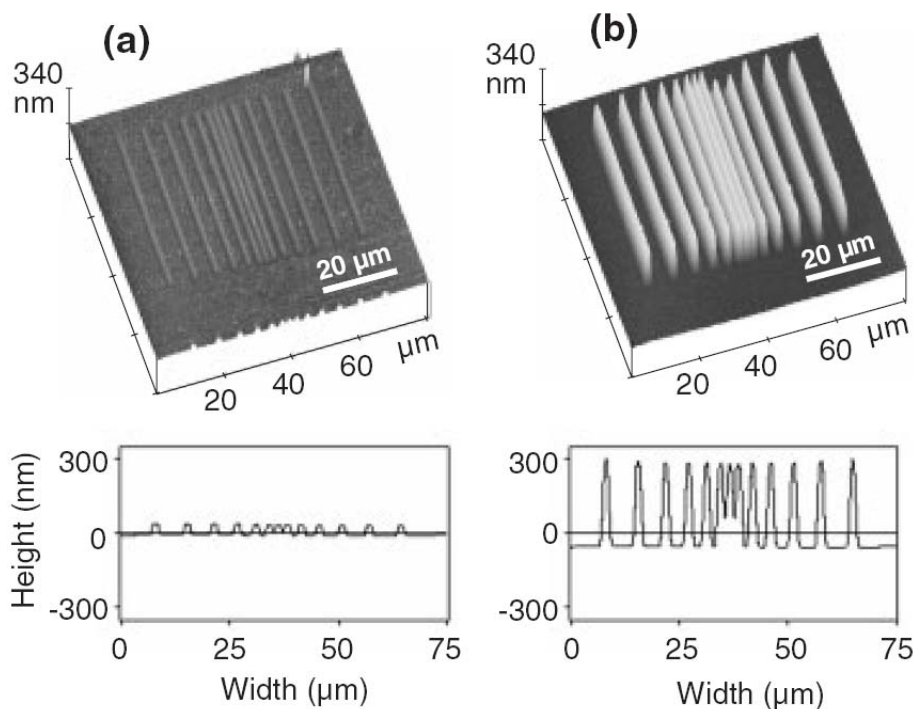


Figure 2.4. Tapping-mode AFM height images displaying a) Au patterns fabricated by EBL-based lithography and b) the subsequently grafted PNIPAM brushes from ATRP initiators immobilized on the previously formed patterns.⁴⁹

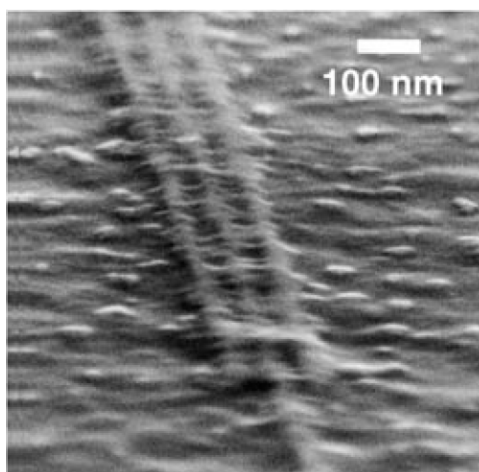


Figure 2.5. Scanning electron microscopy images of polystyrene nano-brushes obtained by EBL of precursor SAMs and subsequent SIP.⁴⁵

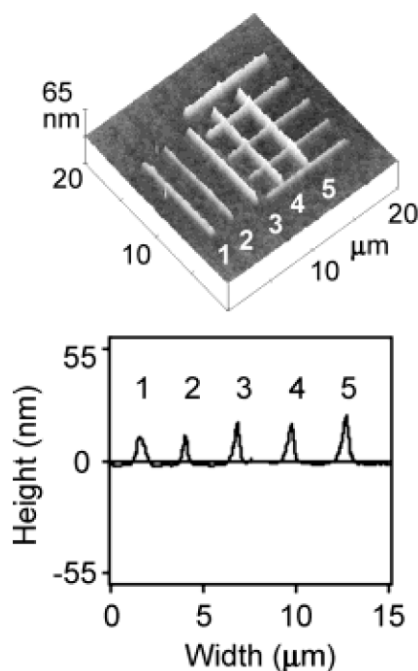


Figure 2.6. AFM contact-mode image displaying PNIPAM brush nanostructures fabricated by AFM-assisted “nano-shaving” technique and following surface-initiated ATRP.⁴⁷

Smaller features were obtained delivering initiators for controlled SIP with AFM dip-pen⁵⁰ or AFM-assisted anodization^{51,52} lithographies. In the first approach the thiol-based initiators were directly deposited from an inked AFM tip onto a gold surface.⁵³ As depicted in Figure 2.7, following the initiator patterning step, the surrounding gold was passivated towards possible contaminations with an inert hydrophobic SAM chemisorbed from solution. Subsequently, surface-initiated ROMP was carried out, accomplishing the controlled grafting of brush nano-structures presenting typical patterns size of 70 nm.

Surface-initiated ROMP was also used to fabricate conductive polymer nano-brushes from initiator-modified features generated on silicon surfaces by AFM-assisted anodization lithography.⁵⁴ This technique allowed the local oxidation of an organic resist deposited on a silicon substrate, hence inducing the formation of silicon oxide patterns which could be subsequently functionalized via solution deposition of silane-based precursors for surface-initiated ROMP. Following the polymerization process, polymeric nano-structures based on conductive brushes were synthesized presenting typical line width of 80-70 nm. The fabricated brushes were also shown to be electrically conductive by electric force microscopy (EFM) and

thus gave a further example of smart systems based on a limited number of polymer grafts characterized by controlled shape, height and distance.

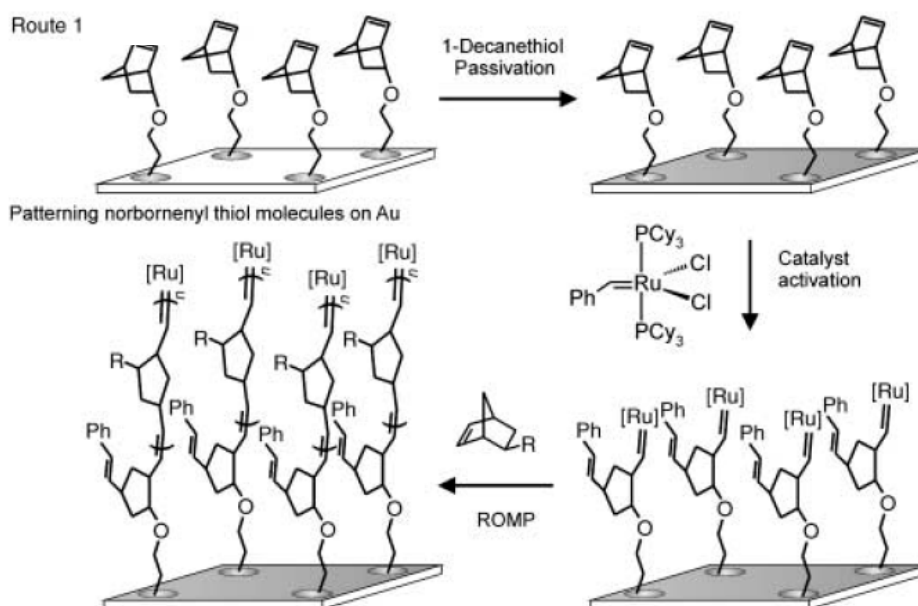


Figure 2.7. Step-wise fabrication method for the preparation of polymer brush nano-structures by immobilization of precursor adsorbates with DPN and subsequent surface-initiated ROMP.⁵³

A further step-forward for a SIP-based nano-lithographic approach is represented by the controlled grafting of single macromolecular species on surfaces. This main target would indeed allow the fabrication of complex architectures based on single molecules with fundamental significance for the designing of bio-sensors and studies of the physical behavior of isolated polymer chains. The synthesis of polymeric structures with sizes of few nanometers was performed exploiting AFM-based field-induced polymerization,⁵⁵ nevertheless, the polymers were not covalently immobilized onto the target surface as in a grafting-from method. Parts of the studies reported in this Thesis will focus on the development of AFM-assisted SIP techniques aiming at the synthesis of so-called polymer “hedge” brushes. Such polymer structures are characterized by line-width resolutions down to few tens of nanometers and thus are constituted by a few to a few tens of grafted chains.

2.4 Summary

Chemical structuring of surfaces using functional polymer brushes and SIP represent fundamental fabrication techniques to obtain polymeric platforms with tunable physical and chemical characteristics. Stimuli-responsive brushes were widely used to design bio-interfaces allowing control over the adhesion of biomolecules and, in some instances, their programmed release. “Smart” polymer brushes were also employed for the fabrication of mixed systems where different polymeric species were sequentially grafted. In this case the surface properties of the polymer layers (e.g. charge, wettability) could be precisely tuned as a function of the properties of the solvent in which the surfaces were immersed. Weak polyelectrolytes were furthermore used as grafted matrixes for the synthesis of hybrid coatings where the polymer species were loaded with optically active nano-objects.

The combination of SIP with nano-lithographic techniques for the localized surface modification on the nano-scale, proved an efficient approach to synthesize brush architectures across the length scales. “Smart” nano-brushes were obtained with SIP-based nanolithography using stimulus-responsive macromolecules, keeping control over the size, shape and inter-feature distance of the polymer grafts.

The advances in these nanofabrication techniques finally allowed the controlled immobilization of a limited number of grafted macromolecules in precise positions at surfaces. Further technological progress in these nano-fabrication methods would eventually allow the patterning of single macromolecules implying fundamental advances in surface polymer science

2.5 References

- (1) Milner, S. T. *Science* **1991**, *251*, 905.
- (2) Alexander, S. *Journal De Physique* **1977**, *38*, 983.
- (3) De Gennes, P. G. *Macrololecules* **1980**, *13*, 1069.
- (4) De Gennes, P. G. *Scaling Concepts in Polymer Physics* Ithaca, NY, 1979.
- (5) Milner, S. T.; Witten, T. A.; Cates, M. E. *Macromolecules* **1988**, *21*, 2610.
- (6) Milner, S. T.; Witten, T. A.; Cates, M. E. *Europhys. Lett.* **1988**, *5*, 413.
- (7) Mansky, P.; Liu, Y.; Huang, E.; Russell, T. P.; Hawker, C. J. *Science* **1997**, *275*, 1458.

- (8) Zhao, B.; Brittain, W. J. *Prog. Polym. Sci.* **2000**, *25*, 677.
- (9) Ito, Y.; Ochiai, Y.; Park, Y. S.; Imanishi, Y. *J. Am. Chem. Soc.* **1997**, *119*, 1619.
- (10) Prucker, O.; Rhe, J. *Langmuir* **1998**, *14*, 6893.
- (11) Jones, D. M.; Brown, A. A.; Huck, W. T. S. *Langmuir* **2002**, *18*, 1265.
- (12) Prucker, O.; Rhe, J. *Macromolecules* **1998**, *31*, 602.
- (13) Baum, M.; Brittain, W. J. *Macromolecules* **2002**, *35*, 610.
- (14) Shah, R. R.; Merreceyes, D.; Husemann, M.; Rees, I.; Abbott, N. L.; Hawker, C. J.; Hedrick, J. L. *Macromolecules* **2000**, *33*, 597.
- (15) Zhao, B.; Brittain, W. J. *Macromolecules* **2000**, *33*, 342.
- (16) Jordan, R.; Ulman, A.; Kang, J. F.; Rafailovich, M. H.; Sokolov, J. *J. Am. Chem. Soc.* **1999**, *121*, 1016.
- (17) Husseman, M.; Malmstrom, E. E.; McNamara, M.; Mate, M.; Mecerreyes, D.; Benoit, D. G.; Hedrick, J. L.; Mansky, P.; Huang, E.; Russell, T. P.; Hawker, C. J. *Macromolecules* **1999**, *32*, 1424.
- (18) Choi, I. S.; Langer, R. *Macromolecules* **2001**, *34*, 5361.
- (19) Wieringa, R. H.; Siesling, E. A.; Geurts, P. F. M.; Werkman, P. J.; Vorenkamp, E. J.; Erb, V.; Stamm, M.; Schouten, A. J. *Langmuir* **2001**, *17*, 6477.
- (20) Wieringa, R. H.; Siesling, E. A.; Werkman, P. J.; Vorenkamp, E. J.; Schouten, A. J. *Langmuir* **2001**, *17*, 6491.
- (21) Otsu, T.; Yoshida, M. *Makromol. Chem. Rapid Commun.* **1982**, *3*, 127.
- (22) Matyjaszewski, K.; Xia, J. H. *Chem. Rev.* **2001**, *101*, 2921.
- (23) Chiefari, J.; Chong, Y. K.; Ercole, F.; Krstina, J.; Jeffery, J.; Le, T. P. T.; Mayadunne, R. T. A.; Meijs, G. F.; Moad, C. L.; Moad, G.; Rizzardo, E.; Thang, S. H. *Macromolecules* **1998**, *31*, 5559.
- (24) Fischer, H. *J. Polym. Sci. Part A: Polym. Chem.* **1999**, *37*, 1885.
- (25) Zhao, B.; Brittain, W. J. *Macromolecules* **2000**, *33*, 8813.
- (26) Samadi, A.; Husson, S. M.; Liu, Y.; Luzinov, I.; Kilbey, S. M. *Macromol. Rapid Commun.* **2005**, *26*, 1829.
- (27) Ramakrishnan, A.; Dhamodharan, R.; Rhe, J. *J. Polym. Sci. Part A: Polym. Chem.* **2006**, *44*, 1758.
- (28) Otsu, T.; Matsumoto, A. *Microencapsulation - Microgels - Iniferters* **1998**, *136*, 75.
- (29) Nakayama, Y.; Matsuda, T. *Langmuir* **1999**, *15*, 5560.
- (30) de Boer, B.; Simon, H. K.; Werts, M. P. L.; van der Vegte, E. W.; Hadziioannou, G. *Macromolecules* **2000**, *33*, 349.
- (31) Magoshi, T.; Ziani-Cherif, H.; Ohya, S.; Nakayama, Y.; Matsuda, T. *Langmuir* **2002**, *18*, 4862.
- (32) Matsuda, T.; Ohya, S. *Langmuir* **2005**, *21*, 9660.

- (33) Alarcon, C. D. H.; Farhan, T.; Osborne, V. L.; Huck, W. T. S.; Alexander, C. *J. Mater. Chem.* **2005**, *15*, 2089.
- (34) Kim, J. B.; Huang, W. X.; Bruening, M. L.; Baker, G. L. *Macromolecules* **2002**, *35*, 5410.
- (35) Rowe, M. A.; Hammer, B. A. G.; Boyes, S. G. *Macromolecules* **2008**, *41*, 4147.
- (36) Rahane, S. B.; Floyd, J. A.; Metters, A. T.; Kilbey, S. M. *Adv. Funct. Mater.* **2008**, *18*, 1232.
- (37) Wang, X.; Xiao, X.; Wang, X. H.; Zhou, J. J.; Li, L.; Xu, J. *Macromol. Rapid Commun.* **2007**, *28*, 828.
- (38) Houbenov, N.; Minko, S.; Stamm, M. *Macromolecules* **2003**, *36*, 5897.
- (39) Ionov, L.; Houbenov, N.; Sidorenko, A.; Stamm, M.; Luzinov, I.; Minko, S. *Langmuir* **2004**, *20*, 9916.
- (40) Klep, V.; Minko, S.; Luzinov, I. *Abstr. Papers Am. Chem. Soc.* **2003**, *226*, U483.
- (41) Gupta, S.; Uhlmann, P.; Agrawal, M.; Chapuis, S.; Oertel, U.; Stamm, M. *Macromolecules* **2008**, *41*, 2874.
- (42) Gupta, S.; Uhlmann, P.; Agrawal, M.; Lesnyak, V.; Gaponik, N.; Simon, F.; Stamm, M.; Eychmuller, A. *J. Mater. Chem.* **2008**, *18*, 214.
- (43) Ionov, L.; Sapra, S.; Synytska, A.; Rogach, A. L.; Stamm, M.; Diez, S. *Adv. Mater.* **2006**, *18*, 1453.
- (44) Wouters, D.; Schubert, U. S. *Angew. Chem. Int. Ed.* **2004**, *43*, 2480.
- (45) Schmelmer, U.; Paul, A.; Kuller, A.; Steenackers, M.; Ulman, A.; Grunze, M.; Golzhauser, A.; Jordan, R. *Small* **2007**, *3*, 459.
- (46) Steenackers, M.; Kueller, A.; Ballav, N.; Zharnikov, M.; Grunze, M.; Jordan, R. *Small* **2007**, *3*, 1764.
- (47) Kaholek, M.; Lee, W. K.; LaMattina, B.; Caster, K. C.; Zauscher, S. *Nano Lett.* **2004**, *4*, 373.
- (48) Kaholek, M.; Lee, W. K.; Ahn, S. J.; Ma, H. W.; Caster, K. C.; LaMattina, B.; Zauscher, S. *Chem. Mater.* **2004**, *16*, 3688.
- (49) Ahn, S. J.; Kaholek, M.; Lee, W. K.; LaMattina, B.; LaBean, T. H.; Zauscher, S. *Adv. Mater.* **2004**, *16*, 2141.
- (50) Piner, R. D.; Zhu, J.; Xu, F.; Hong, S. H.; Mirkin, C. A. *Science* **1999**, *283*, 661.
- (51) Avouris, P.; Hertel, T.; Martel, R. *Appl. Phys. Lett.* **1997**, *71*, 285.
- (52) Dagata, J. A.; Inoue, T.; Itoh, J.; Yokoyama, H. *Appl. Phys. Lett.* **1998**, *73*, 271.
- (53) Liu, X. G.; Guo, S. W.; Mirkin, C. A. *Angew. Chem. Int. Ed.* **2003**, *42*, 4785.
- (54) Lee, W. K.; Caster, K. C.; Kim, J.; Zauscher, S. *Small* **2006**, *2*, 848.
- (55) Martinez, R. V.; Losilla, N. S.; Martinez, J.; Huttel, Y.; Garcia, R. *Nano Lett.* **2007**, *7*, 1846.

Chapter 3

Effect of Initiator Surface Coverage on the Polymerization Kinetics, Morphology and Properties of Poly(methacrylic acid) Grafts*

In this Chapter we introduce the SIP method based on initiator-transfer-terminator agents (iniferter) focusing on polymerization kinetics. Poly(methacrylic acid) (PMAA), used as model polymer for this study, was photografted by iniferter-SIP from self-assembled monolayers (SAMs) of initiator molecules immobilized on Au via disulfide linkages, mixed with disulfide alkanes. The influence of initiator coverage on the growth rates of film thickness, surface morphology and nanoscale mechanics of the grafts was studied. Film thickness was measured by ellipsometry and atomic force microscopy (AFM), while mechanical performance was assessed by AFM compression force. Remarkably, the film thickness growth rate by ellipsometry did not show any significant variation with initiator coverage. However, surface morphology visualized by AFM showed a clear influence of the composition of the initiating SAMs. This was explained by the influence of initiator coverage on the rate of termination reactions.

In the second part of this Chapter, in order to investigate the early stages of the grafting process, polymerization was performed in situ, using a quartz crystal microbalance with a dissipation setup (QCM-D). The mass increment during the photografting was evaluated using concentrated and diluted SAMs of the initiator. A remarkably higher number of grafted chains in the case of concentrated SAMs was observed. By comparing this result with the AFM measurements, a broader

* Part of this Chapter was published in: Benetti, E.M.; Reimhult, E.; de Bruin, J.; Zapotoczny, S.; Textor, M.; Vancso, G.J. *Macromolecules* 2009, *in press*.

chain length distribution, originating from termination reactions in dense systems, was confirmed to affect the surface morphology of the layers.

3.1 Introduction

During the last decade, the development of different surface-initiated polymerization (SIP) techniques has followed closely the advances in controlled polymerization methods, especially based on radical mechanism. Following the fundamental works of R uhe and Prucker^{1,2} who systematically studied the surface-confined synthesis of polymers from flat surfaces using free radical polymerization methods, emerging controlled radical techniques, such as atom transfer radical polymerization (ATRP),^{3,4} reversible addition fragmentation-chain transfer processes (RAFT)⁵ and nitroxide-mediated radical polymerization⁶ were mostly employed for the grafting of polymeric films. As described in the introduction of this Thesis, in all these approaches, the universal platform for the grafting process encompassed self-assembled monolayers of initiator molecules (SAMs). SAMs can be easily prepared on a variety of substrates, metallic and non-metallic. In addition, their composition can theoretically be easily tuned by mixing adsorbates bearing initiator functionalities with corresponding inert molecules characterized by similar anchoring chemistry.⁷⁻¹⁰ Platform engineering of the precursor SAMs by using mixed monolayers (or alternatively, accomplishing surface-dilution of initiator species) was used in order to investigate the effects of the grafting site density on the morphology of the grown polymer chains.¹¹

Numerous studies reported that the thickening rate of grafted films decreased with increasing dilution of the initiator at the precursor surface.¹¹⁻¹⁵ On the other hand, possible kinetic or morphological effects caused by radical recombination in the case of very high surface concentration of growing chains was not univocally recognized, with the exception of an irreversible deceleration of the film's growth-rate but specifically following long reaction periods.^{16,17} The latter phenomenon was reported to limit the maximum film thickness achievable to some hundreds of nanometers, in the case of ATRP-based systems, and after several hours of reaction.¹⁶ Thus, although it has been not systematically addressed yet, the composition of the initiating surface may have direct consequences for the thickness, the density and the

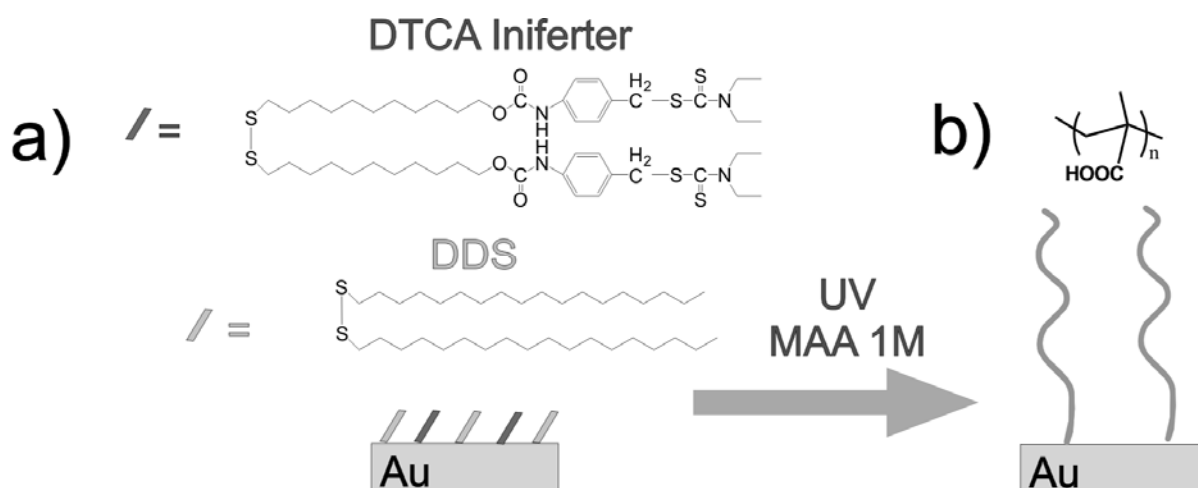
morphology of the layers. In addition, varying the surface density of initiators could influence the polymerization mechanism itself also affecting the chain length distribution of the grafted polymer. The degree of polydispersity characteristic of a grafted system, on the other hand, is difficult to estimate: direct measurements on detached films are often a difficult task and the estimation by using samples synthesized from sacrificial initiator in solution may be not always representative of the reality of the surface grafting process. Thus, other parameters such as thickening rate, surface nano/micro-morphology and swelling properties may be used to interpret the factors which influence the grafting mechanism.

Aiming to investigate how the composition of initiating SAMs could influence the grafting of polymer films, we present here a systematic study focused on the role of initiator surface coverage on the kinetics, the morphology and the properties of photo-polymerized PMAA layers.

The initiating system studied was based on dithiocarbamate-bearing adsorbates which, in the form of disulfides (Scheme 3.1) can easily self-assemble on the Au surface. The dithiocarbamate species, introduced as photoinitiators (or *iniferters*: initiator-transfer-terminator agents) by Otsu,^{18,19} have the peculiarity to cleave upon UV irradiation forming a radical pair constituted by a reactive carbon radical, which initiates the polymerization, and a less reactive, sulfur-centered radical which can act as reversible capping agent during the polymerization process. Disulfide-based initiators were thus used in the presence of similar but inert disulfide species (see experimental section) to form mixed monolayers of variable relative composition. Poly(methacrylic acid) was subsequently photo-grafted from SAMs with different surface concentration of the initiator and the thickening rate of the films was evaluated by ex-situ ellipsometry. The surface morphology and the swelling properties of different films grafted from full and diluted monolayers of initiators were investigated by atomic force microscopy (AFM), showing relevant influence of the composition of the SAM on the characteristics of the subsequently grafted polymer films.

In order to get more insight into the mechanism of polymerization and the influence of the surface concentration of initiating species, the actual increment in hydrated polymer mass was measured in real time during the early stages of the process by quartz crystal microbalance with dissipation monitoring (QCM-D).

The combination of different characterization techniques showed a relevant influence by the surface density of initiating species on the morphology and the properties of the subsequently grafted polymer films.



Scheme 3.1. Synthesis of PMAA grafts from mixed SAMs on Au; a) formation of mixed initiating SAMs of DTCA initiator and DDS diluent agent; b) photopolymerization of methacrylic acid and formation of surface tethered PMAA films.

3.2 Results and Discussion

3.2.1 Mixed Initiating SAMs

In Scheme 3.1, the molecular structure of the two different adsorbates, *iniferter*-bearing disulfide (which is described in the experimental section and we named DTCA) and 1,2-Dioctadecyldisulfane (DDS), used to form the mixed initiating SAMs on Au are depicted. As already described, mixed SAMs deposited from feeding solutions containing different molar ratios of the two components were prepared in order to investigate the role of the surface concentration of photo-labile groups in the subsequent grafting of PMAA. In Figure 3.1 the surface composition of the SAMs, measured with XPS after overnight incubation, was plotted, expressing the molar fraction of DTCA in the monolayers $\Phi^{\text{DTCA}}_{\text{surface}}$, as function of the molar fraction in the feed solution, $\Phi^{\text{DTCA}}_{\text{solution}}$.

As one can see from Figure 3.1a, the data points lie in proximity of the line of unity slope (corresponding to no preferential adsorption of one component with respect to the other) showing a slight synergetic effect. Thus, the surface concentration of DTCA molecules can be precisely tuned by varying $\Phi^{\text{DTCA}}_{\text{solution}}$ of the corresponding feeding solutions.

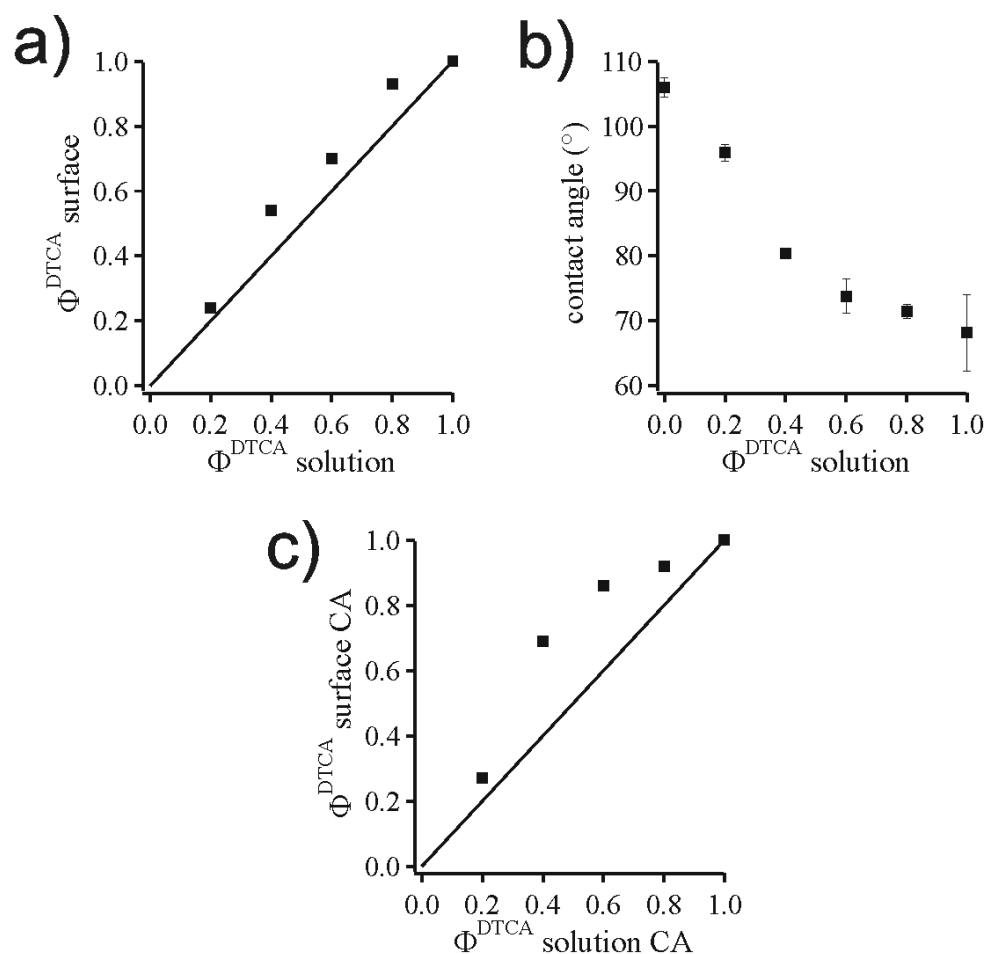


Figure 3.1. a) Molar fraction of DTCA molecules on the SAMs ($\Phi^{\text{DTCA}}_{\text{surface}}$) measured by XPS analysis, expressed as a function of the molar fraction of DTCA present in the feeding solution $\Phi^{\text{DTCA}}_{\text{solution}}$; b) Static water contact angle values recorded on SAMs prepared from feeding solutions with different molar fraction of DTCA ($\Phi^{\text{DTCA}}_{\text{solution}}$); c) Molar fraction of DTCA molecules on the SAMs ($\Phi^{\text{DTCA}}_{\text{surface CA}}$) calculated from contact angle data by using the Cassie equation, expressed as a function of the molar fraction of DTCA present in the feeding solution $\Phi^{\text{DTCA}}_{\text{solution CA}}$.

In the case of mixed precursor SAMs for SIP, several studies in the literature reported on the fine control of the actual surface concentration of initiating adsorbates as a difficult task.^{15,17} In the present case, the values of $\Phi^{\text{DTCA}}_{\text{surface}}$ compared to $\Phi^{\text{DTCA}}_{\text{solution}}$ were only slightly higher (between the 15 and the 35%). This effect was probably due to the higher polarity of DTCA functionalities with respect to the CH₃ terminating DDS, which thus makes the chemisorption of the former compound on the Au surface energetically favoured.⁷

The increase in surface concentration of the more polar DTCA molecules also influenced the wettability of the initiating SAMs. As can be seen in Figure 1b the static water contact angle measured on SAMs with different surface composition of the two components, steadily decreased with the increase of $\Phi^{\text{DTCA}}_{\text{solution}}$, confirming the presence of DTCA species on the surface.

Using the obtained values of contact angles in the well known Cassie equation it was possible to calculate the experimental surface composition of the SAMs,²⁰ expressed as $\Phi^{\text{DTCA}}_{\text{surface}}\text{CA}$, as a function of the relative composition of the feeding solutions $\Phi^{\text{DTCA}}_{\text{solution}}\text{CA}$. By plotting the two series of values (Figure 3.1c) a curve very similar to the one obtained through the XPS analysis was obtained. Also in this case the experimental values lay in the vicinity but above the line of no preferential adsorption, reflecting a control over the surface composition of the SAMs and a slight energetically favoured adsorption of DTCA molecules compared to DDS.

3.2.2 Photografting of PMAA

The UV-initiated polymerization from SAMs on gold has been considered as impossible (or notoriously difficult) task due to the instability of the thiol-gold bond under UV light.²¹ However, the studies reported in this Thesis demonstrated that by using lamps emitting at 300 nm coupled with a 280 nm cut-off filter as a precaution, it is possible to perform a controlled photopolymerization and avoid any degradation of the starting monolayer.

The kinetics of SIP using iniferter initiators on flat surfaces was first investigated by Hadziioannou et al.²¹ and recently by Metters et al.²² In the first study a linear increase of the film thickness with the polymerization time for the grafting of poly(methyl methacrylate) (PMMA) was found, thus the living character of this

particular SIP method was demonstrated. In the latter report, the grafting of PMMA from initiator-modified silicon oxide surfaces was investigated observing irreversible slowing down of the polymerization with time. This phenomenon translated into a non-linear growth of PMMA layers with the irradiation time. This was described as a direct consequence of the loss of surface-tethered radicals by recombination reactions.

The number of tethered chains is directly related to the number of the initiator molecules on the surface which effectively initiate and propagate the growth of polymers. Thus the surface concentration, or alternatively the distance between grafting points, is a parameter which should play a fundamental role in the subsequent film growth.

In the present study we have photopolymerized PMAA from SAMs on Au bearing different initiator concentrations, deposited from solutions of 1.0, 0.8, 0.6, 0.4 and 0.2 $\Phi^{\text{DTCA}}_{\text{solution}}$ corresponding to $\Phi^{\text{DTCA}}_{\text{surface}} = 1.0, 0.9, 0.7, 0.5$ and 0.2, respectively. The polymerization reactions were all performed keeping the monomer concentration constant and, for each sample, the dry ellipsometric thickness of the synthesized PMAA layers was measured after time intervals ranging from 10 to 80 minutes.²³

In Figures 3.2a, 3.2b and 3.2c the dry thickness measured as a function of the polymerization time was plotted for all the samples studied. In order to simplify the graphical representation, the growth rate was plotted in Figure 3.2a, for films grafted from 1.0 SAMs (full initiator coverage), in Figure 3.2b, in the case of semi-diluted SAMs (corresponding to 0.8, and 0.6 $\Phi^{\text{DTCA}}_{\text{solution}}$) and finally in Figure 3.2c for highly diluted, 0.4 and 0.2 SAMs.

In general, it is interesting to note that very thick films, up to 400 nm, can be synthesized during 80 minutes of irradiation for the entire range of DTCA molar ratios considered. The polymerization rates observed are thus remarkably higher if compared to the values for SIP of methyl methacrylate (MMA) initiated from a similar system.^{21,22} However, the shapes of the thickening rate curves are rather similar to the ones typical of *iniferter*-mediated SIP.²²

In addition, an apparent induction time can be recognized for all the samples studied as an initial slow thickening rate during the first 20-30 minutes of irradiation, followed by acceleration of films' growth. Such slow initial polymerization rate might be caused by radical transfer to oxygen still present in the

reaction medium at the early stages of the process. More interestingly, as it was already observed by Metters et al. studying the *iniferter*-mediated photo-grafting of MMA, slow initial increase in thickness followed by rapid growth can be interpreted as a consequence of different configurations of the surface-tethered chains, namely related to a “mushroom-to-brush” transition.²²

It is also interesting to notice that for all the six different surface concentrations of initiator reported, no relevant slowing down of the film thickening was recorded after long irradiation times and thus chain termination reactions do not seem to play a role in limiting the final thickness values which could be achieved.

Ellipsometry measurements of the film thickness showed no significant influence of the surface composition of the starting SAMs on the films' thickening rate. PMAA films grafted from SAMs of DTCA (DTCA 1.0 in Figure 3.2a) with full coverage were shown to grow following a similar rate with respect to the cases where DTCA molecules were diluted with DDS inert analogues. This behavior was observed down to high dilutions, like in the case of layers grafted from 0.2 SAMs (most diluted studied).

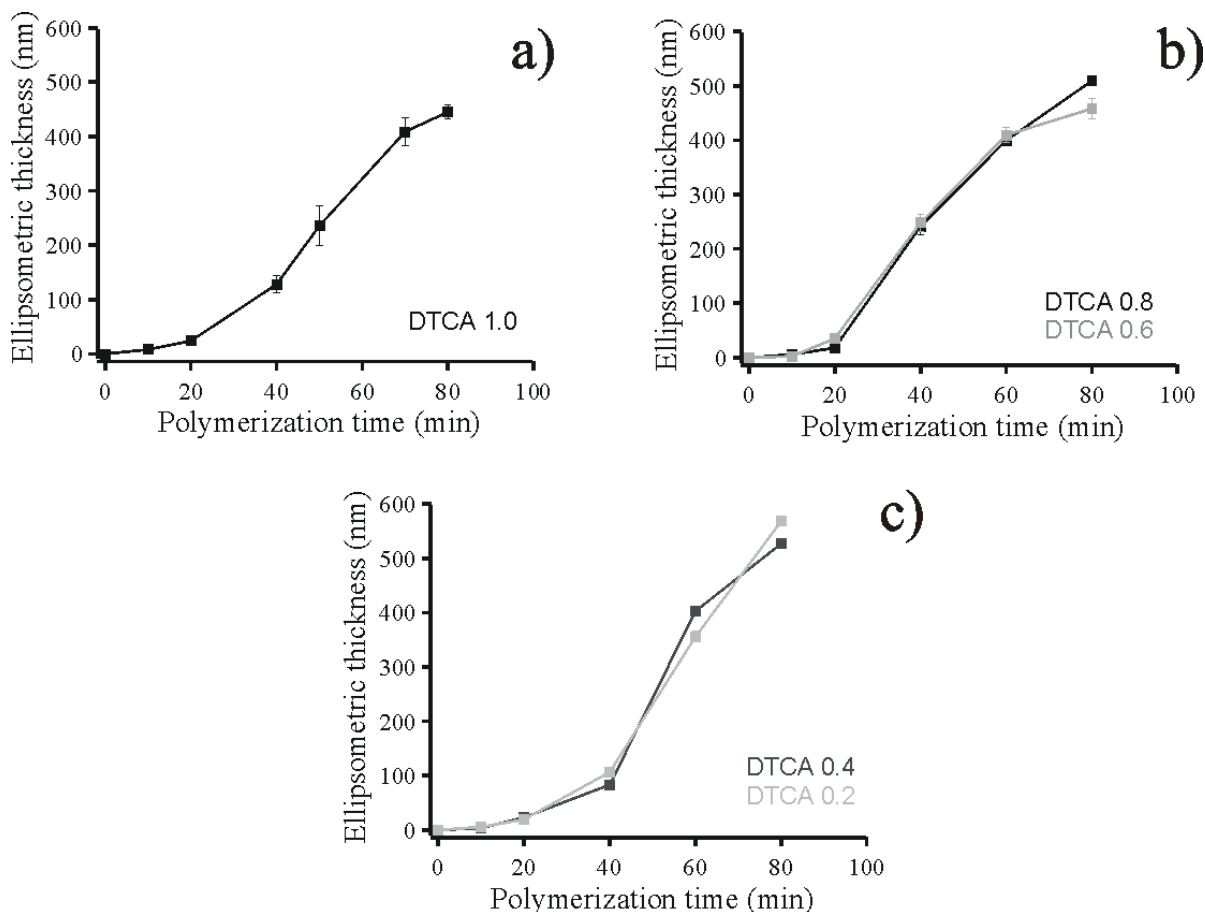


Figure 3.2. Ellipsometric thickness of PMAA films as a function of UV-irradiation time plotted for films grafted from a) 1.0 SAMs, b) from 0.8 and 0.6 SAMs and c) from 0.4 and 0.2 SAMs.

An explanation for this apparently unexpected behavior is offered by considering the effect of high surface concentration of radicals for high molar ratios of DTCA. In support of this idea, Baker et al.¹⁴ observed that, using ATRP, the polymerization rate from SAMs with decreasing initiator concentrations did not show a relevant slowdown over a wide range of concentrations. This result was justified by an increase of bimolecular termination reactions for high surface concentrations of the initiator, thus indirectly assuming that only a fraction of growing chains actually contributed to the formation of the grafted film if compared to the “potential” grafting points present in the precursor SAM. Comparing the results obtained here, this phenomenon seemed to play a more important role for *iniferter*-based initiators when compared with ATRP-based SIP.¹⁴ If bimolecular termination strongly influenced the photo-grafting of PMAA and considering that similar thickening rates were obtained even though the surface coverage of initiator

was varied, thus a high number of growing chains should have undergone deactivation during the early stages of SIP, and, most importantly, in the cases of high surface concentration of initiator.

3.2.3 Surface Morphology of PMAA by AFM

In order to monitor whether the occurrence of termination reactions influenced the micro/nano-morphology of photo-grafted PMAA films, AFM topography images of PMAA films grafted from samples 1.0 and 0.2 were recorded at the early stages of polymerization, namely after 10, 15 and 20 minutes (Figure 3.3a, b, c, d, e, and f) of UV exposure.

As the AFM images show, for films grown from 1.0 SAMs, the average roughness (root mean square, RMS) showed a significant increase following polymerization. We observed an increase of roughness from 0.9 nm (measured on an area of $10 \times 10 \mu\text{m}^2$) after 10 minutes of photoirradiation to 1.0 nm after 15 minutes, reaching 2.0 nm following 20 minutes of reaction (corresponding to a 120 % overall increase). However, in the case of PMAA layers grown from 0.2 SAMs (as it can be seen by comparing Figures 3.3b, 3.3d and 3.3f) such strong roughening with polymerization time was not pronounced. In the latter cases the average RMS values after 10, 15 and 20 minutes of photografting were respectively 0.5, 0.6 and 0.7 nm (measured on an area of $10 \times 10 \mu\text{m}^2$), with an overall increment by 40% during the polymerization time studied. (For the smoother films obtained from SAMs with low coverage, peculiar dot-like features of uniform size can be seen. We speculate that these might be precipitated chains grown in the solution).

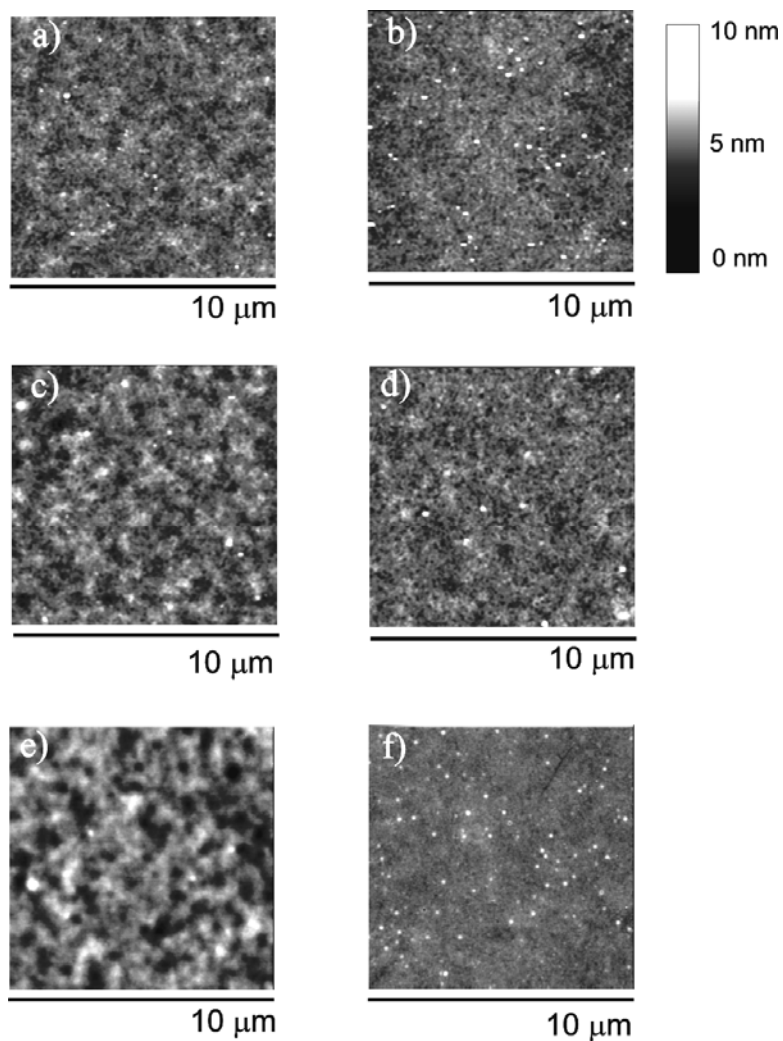


Figure 3.3. a), c) and e) depict topography images by TM-AFM for layers grafted from 1.0 SAMs, respectively, after 10, 15 and 20 minutes of photoirradiation; b), d) and f) depict topography images by TM-AFM for layers grafted from 0.2 SAMs, respectively, after 10, 15 and 20 minutes of photoirradiation.

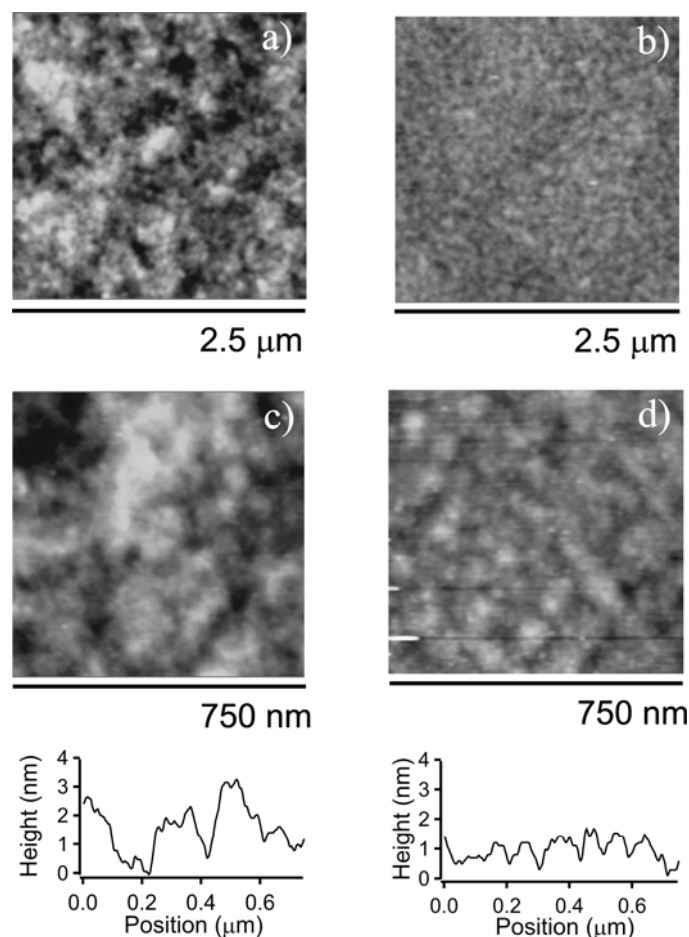


Figure 3.4. a) and c) depict high-resolution topography images by TM-AFM for layers grafted from 1.0 SAMs, the corresponding cross sectional profile is given below; b) and d) depict high-resolution topography images by TM-AFM for layers grafted from 0.2 SAMs, the corresponding cross sectional profile is given below (vertical scale from black to white 10 nm).

Comparing the two different behaviors, a higher roughening rate was found in the case of films grafted from SAMs with high concentration of DTCA.

In addition to the average RMS roughness, also the surface nano-morphology showed important differences comparing films grafted from 1.0 and 0.2 SAMs. As it can be seen in the high resolution micrographs in Figure 3.4, in the case of 1.0 films polymer aggregates with typical lateral dimensions ranging from 50 to 200 nm are present on the brush surface. These “bunches” of grafted macromolecules extend out of the surrounding surface producing peak-to-peak values which, in many cases, reach 2.5-3.5 nm (compare corresponding cross section). On the other hand, the surface of PMAA films grown from 0.2 SAMs showed a regular and continuous nano-

morphology characterized by polymer structures presenting peak-to-peak values of 0.5-0.7 nm.

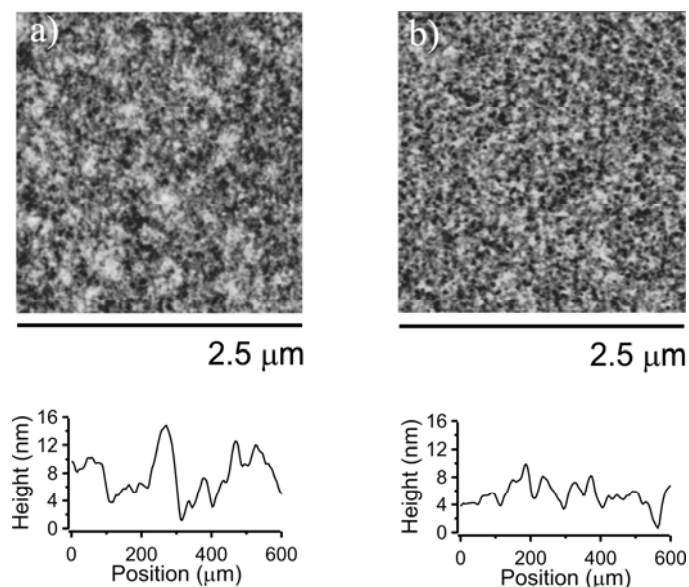


Figure 3.5. a) topography image by TM-AFM for PMMA layers grafted from 1.0 SAMs during 30 minutes of irradiation, the corresponding cross sectional profile is given below; b) topography images by TM-AFM for PMMA grafted from 0.2 SAMs during 30 minutes of irradiation, the corresponding cross sectional profile is given below (vertical scale from black to white 25 nm).

It has to be mentioned that an enhancement of surface roughness for grafted polymer films was related to crosslinking in some reports.^{24,25} In the present case we believe that surface asperities produced by polymer aggregates were caused by broader chains length distributions consequent to high occurrence of termination reactions when PMAA films were grafted from 1.0 SAMs.

Aiming to confirm our theory we grafted PMMA, a polymer much more inert than PMAA towards possible spontaneous crosslinking, alternatively from 1.0 and 0.2 SAMs, following similar experimental conditions reported by Rahane et al.²² Following 30 minutes of irradiation the PMMA films were analyzed by TM-AFM. As it can be seen by comparing Figure 3.5a and 3.5b, PMMA grafts grown from 1.0 SAMs presented enhanced surface roughness if compared to films grafted from 0.2 SAMs, showing very similar morphological differences with respect to the corresponding PMAA films.

3.2.4 Properties of PMAA Grafts

PMAA films grown from 1.0 SAMs during short irradiation times, are supposed to be formed by denser assemblies of grafts if compared to polymer films photo-polymerized from 0.2 starting SAMs. Thus the two different layers, presenting similar thicknesses (~20 nm by ellipsometry) should also show different resistance towards mechanical scratching.

An “easy” scratching experiment can thus highlight the completely different properties of the layers since polymer films presenting comparable thicknesses but different density of anchoring points to the underlying substrate should also show different mechanical resistance. An immediate demonstration of this peculiar behavior can be obtained by mechanically removing the dry films using plastic tweezers and subsequently imaging the scratched regions with an optical microscope (Figure 3.6a and 3.6b). The PMAA film grafted from sample 1.0 could not be completely removed; however scratching removed virtually the entire contacted sections of the 0.2 films. These differences could clearly be seen when, after scratching of the films, the two surfaces were wetted with a water drop. Comparing the insets of the two images in Figure 3.6a and 3.6b it can be clearly seen how the scratched regions of 0.2 could not be wetted, exposing the rather hydrophobic initiating SAMs, while the surface of 1.0 stayed completely covered by the water drop evidencing much more resistance towards film detachment.

The swelling properties of these two different films should also be influenced if the mechanical and morphological differences were related to different chains characteristics. In order to investigate the swelling properties of PMAA, layers grafted from 1.0 and 0.2 SAMs were first scratched with plastic tweezers in order to accomplish the complete removal of polymer also in the case of PMAA grafted from 1.0 SAMs. Following scratching the samples were immersed in PBS solution (pH 7.0) and the height of the swollen grafts was measured by CM-AFM as a difference between scratched regions and the surrounding intact PMAA film (shown e.g. by the arrows in Figure 3.6a and 3.6b). Films presenting dry step-height of 20 nm and 30 nm (synthesized during 20 minutes of UV-irradiation from 1.0 and 0.2 SAMs, respectively), when immersed in the liquid swelled profusely reaching a height of 500

nm, if grown from 1.0 SAMs, and 550 nm from 0.2. The degree of swelling measured for the two layers was in good agreement with reported values for PMAA brushes synthesized by free radical polymerization methods,²⁶ nevertheless, no relevant differences (within the experimental errors measured) were observed between the two samples which would be expected in the case of different grafting densities.^{14,27}

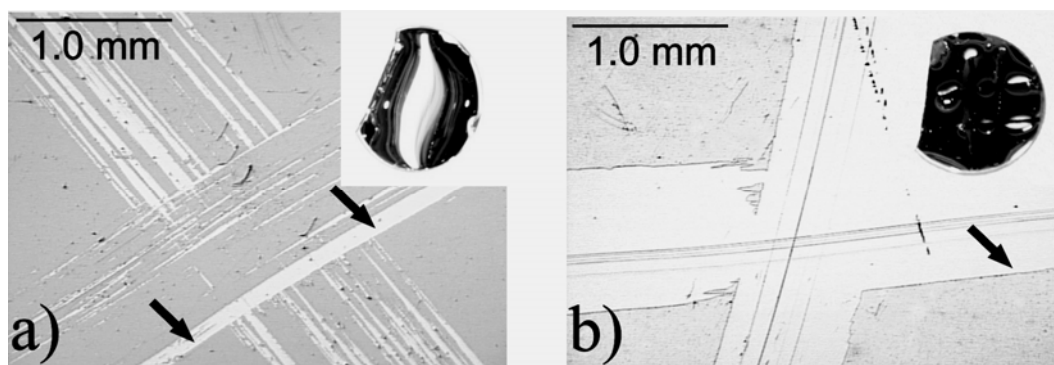


Figure 3.6. a) Scratched films of PMAA grafted during 20 minutes of irradiation from 1.0 SAMs imaged with an optical microscope and b) similar PMAA films grafted during the same polymerization time but from 0.2 SAMs. In the insets (size: 3x3 cm²) of Figures 6a and 6b pictures from a digital video camera showing the wettability of the respective films over the scratched regions are shown. Regarding the arrows see explanation in the text.

To test the compressibility of the two grafted layers in this medium the edge of the polymer films was scanned applying different loads by the AFM tip and the step-height between the polymer and the underlying substrate was recorded. In Figure 3.7a and 3.7b typical cross sections depicting the height between the polymer films and the solid supports at different applied loads (at 12, 26, 34, and 43 nN) were shown, with the corresponding plots reporting the relative compressibility values normalized to the height observed at the lowest load (insets of Figures 3.7a and 3.7b, respectively, for films grafted from 1.0 and 0.2 SAMs). The average height of the film decreased under increasing load in a similar way for both samples, but the films grafted from 1.0 showed a much higher variability in the compressibility, as evidenced by the much larger standard deviations in the inset to Figure 3.7a, when a large number of compression data from different sections of the film was compared.

We believe that this larger heterogeneity is a result of the inhomogeneous morphology of this film.

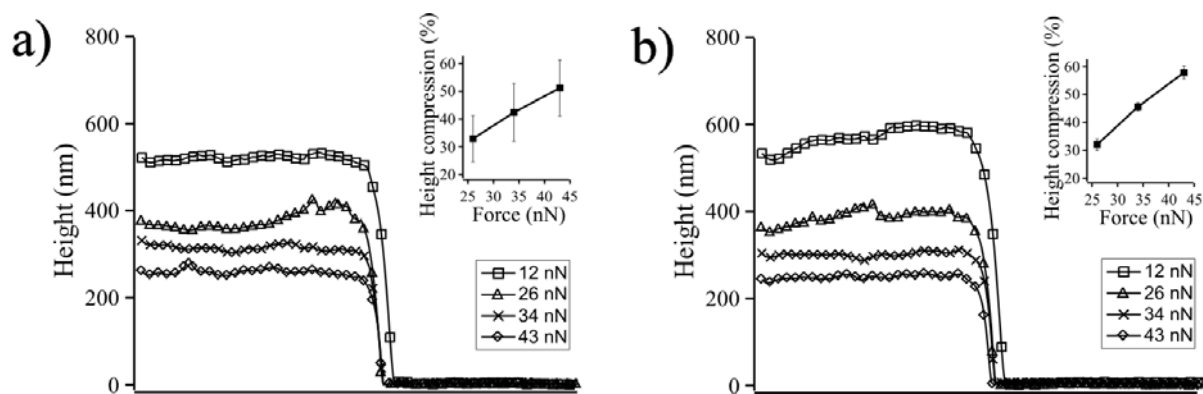


Figure 3.7. Representative cross sections showing the step-height of PMAA films grafted from a) 1.0 and b) 0.2 SAMs recorded by CM-AFM in PBS solution at pH 7.4 by applying increasing load (from 12 to 43 nN). The corresponding insets in Figures 7a and 7b show the compression values measured as relative height decrease as a function of the load.

In summary, distinct differences were observed from the morphological characterization performed in air and from the swelling properties of films synthesized after short irradiation times from very diluted and concentrated initiating SAMs, respectively. Since these films displayed similar growth rates in the entire range of polymerization times studied, it is possible to speculate that bimolecular termination reactions, predominant in films grown from 1.0, directly affected the film morphology and were presumably more frequent at the early stages of the polymerization process, i.e. within the first 20 minutes of irradiation.

3.2.5 *In-situ* QCM-D Measurements

In order to investigate the growth of PMAA, *in situ*, during the early stages of polymerization, Au coated quartz crystals functionalized with 1.0 and 0.2 initiating SAMs were used as substrates for the subsequent photografting of PMAA. In the present study, the functionalized sensors were placed inside a QCM measurement

cell equipped with a quartz window which could thus expose the substrates' surface to the external UV-irradiation source in a cross linking chamber. A degassed solution of MAA was pumped into the cell, and fully covered the exposed functionalized sensor surface, and this set-up was finally irradiated for 20 minutes recording the Δf and ΔD values as function of the polymerization time.²⁸

In Figure 3.8a and 3.8b are shown the frequency shift, Δf , recorded for three different overtones for polymerization performed on sensors modified with 1.0 and 0.2 SAMs, respectively. Following the frequency traces, the starting and the ending of the UV irradiation are highlighted by two arrows, respectively at times corresponding to 0 and 20 minutes. During this period, the decrease in resonant frequency, observed for both SAMs, corresponded to an increase in mass coupled to the sensor, which was caused by the growth of surface tethered polymer chains. The decrease of Δf was accompanied (Figure 3.8a and 3.8b) by a concomitant increase in dissipation, ΔD (Figure 3.8c and 3.8d), which is consistent with the surface growth of hydrated polymer chains covering the sensor.

The onset of shifts in Δf and ΔD was observed 5-7 minutes after the beginning of UV-irradiation. Before that time only a small transient increase in Δf due to the UV light itself on the sensor was observed (see Figure 3.9). We interpreted this delay as most likely due to an induction time during which the propagation of growing chains is very slow and also partly masked by the initial UV-induced transient response of the sensor itself.

Interestingly, the frequency decrease and dissipation increase for the two different SAMs did not follow the same kinetics and also had very different rates of change. The layers grown on 1.0 showed a faster Δf decrease and ΔD increase compared to the photografting on 0.2 SAMs. Furthermore, after the switching-off of UV light, for 0.2 initiating SAMs, the variations of Δf and ΔD immediately leveled off, indicating the interruption of polymer grafting. In the case of 1.0 SAMs, instead, the variation rate of frequency and dissipation did not become 0 when UV was switched off. Instead it reached a steady state slowly leveling off during 10 minutes following the end of the polymerization. We suggest that this phenomenon may be due to an increase of viscosity by polymerization initiated in the medium when films were grafted from 1.0 starting layers. In support of this assumption we reason that the UV irradiation of MAA solutions, even in the absence of any initiating functionalized

surface, were shown to induce a gradual decrease of Δf following the irradiation time (Figure 3.10).

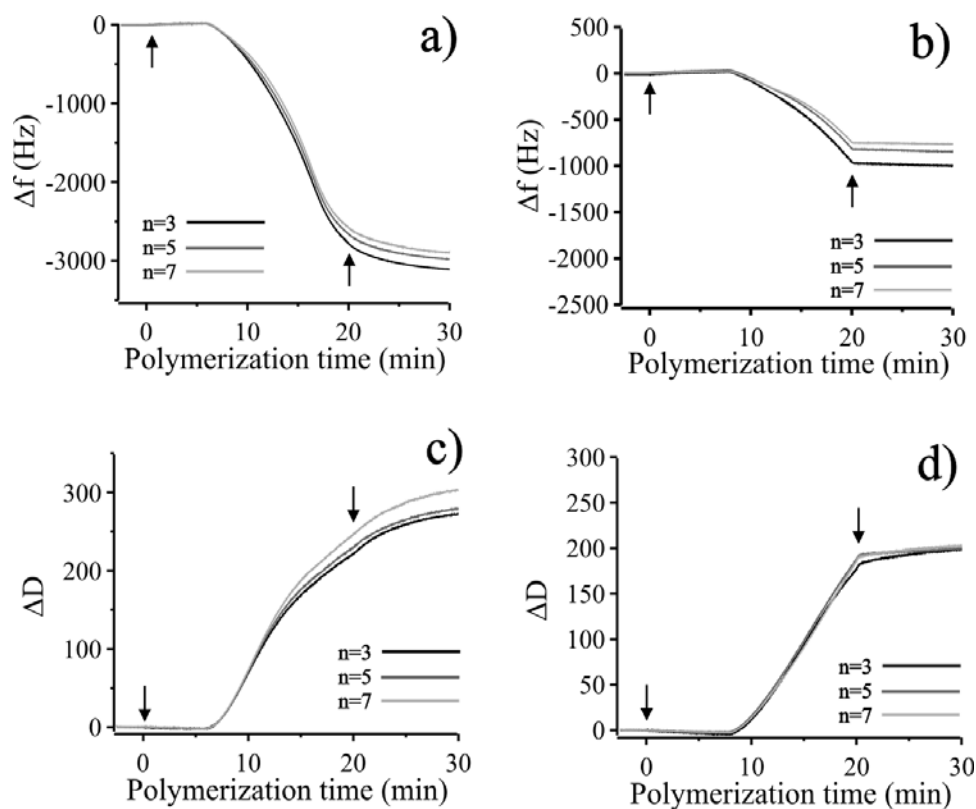


Figure 3.8. Change in frequency Δf (3.8a and 3.8b) and dissipation ΔD (3.8c and 3.8d) of a quartz crystal microbalance with dissipation recording of the photopolymerization process. Starting and ending times are indicated by black arrows in the graphs. The changes in Δf and ΔD were respectively recorded in the case of PMAA grafted from 1.0 (3.8a and 3.8c) and from 0.2 SAMs (3.8b and 3.8d).

The differences between the two samples become more evident if the mass uptake as function of the irradiation time, obtained by fitting the Δf and ΔD response using the Voigt model for the three overtones displayed, was compared for 1.0 and 0.2 SAMs. The difference between the two trends in Figure 3.11 highlights that the total film mass (expressed as ng/cm^2) grafted from 1.0 SAMs exhibits a much more accelerated growth compared to the 0.2 SAMs during the first 20 minutes of polymerization. The measured values must be interpreted as “total’ mass increment,

considering the polymer chains as hydrated and trapping a substantial amount of excess water and possibly monomers within the brush.

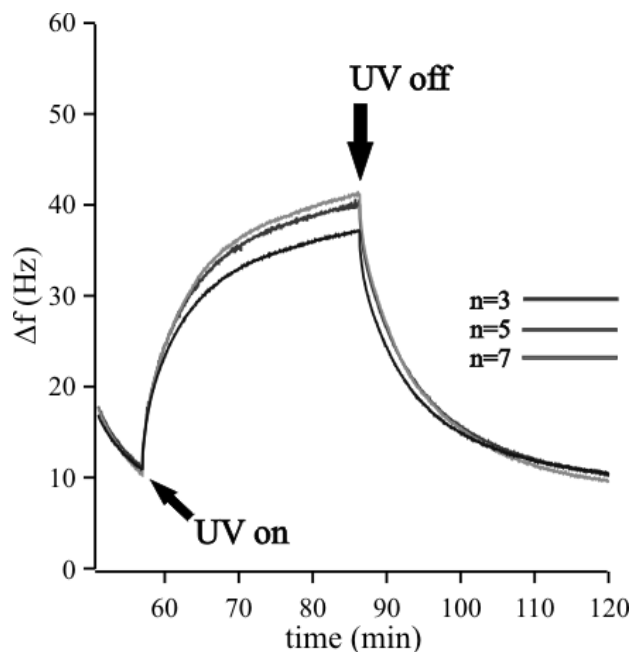


Figure 3.9. Change in frequency Δf of a quartz crystal microbalance with dissipation during the UV irradiation of the gold sensor immersed in milli-q water. Starting and ending times are indicated by black arrows in the graphs.

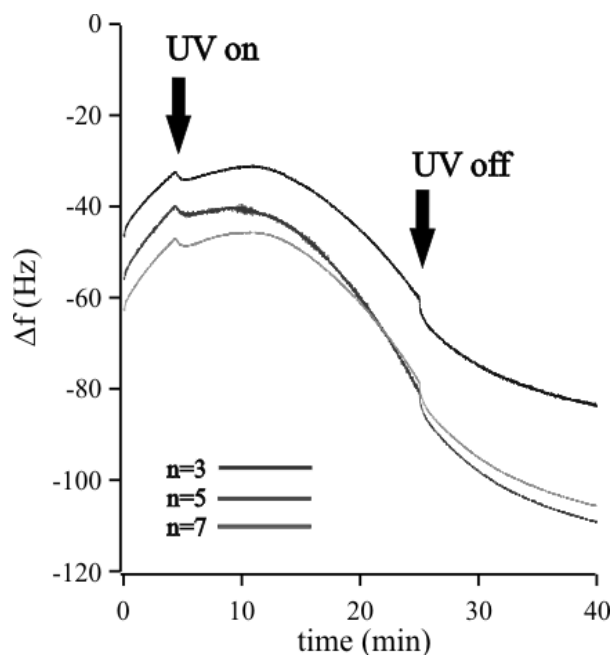


Figure 3.10. Change in frequency Δf of a quartz crystal microbalance with dissipation during the UV irradiation of the gold sensor immersed in 1M MAA water solution. Starting and ending times are indicated by black arrows in the graphs.

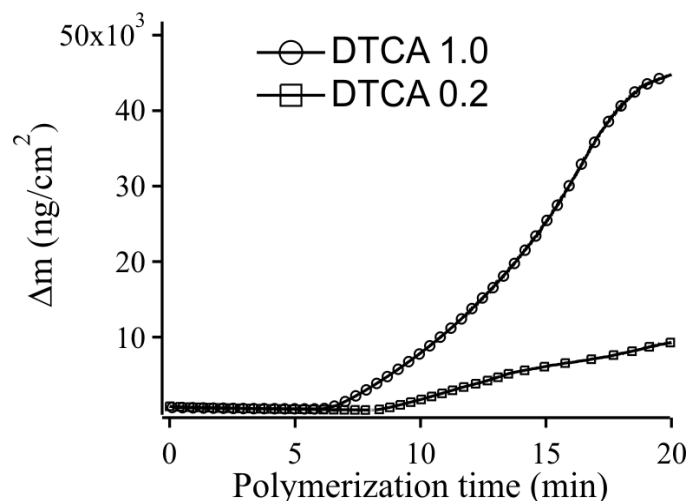


Figure 3.11. Hydrated mass uptake (expressed as ng/cm²) estimated by fitting Δf and ΔD values obtained during the photopolymerization of PMAA to a Voigt model for the adsorbed film, for 1.0 (circles) and 0.2 SAMs (squares), respectively.

While the increase in dry mass is relatively similar for the two initiator concentrations once the growth has become significant (see Figure 3.2), the increase in hydrated mass is much more rapid for the 1.0 SAMs and also starts earlier as evidenced by the shorter lag phase observed. Furthermore, the ratio of ΔD to Δf (roughly incremental viscous losses per mass unit adsorbed), reported in Figure 3.12, is higher for the 0.2 SAMs than for the 1.0 SAMs, which indicates a denser, more rigid, film initially forming in the latter case, while it becomes similar after the slowdown in mass growth occurring for the 1.0 SAM after 15 min.

These results demonstrate that a higher number of polymer chains were initially grafted from full initiators SAMs compared to initiating layers presenting DTCA diluted with DDS. In addition, most likely as a consequence of the structural heterogeneity of 1.0 samples (evidenced by peculiar surface morphology and by film compressibility measures by AFM) the film can take up more water, as evidenced by the higher total hydrated mass. When dried, the amount of polymer for the two initiator coverages becomes comparable as shown by ellipsometry. The observed initial very large difference between ellipsometric mass and QCM-D mass might also be partly related to a faster growing of the 1.0 SAM initiated PMAA film due to the higher density of chains, since it was reproducibly observed that the Voigt modeled mass (as well as the untreated data) showed a significant decrease in growth rate

between 15 and 20 minutes of irradiation and that the Voigt mass growth rates at 20 min became similar for high and low initiator density SAMs. Thus, the crowding of growing chains favoring bimolecular reactions and affecting the subsequent thickening rate by decreasing the effective number of tethered macroradicals, might become dominant around this time. As a consequence of this decrease of growing chains, the film thickening vs. polymerization time showed very similar trends in the case of thick films grown from full layers of initiators with respect to SAMs where the initiators are diluted with inert adsorbates. The AFM images of dry films showing evidence of a higher structural heterogeneity for full iniferter coverage support this interpretation.

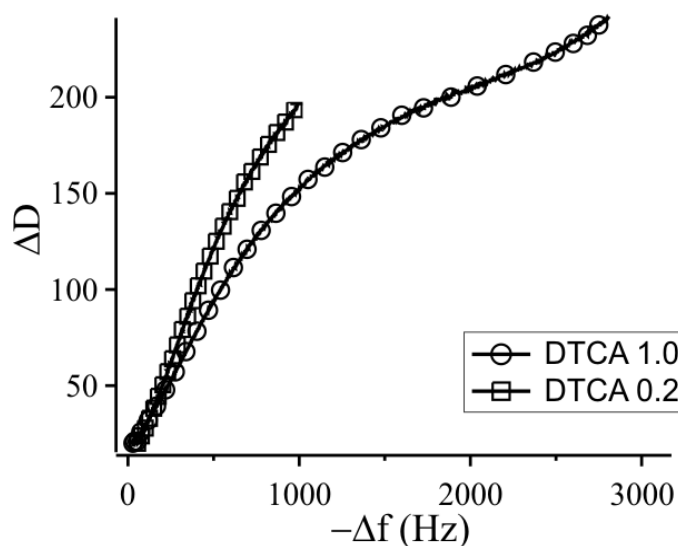


Figure 3.12. Change in frequency ΔD as a function of the change in Δf (expressed as $-\Delta f$ for clarity) of a quartz crystal microbalance with dissipation recorded during the photopolymerization process. The changes in ΔD were respectively recorded in the case of PMAA grafted from 1.0 (circles) and from 0.2 SAMs (squares).

3.3 Conclusions

In summary we investigated here the photografting of PMAA using mixed initiating systems based on SAMs containing iniferter-based adsorbates, demonstrating how the fine tuning of the composition of the starting layers could influence the morphology and the properties of the subsequently grafted films.

Very thick PMAA grafts could be synthesized after relatively short reaction times for the entire range of surface concentrations of initiator studied. The film growth rate, measured with ex situ ellipsometry in the dry state, did not show a significant dependence on the composition of the starting SAMs, implying that radical recombination reactions played a role in the surface grafting process. Comparing the extreme cases of PMAA grafts from full SAMs of initiators and highly diluted SAMs, important morphological differences and different swelling properties were found after short irradiation times. We concluded that this is related to different kinetics of the grafting process in the two model substrates studied as demonstrated by in situ QCM-D measurements. Taken into consideration the initial film mass growth and viscoelastic properties for the two systems as measured by QCM-D, a higher number of chains are initially grown in the case of concentrated SAMs of initiators. Nevertheless, due to termination reactions, this potential grafting efficiency did not turn into a higher thickening rate during the course of the polymerization with respect to films grown from diluted SAMs.

3.4 Experimental

Materials. The synthesis of the disulfide photo-initiator dithiodiundecane-11,1-diylbis[4({[(diethylamino)carbonothioyl]thioethyl)phenyl}carbamate} (DTCA) followed three different steps. First 11-mercaptoundecan-1-ol was oxidized to the corresponding disulfide, 11,11'-dithiodiundecan-1-ol, using an equimolar aqueous solution of iodine and potassium iodide. The disulfide was then reacted with 4-(chloromethyl)phenyl isocyanate in chloroform with dibutyltin dilaurate as a catalyst, giving dithiodiundecane-11,1-diylbis{[4-(chloromethyl)phenyl]carbamate} as a product. The latter compound was finally reacted with the diethylammonium salt of diethyldithiocarbamic acid in THF at 40°C giving the final compound dithiodiundecane-11,1-diylbis[4({[(diethylamino)carbonothioyl]thioethyl)phenyl}carbamate} (DTCA).

Methacrylic acid (MAA) and methyl methacrylate (MMA) were obtained by Sigma and purified from inhibitors by condensation under high-vacuum. 1,2-Dioctadecyldisulfane (DDS) was obtained by oxidation of octadecane-1-thiol (ODT, Sigma) in chloroform using an equimolar aqueous solution of iodine and potassium

iodide (Merck and Sigma, respectively). Gold substrates were purchased from Ssens B.V. (Hengelo, the Netherlands). All solvents were used in high purity and milli-q water was obtained from a Millipore system (Millipore S.A.S., Molsheim, France).

Photopolymerization. In a typical procedure, 1 mM mixed chloroform solutions of DTCA and DDS with molar ratios of initiator equal to 0.2, 0.4, 0.6, 0.8 and 1.0 were used to form the initial SAMs. Gold substrates with area of 6 cm² were cleaned with a “piranha” (30% HB₂B₂O₃ / 70% HB₂B₂SO₄) solution and after extensive rinsing with milli-q water, ethanol and dichloromethane were immersed in the corresponding DTCA-DDS solution overnight at room temperature. The so-prepared samples were subsequently placed in a quartz flask containing a 1.0 M aqueous solution of MAA. They were extensively purged with argon and finally irradiated through a 280 nm cut-off filter for the necessary polymerization time by an array of six UV-B lamps (15W, G15T8E, Ushio, Japan, sample-to-lamp distance: 20 cm). After carrying out the photopolymerization for the desired time, the substrates were rinsed with milli-q water overnight. MMA was grafted following similar experimental procedures with the exception of toluene used as solvent and the final monomer concentration which was set to 4.5 M.

Surface Characterization. Contact angle measurements were performed on the SAM functionalized gold substrates in order to monitor the changes in wettability following chemisorption of different relative concentrations of DTCA with respect to DDS. Static water contact angle measurements were performed by the sessile drop technique using an optical contact angle device equipped with an electronic syringe unit (OCA15, Dataphysics, Germany). This set-up was then connected to a charge-coupled device (CCD) video camera. The sessile drop was deposited onto the polished surface of the materials with the syringe, and the drop contour was fitted by the Young-Laplace method. Twenty measurements of each specimen were performed.

X-ray photoelectron spectroscopy (XPS) was used to evaluate the actual surface concentration of initiator in SAMs prepared from feeding solutions containing different molar fraction of DTCA/DDS. XPS spectra were obtained on a Quantera XPS instrument (Physical Electronics) using monochromatized Al K α radiation (1486.6 eV) with an X-ray beam diameter of 100 μ m and at an angle of 45° relative to the substrate’s surface. Each sample was measured over a set of eight different locations. In order to evaluate the relative concentration of DTCA on the

surface, high resolution XPS elemental scans for the O1s, N1s and C1s signals were recorded. The ratios between elemental concentrations C/N and C/O were evaluated as a function of the molar fraction of DTCA initially present in the corresponding feeding solutions ($\Phi^{\text{DTCA}}_{\text{solution}}$). Thus, combining the values obtained for each sample, the relative composition of the SAMs (expressed as $\Phi^{\text{DTCA}}_{\text{surface}}$) with respect to $\Phi^{\text{DTCA}}_{\text{solution}}$ was calculated.

The dry thickness of the subsequently grafted PMAA films was measured using a computer-controlled null ellipsometer (Philips Plasmon) working with a He-Ne laser ($\lambda = 632.8 \text{ nm}$) at an angle of incidence of 70° . The measurements were formed at 22°C and 30% relative humidity and the data obtained were averaged over 40 points at the surface of each sample. For the grafted PMAA layers, a refractive index of 1.475 was used.²⁹

The surface morphology of the films was evaluated by atomic force microscopy in tapping mode (TM-AFM) using a Dimension 3100 setup (Digital Instruments, Veeco, Santa Barbara, CA, USA) and recording topography images over several areas of each substrate. The same instrument, equipped with a liquid-cell, was used in contact mode in order to evaluate the properties of the PMAA layers when immersed in PBS buffer at pH 7. In order to monitor the swelling behavior and the resistance to compression of the grafted PMAA, the polymer layers were mechanically removed (scratched) with plastic tweezers and the height between the unscratched and scratched regions was measured in contact mode upon application of variable loads by the AFM tip.

QCM-D measurements³⁰ were performed in order to monitor the polymer growth during the first stages of the polymerization process. AT-cut quartz crystals (Q-Sense, Gothenburg, Sweden) with a fundamental resonance frequency of 5 MHz were used as substrates for the grafting of PMAA. The gold electrode on the quartz crystal sensor was functionalized *ex situ* with initiating SAMs following the same procedures reported in the materials section, with 0.2 and 1.0 molar ratios of DTCA to DDS respectively. The sensors were subsequently placed inside a QCM-D chamber equipped with a liquid flow system on a Q-Sense E4 measurement system (Q-Sense, Gothenburg, Sweden). A quartz window in the chamber allowed for effective UV illumination of the sensor surface with the unit placed under an array of 6 UV-B lamps (15W, G15T8E, Ushio, Japan, sample-to-lamp distance: 20 cm). Degassed MAA solution was pumped inside the system via an external syringe and finally

irradiated by the already described UV set-up. The Q-Sense E4 system allows for simultaneous recording of changes in resonant frequency (Δf) and energy dissipation (ΔD) recorded at multiple overtones (5, 15, ..., 65 MHz). As a first approximation the system has a mass sensitivity of 17.7 ng/cm² per Hz using the Sauerbrey relation.³¹ However, acoustic sensors like QCM-D measure the adsorbed mass including dynamically coupled water and are sensitive to the viscoelastic properties of the adsorbed film, as well.^{32,33} Thus, in order to calculate the variation in grafted polymer mass, a Voigt-based model was used to fit the experimental data for Δf and ΔD at several overtones, which takes the effect of viscoelasticity into account.^{34,35} The hydrated polymer grafts were considered as a homogenous viscoelastic film characterized by viscosity ηB_{PB} varying between 0.001 and 0.01 kg/ms and a swollen thickness d varying between 0 and 1 μm .

3.5 References

- (1) Prucker, O.; R uhe, J. *Langmuir* **1998**, *14*, 6893.
- (2) Prucker, O.; R uhe, J. *Macromolecules* **1998**, *31*, 602.
- (3) Matyjaszewski, K.; Xia, J. H. *Chem. Rev.* **2001**, *101*, 2921.
- (4) Patten, T. E.; Matyjaszewski, K. *Adv. Mater.* **1998**, *10*, 901.
- (5) Chiefari, J.; Chong, Y. K.; Ercole, F.; Krstina, J.; Jeffery, J.; Le, T. P. T.; Mayadunne, R. T. A.; Meijs, G. F.; Moad, C. L.; Moad, G.; Rizzardo, E.; Thang, S. H. *Macromolecules* **1998**, *31*, 5559.
- (6) Georges, M. K.; Veregin, R. P. N.; Kazmaier, P. M.; Hamer, G. K. *Macromolecules* **1993**, *26*, 2987.
- (7) Bain, C. D.; Evall, J.; Whitesides, G. M. *J. Am. Chem. Soc.* **1989**, *111*, 7155.
- (8) Bertilsson, L.; Liedberg, B. *Langmuir* **1993**, *9*, 141.
- (9) Folkers, J. P.; Laibinis, P. E.; Whitesides, G. M.; Deutch, J. J. *J. Phys. Chem.* **1994**, *98*, 563.
- (10) Atre, S. V.; Liedberg, B.; Allara, D. L. *Langmuir* **1995**, *11*, 3882.
- (11) Jones, D. M.; Brown, A. A.; Huck, W. T. S. *Langmuir* **2002**, *18*, 1265.
- (12) Wu, T.; Efimenko, K.; Vlcek, P.; Subr, V.; Genzer, J. *Macromolecules* **2003**, *36*, 2448.
- (13) Harris, B. P.; Metters, A. T. *Macromolecules* **2006**, *39*, 2764.
- (14) Bao, Z. Y.; Bruening, M. L.; Baker, G. L. *Macromolecules* **2006**, *39*, 5251.

- (15) Tugulu, S.; Barbey, R.; Harms, M.; Fricke, M.; Volkmer, D.; Rossi, A.; Klok, H. A. *Macromolecules* **2007**, *40*, 168.
- (16) Huang, W. X.; Kim, J. B.; Bruening, M. L.; Baker, G. L. *Macromolecules* **2002**, *35*, 1175.
- (17) Ma, H. W.; Hyun, J. H.; Stiller, P.; Chilkoti, A. *Adv. Mater.* **2004**, *16*, 338.
- (18) Otsu, T.; Yoshida, M. *Makromol. Chem. Rapid Commun.* **1982**, *3*, 127.
- (19) Otsu, T. *J. Polym. Sci. Part A: Polym. Chem.* **2000**, *38*, 2121.
- (20) Cassie, A. B. D. *Discuss. Faraday Soc.* **1948**, *3*, 11.
- (21) de Boer, B.; Simon, H. K.; Werts, M. P. L.; van der Vegte, E. W.; Hadziioannou, G. *Macromolecules* **2000**, *33*, 349.
- (22) Rahane, S. B.; Kilbey, S. M.; Metters, A. T. *Macromolecules* **2005**, *38*, 8202.
- (23) During this time interval the viscosity of the reaction solution did not increase since no relevant amount of polymer in solution was formed by auto-initiation. For irradiation times longer than 80 minutes, solution polymerization was observed to take place thus causing contamination of the polymer layers and affecting the values of film thickness.
- (24) Edmondson, S.; Huck, W. T. S. *J. Mater. Chem.* **2004**, *14*, 730.
- (25) Pinto, J. C.; Whiting, G. L.; Khodabakhsh, S.; Torre, L.; Rodriguez, A. B.; Dalgliesh, R. M.; Higgins, A. M.; Andreasen, J. W.; Nielsen, M. M.; Geoghegan, M.; Huck, W. T. S.; Sirringhaus, H. *Adv. Funct. Mater.* **2008**, *18*, 36.
- (26) Biesalski, M.; Johannsmann, D.; Ruhe, J. *J. Chem. Phys.* **2002**, *117*, 4988.
- (27) Cheng, N.; Azzaroni, O.; Moya, S.; Huck, W. T. S. *Macromol. Rapid Commun.* **2006**, *27*, 1632.
- (28) The latter time of UV exposure was chosen in order to investigate the physical characteristics of the films during the initial polymer growth. The irradiation of MAA solutions for longer times would cause a large change in density and viscosity of the medium due to the formation of polymer in solution. This would greatly affect the response of the QCM-D and distort the interpretation of changes to the surface-polymerized film.
- (29) Brandrup, J.; Immergut, H. E.; Grulke, E. A. *Polymer Handbook, 4th Ed.*; J. Wiley&Sons: New York, 1999.
- (30) Rodahl, M.; Hook, F.; Krozer, A.; Brzezinski, P.; Kasemo, B. *Rev. Sci. Instrum.* **1995**, *66*, 3924.
- (31) Sauerbrey, G. *Z. Phys.* **1959**, *155*, 206.
- (32) Hook, F.; Kasemo, B.; Nylander, T.; Fant, C.; Sott, K.; Elwing, H. *Anal. Chem.* **2001**, *73*, 5796.
- (33) Reimhult, E.; Larsson, C.; Kasemo, B.; Hook, F. *Anal. Chem.* **2004**, *76*, 7211.

- (34) Domack, A.; Prucker, O.; Ruhe, J.; Johannsmann, D. *Phys. Rev. E* **1997**, *56*, 680.
- (35) Voinova, M. V.; Rodahl, M.; Jonson, M.; Kasemo, B. *Phys. Scr.* **1999**, *59*, 391.

Chapter 4

Tunable Temperature-Responsive Polymer Brushes on Gold by Iniferter-Based Surface-Initiated Polymerization*

With the primal aim of showing a potential application of photo-iniferter-SIP in the chemical structuring of stimulus-responsive polymeric platforms, we report in this Chapter on the synthesis of Poly-N(isopropylacrylamide) (PNIPAM) brush layers. These thermoresponsive brushes were grafted in a controlled way to gold substrates demonstrating the capability to tune the structure and properties of the polymer grafts. The chain length of the polymers was controlled using UV-light as a trigger and the end groups exposed were shown to be easily exchangeable following the grafting process. Reversible volume shrinkage/expansion, roughening and variation of adhesion were observed by in-situ real time AFM upon cycling the temperature around the LCST.

4.1 Introduction

The surface tethering of “smart” polymers has thus far been explored with a variety of methods, including the “grafting to” approach,¹ physical adsorption^{2,3} and the “grafting from” technique.⁴⁻⁸ The latter method is recognized as being very versatile, and enables the formation of patterned polymeric brushes. It exploits such techniques as micro contact printing (μ CP)⁹ as well as tip-assisted nano-lithography⁷ in order to deposit the initiators from which the polymer chains may eventually be

* Part of this Chapter was published in: Benetti, E.M.; Zapotoczny, S; Vancso, G.J. *Adv. Mater.* **2007**, *19*, 268.

grown. Great interest has been vested in using poly-N(isopropylacrylamide) (PNIPAM) as prototype “smart” polymer in biological applications as it exhibits a lower critical solution temperature (LCST) in aqueous environments. Upon passing the LCST by heating, PNIPAM precipitates at physiologically relevant temperatures, which forms the basis for responsive applications. PNIPAM is also a prime target polymer for surface and interface-related use, as many biological, biomedical and sensing applications such as protein adsorption, cell adhesion, and biosensors benefit from thermal control of the conformation of surface-grafted chains.¹⁰⁻¹⁴ The possibility to control the chemistry and, at the same time, the topography of a surface-bound stimulus-responsive polymeric platform, represents a fundamental issue in materials science as well as in biotechnology.¹⁵⁻¹⁹

In this Chapter we report on the synthesis of thermosensitive surfaces, by controlled grafting of PNIPAM brushes using the already introduced disulfide-containing photo-*iniferter* immobilized on Au, and on in-situ AFM monitoring of reversible changes of the volume and adherence of grafted patterns. Our approach allows for tuning the composition of the polymer chain terminal groups exposed to the brush-liquid interface. The system proposed here is furthermore fully compatible with a successive single molecule level fabrication exploiting AFM tip-assisted nanomodification techniques.²⁰

PNIPAM brushes were grafted in a controlled manner from mixed self-assembled monolayers (consisting of an alkane thiol and the disulfide initiator) on gold substrates. The “grafting-from” polymerization was carried out by employing the *iniferter* DTCA as initiator²¹ for photopolymerization (which was introduced in Chapter 3 and which is depicted in Figure 4.1).

The choice of gold as a substrate has several advantages as compared to the already reported photo*iniferter*-based grafting from silicon surfaces.^{5,22} Self-assembled monolayers (SAMs) of thiols or disulfides on gold surfaces are well-ordered, their compositions may be easily varied, the deposition procedure is compatible with the lithographic techniques mentioned above, and this chemistry is not sensitive to ambient (humidity) variations.²³⁻²⁶

As it was demonstrated in the previous Chapter, DTCA photo-*iniferter* can be easily deposited on gold and will initiate a controlled radical polymerization from aqueous N-isopropylacrylamide (NIPAM) solutions, which can be triggered by UV light and performed at room temperature. The diethyldithiocarbamil group remains

at the end of the growing tethered chain,²¹ which allows one to tune the chain length by variation of the irradiation time (see Chapter 3). In addition, the use of this polymerization reaction gives control over the end groups, which can be easily exchanged or chemically modified.¹⁹ The biocompatibility of this technique should also be underlined since no organic solvents are used and no toxic metal/compounds are involved in the polymerization process.

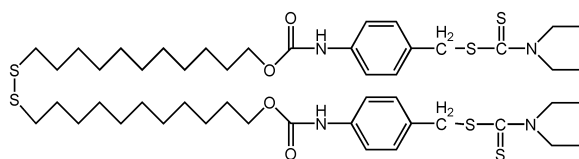


Figure 4.1. Disulfide-based photoiniferter (DTCA).

4.2 Results and Discussion

4.2.1 Iniferter-Based Photografting of NIPAM

The UV-initiated polymerization of NIPAM from SAMs on Au was performed following a similar procedure to the one previously reported in Chapter 3. Thus lamps emitting at 300 nm coupled with a 280 nm cut-off filter were used in order to avoid SAMs degradation.²² A diluted solution of octadecylthiol (ODT) (40 mol-%) mixed with DTCA (60 mol-%, with respect to the iniferter groups) in ethanol was placed in contact with gold using a PDMS elastomeric stamp, thus forming regular patterns consisting of mixed SAMs. Surface dilution of initiator plays an important role in the subsequent “grafting-from” photopolymerization, since, as it was shown in Chapter 3, allowed us to reduce the recombination of the radicals that are formed on the surface.^{5,27-29}

The gold substrate covered with a printed pattern of mixed SAM consisting of parallel stripes with a 15 μm width separated by 5 μm Au was immersed in a deoxygenated aqueous solution of the monomer N-isopropylacrylamide (NIPAM) and subsequently irradiated with UV light. Figure 4.2 presents height images from AFM measurements in tapping mode of the patterned surface with the grafted

PNIPAM chains in the dry state. After only 5 min of irradiation of the sample immersed in a 5% monomer solution, height features of 10 ± 2 nm were obtained (Figure 4.2a) on the initiator covered stripes. We performed a chain extension test by placing the sample, following interruption of polymerization, back in the monomer solution and irradiating for another 5 min. As can be seen in Figure 2b, the height of the brushes doubled after the second irradiation step, reaching values of 20 ± 3 nm.

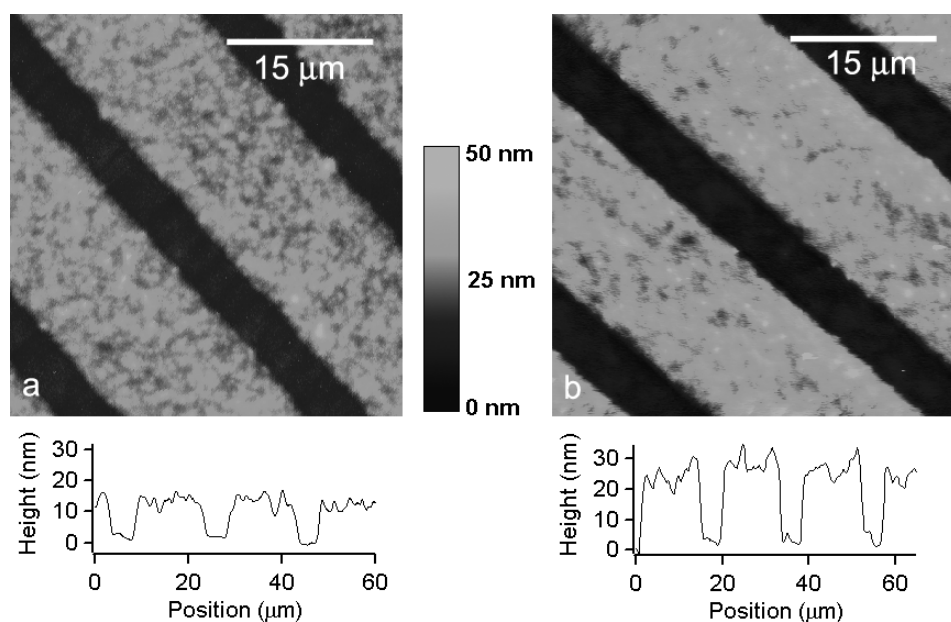


Figure 4.2. Height images from AFM measurements in tapping mode of the patterned surface with the grafted PNIPAAm chains (in the dry state) after a) 5 minutes and b) an additional 5 minutes of irradiation. The respective cross sections are displayed below each image.

4.2.2 Temperature Response by In-Situ AFM

The sample obtained was subsequently imaged in an aqueous medium to monitor the morphological changes of the PNIPAM brushes at temperatures around the LCST. Whereas in recent years the works of Kidoaki et al.⁴ and of Jones et al.⁹ focused on AFM force measurements below and above the LCST, to our knowledge, this is the first study providing AFM topography images and force volume measurements recorded in situ at several temperatures in the range 30-36°C. In Figure 4.3 height images of the PNIPAAm brushes at 31.0 and 36.0°C can be seen.

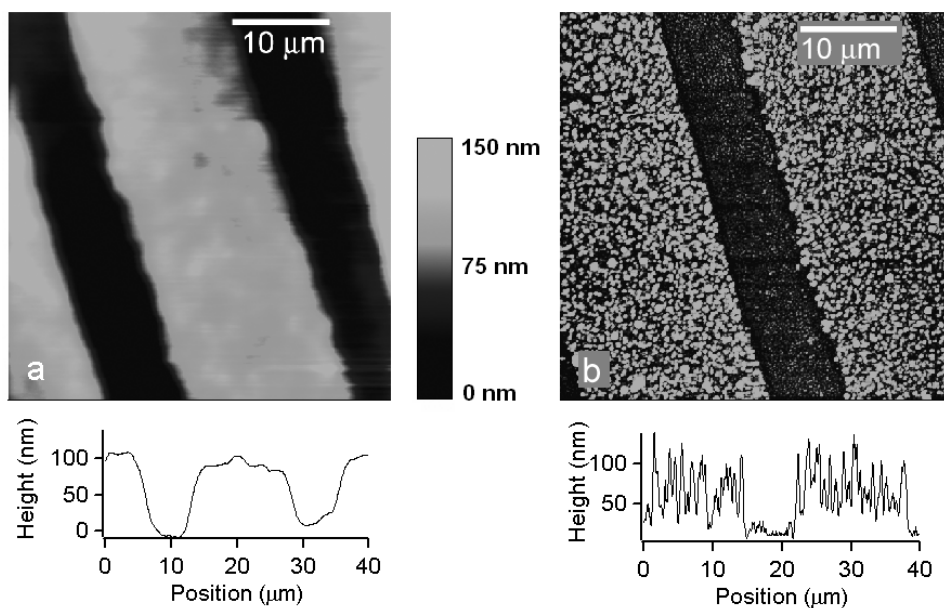


Figure 4.3. Height images from AFM measurements in tapping mode of the patterned surface with the grafted PNIPAAm chains in water at a) 31.0°C and b) 36.0°C. The respective cross sections are displayed below each image.

Representative height images at 31.0°C in Figure 4.3a, show how the polymeric features that exhibited an average height of 20 nm in the dry state swelled profusely and gave rise to height values of 109 ± 6 nm when immersed in water (Figure 4.3a). Assuming that in the presence of a good solvent the height of the stretched brushes h is comparable to the length of the polymer chains L ,³⁰ we can estimate the average molar mass M_n knowing the monomer length l . Assuming l to be 3 Å for acrylic monomers³¹ we estimated an M_n value for the grafted chains of 40000 g/mol. If compared with experiments carried out in bulk systems with a similar *iniferter*-based initiator, the values for number average molar mass were in the same order of magnitude as compared to the values obtained by GPC measurements (data not shown). The grafting density can thus be estimated to be 0.33 chain/nm² confirming the formation of a tightly packed brush.³²

When the temperature was raised to above the LCST value (32.0 °C measured in the bulk for this polymer), the chains collapsed, aggregated and formed globular features (Figure 4.3b, image captured at 36.0 °C). The calculated average height of the polymeric features dropped to 34 nm but the height profiles in Figure 4.3b clearly display that the chains not only shrank but, in many cases, aggregated

without any significant difference in peak height. The aggregation of the polymer brushes was accompanied by the exclusion of water from the polymeric structure. From the bearing analysis on the AFM micrographs we concluded that the volume occupied by the polymer decreased more than twice, from $0.046 \pm 0.002 \mu\text{m}^3/\mu\text{m}^2$ at 31°C to $0.022 \pm 0.002 \mu\text{m}^3/\mu\text{m}^2$ at 36°C . The formation of hydrophobic polymeric aggregates caused an abrupt change in the morphology leading to a dramatic increase in the values of root-mean-squared (RMS) roughness of the surface from $4.9 \pm 0.8 \text{ nm}$, at 31°C , to $37 \pm 2 \text{ nm}$ at 36°C (values calculated over $10 \mu\text{m} \times 10 \mu\text{m}$ area).

The surface properties of the grafted polymer were monitored by AFM in the force-volume mode (capturing adherence images). As shown in Figure 4.4, the adherence can be easily tuned by a repetitive heating-cooling sequence, which causes the polymer features to alternate between swollen and collapsed states (compare height images in Figure 4.3).

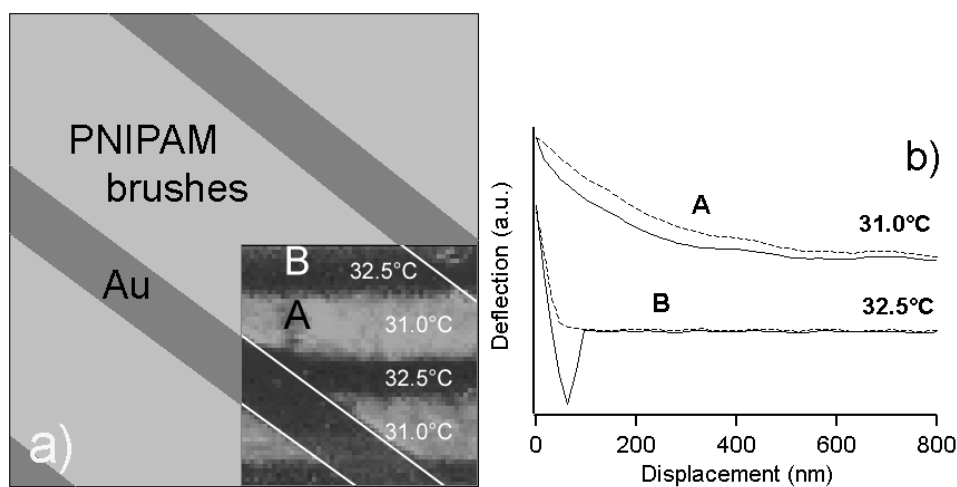


Figure 4.4. a) The area captured shows a $40 \times 40 \mu\text{m}$ section exhibiting a schematic of the structure of the surface grafted polymer platform. The bottom right is an experimental AFM force volume image ($20 \times 20 \mu\text{m}$) of the grafted PNIPAM chains in water. The grey scale in the AFM image corresponds to areas of high (dark) and low (bright) adherence. The temperature was cycled between 31.0°C and 32.5°C . b) Force-displacement curves for the two regimes, captured on the polymeric features.

The tip-sample interaction at 31.0°C was dominated by repulsive forces (brighter horizontal areas, and force curve A in Figure 4.4) as compared to adhesive interactions with the non-printed gold surface. At 32.5°C the contrast between Au

and polymer disappeared as a result of the transition of the brushes to collapsed aggregates above the LCST. This resulted in attractive interactions and “conventional” adhesive pull-off forces upon tip withdrawal (see force curve B in Figure 4.4). The typical force-distance curves at the two temperatures (Figure 4.4b) confirm that the repulsive forces upon compression of the swollen chains at 31.0°C, which are typical for packed brushes,³²⁻³⁴ disappeared at 32.5°C, above the LCST.⁹

4.2.3 Control Over Chain Ends via Radical Exchange

As mentioned earlier, the grafting procedure should permit the control of the chain ends of the tethered polymers. In order to test this notion, diethyldithiocarbamyl groups were exchanged with stable 2,2,6,6-tetramethylpiperidyl-1-oxyl (TEMPO) radicals.³⁵

The tethered polymer chains were irradiated in the presence of 4-amino-TEMPO radicals that irreversibly couple at room temperature with the in situ formed macroradicals. Figure 4.5a displays a schematic representation of this exchange procedure. In the next step a fluorophore (fluorescamine) was reacted with the primary amine moieties of the exchanged groups. The contrast shown in the fluorescent microscope image in Figure 4.5b comes from the fluorescamine adducts formed at the chain ends of the polymers grafted from the μ CP patterns. Thus, with chain terminal group exchange strategies such as the approach we used, it is possible to easily introduce the desired functionalities at the end of the tethered polymer brushes.

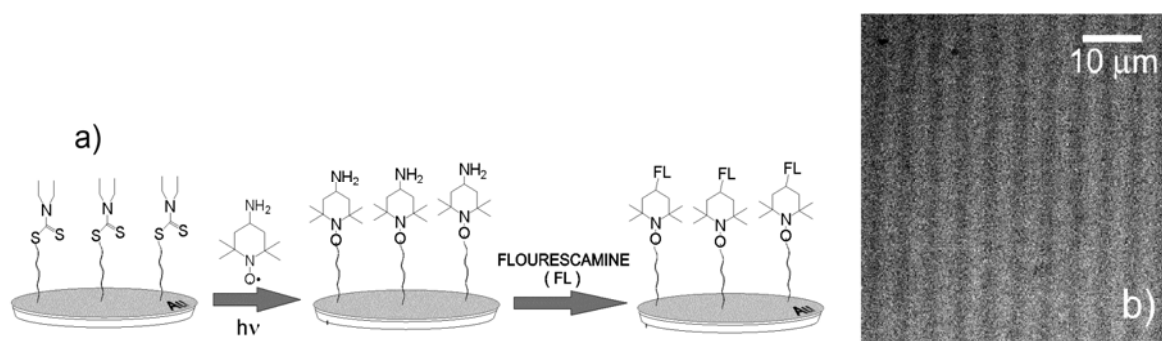


Figure 4.5. a) Scheme of the exchange procedure of the PNIPAM polymer brush end groups with the stable 4-amino-TEMPO radicals and the subsequent fluorescent labeling of the amino groups with

fluorescamine. b) A fluorescent microscope image of the patterned PNIPAM brushes modified according to the mentioned procedure.

4.3 Conclusions

In this Chapter we reported on the use of DTCA photo-*iniferter* for the controlled surface grafting of tunable, temperature-responsive PNIPAM brushes. The length of tethered chains can be controlled by the irradiation time. We monitored by in situ AFM, the temperature induced morphology and adherence changes of microscale-patterned surfaces of the brush around its LCST.

Furthermore, the method presented enabled control of chain ends as was proven by a radical exchange experiment. All these characteristics make the present grafting technique a promising tool for producing “smart”, temperature-responsive platforms, with a potential of chemical control of the chain terminating groups.

4.4 Experimental

Photopolymerization: In order to obtain brush micro-patterns a mixture of the initiator DTCA (synthesized as described in Chapter 3) and ODT in ethanolic solution was deposited on Au substrates with a polydimethylsiloxane (PDMS) stamp. The gaps between the patterned areas were subsequently functionalized with an ODT monolayer via deposition from a 1 mM ethanolic solution overnight. The samples were then placed in quartz flasks equipped with a 280 nm cut-off filter and containing 5% aqueous solution of NIPAM. They were purged with nitrogen and subsequently irradiated for the necessary time by 6 UV-B lamps (15W G15T8E, Ushio Japan) at a distance of 20 cm. After the photopolymerization, the substrates were extensively rinsed with water and methanol.

Chain-end exchange experiment: After the grafting of PNIPAM, the substrates were covered with a drop of 0.01 M aqueous solution of 4-amino-TEMPO (4-amino-2,2,6,6-tetramethylpiperidyl-1-oxyl) free radicals and irradiated for 5 min with UV light in the above described system. The samples were subsequently rinsed with water and placed in an acetone solution of fluorescamine (0.5 mg/ml) for a further 5

minutes. After extensive rinsing with acetone the substrates were imaged with a fluorescent microscope (Olympus IX71).

AFM measurements: The AFM measurements in tapping mode were carried out on a NanoScope III multimode AFM (Digital Instruments/Veeco, Santa Barbara, USA) equipped with a heating stage, a liquid cell and an external thermocouple that allowed the control of the actual temperature of the medium.

4.5 References

- (1) Cho, E.C.; Kim, Y.D.; Cho, K. *Polymer* **2004**, *45*, 3195
- (2) Tanahashi, T.; Kawaguchi, M.; Honda, T.; Takahashi, A. *Macromolecules* **1994**, *27*, 606.
- (3) Callewaert, M.; Grandfils, C.; Boulangè-Petermann, L.; Rouxhet, P.G. *J. Colloid Interface Sci.* **2004**, *276*, 299.
- (4) Kidoaki, S.; Ohya, S.; Nakayama, Y.; Matsuda, T. *Langmuir* **2001**, *17*, 2402.
- (5) Ista, L.K. ; Mendez, S. ; Pèrez-Luna, V.H. ; Lòpez, G.P. *Langmuir* **2001**, *17*, 2552.
- (6) Biesalski, M.; Johannsmann, D.; Rùhe, J. *J. Chem. Phys.* **2002**, *117*, 4988.
- (7) Kaholek, M.; Lee, W.; Ahn, S.; Ma, H.; Caster, K.C.; LaMattina, B.; Zauscher, S. *Chem. Mater.* **2004**, *16*, 3688.
- (8) Tu, H.; Heitzman, C.E.; Braun, P.V. *Langmuir* **2004**, *20*, 8313.
- (9) Jones, D.M.; Smith, J.R.; Huck, W.T.S.; Alexander, C. *Adv. Mater.* **2002**, *14*, 1130.
- (10) Heskins, M. ; Guillet, J.E. *Macromol. Sci. Chem.* **1968**, *A2*, 144.
- (11) Hoffmann, A.S. *J. Control. Rel.* **1987**, *6*, 297.
- (12) Schild, H.G. *Prog. Polym. Sci.* **1993**, *17*, 163.
- (13) Huber, D.L.; Manginell, R.P.; Samara, A.; Kim, B.; Bunker, B.C. *Science* **2003**, *301*, 352.
- (14) Canavan, H.E.; Cheng, X.; Graham, D.J.; Ratner, B.D.; Castner, D.G. *Langmuir* **2005**, *21*, 1949.
- (15) Ikada, Y. *Biomaterials* **1994**, *15*, 725.
- (16) Webb, K.; Hlady, V.; Tresco, P.A.; Altankov, G.; Grinnell, F.; Groth, T. *J. Biomed. Mater. Res.* **1996**, *30*, 385.
- (17) Elbert, D.L.; Hubbel, J.A. *Biomacromolecules* **2001**, *2*, 430.
- (18) Magoshi, T.; Ziani-Cherif, H.; Ohya, S.; Nakayama, Y.; Matsuda, T. *Langmuir* **2002**, *18*, 4862.

- (19) Matsuda, T.; Ohya, S. *Langmuir* **2005**, *21*, 9660.
- (20) Piner, R.D.; Zhu, J.; Xu, F.; Hong, S.; Mirkin, C.A. *Science* **1999**, *283*, 661.
- (21) (a) Otsu, T.; Yoshida, M.; *Makromol. Chem. Rapid Commun.* **1982**, *3*, 127. (b) Otsu, T.; Yoshida, M.; Tazaki, T. *Makromol. Chem. Rapid Commun.* **1982**, *3*, 133. (c) Otsu, T.; Matsumoto, A. *Adv. Polym. Sci.* **1998**, *136*, 75.
- (22) de Boer, B.; Simon, H.K.; Werts, M.P.L.; van der Vegte, E.W.; Hdzioannou, G. *Macromolecules* **2000**, *33*, 349.
- (23) Bain, C.D.; Evall, J.; Whitesides, G.M. *J. Am. Chem. Soc.* **1989**, *111*, 7155.
- (24) Dubois, L.H. ; Nuzzo, R.G. *Annu. Rev. Phys. Chem.* **1992**, *43*, 437.
- (25) Poirier, G.E. ; Pylant, E.D. *Science* **1996**, *272*, 1145.
- (26) Love, J.C.; Estroff, L.A.; Kriebel, J.K.; Nuzzo, R.G.; Whitesides, G.M. *Chem. Rev.* **2005**, *105*, 1103.
- (27) Niwa, M.; Date, M.; Higashi, N. *Macromolecules* **1996**, *29*, 3681.
- (28) Zhao, B.; Brittain, W.J.; *Macromolecules* **2000**, *33*, 342.
- (29) Jones, D.M.; Brown, A.A.; Huck, W.T.S. *Langmuir* **2002**, *18*, 1265.
- (30) Milner, S.T.; Witten, T.A.; Cates, M.E. *Macromolecules* **1988**, *21* 2610.
- (31) Carey, F.S. in *Organic Chemistry*, 2nd ed., Mc Graw Hill: New York **1992**.
- (32) Yamamoto, S.; Ejaz, M.; Tsujii, Y.; Fukuda, T. *Macromolecules* **2000**, *33*, 5608.
- (33) Overney, R.M.; Leta, D.P.; Pictroski, C.F.; Rafailovich, M.H.; Liu, Y.; Quinn, J.; Sokolov, J.; Eisenberg, A.; Overney, G. *Phys. Rev. Lett.* **1996**, *76*, 1272.
- (34) Kelley, T.W.; Schorr, P.A.; Johnson, K.D.; Tirrel, M.; Frisbie, C.D. *Macromolecules* **1998**, *31*, 4297.
- (35) Beckwith, A.L.J.; Bowry, V.W.; Ingold, K.U. *J. Am. Chem. Soc.* **1992**, *114*, 4983.

Chapter 5

RGD-Functionalized Poly(methacrylic acid) Brushes: Control Over Cell Adhesion via Chemical Structuring*

In this Chapter the use of iniferter-mediated SIP is demonstrated to synthesize quasi 3-D structured hybrid peptide-polymer layers. This controlled SIP is used to graft poly (methacrylic acid) (PMAA) brush layers obtained from surface-attached iniferters in self assembled monolayers to a gold surface. The tethered chains are subsequently functionalized with the cell-adhesive arginine-glycine-aspartic acid (RGD) motif. The modified brushes are extended by reinitiating the polymerization to obtain an additional layer of PMAA, thereby burying the peptide-functionalized segments inside the brush structure. Contact angle measurements and Fourier transform infrared spectroscopy (FTIR) are employed to characterize the wettability and the chemical properties of these platforms. Time-of-flight secondary ion mass spectroscopy (TOF-SIMS) measurements are performed to monitor the chemical composition of the polymer layer as a function of the distance to the gold surface and to obtain information concerning the depth of the RGD motifs inside the brush structure. The brush thickness is evaluated as a function of the polymerization (i.e. UV-irradiation) time with atomic force microscopy (AFM) and ellipsometry.

In the second part of this Chapter, cell adhesion tests employing human osteoblasts are reported. These are performed on substrates with the RGD peptides exposed at the surface of substrates, as well as covered by a PMAA top brush layer. In addition, immunofluorescence studies demonstrate a variation of the cell

* Part of this Chapter was published in: Navarro, M.E.; Benetti, E.M.; Zapotoczny, S.; Planell, J.A.; Vancso, G.J. *Langmuir* **2008**, *24*, 10996.

morphology as a function of the position of the peptide units along the grafted chains.

5.1 Introduction

Platform fabrication efforts to obtain suitable surfaces for cell-adhesion studies have to a large extent been focused on surface modification approaches with specific molecular motifs which influence the adhesion and/or the behavior of cells at surfaces.^{1,2} Cell-adhesive protein motifs³ such as RGD have been successfully employed to modify polymeric scaffolds for bone-tissue regeneration, thus enhancing the adhesion and survival of cells.⁴ Cell adhesion depends not only on the receptor/ligand or integrin/RGD interactions but also on the clustering of the receptor (integrins) to form cell focal points.⁵ When the peptide sequence is coupled to brushes, the internal mobility of the polymers that constitute the film can promote the formation of such clusters.

Functional polymer brushes have been employed as versatile platforms for the immobilization of such peptides.^{6,7} The use of tethered polymer chains as engineered substrates for the preparation of bio-interfaces has several advantages: polymer brushes provide multiple binding points for biomolecules,⁸ their flexible nature enables the reorganization of chemical functional units of the tethered chains upon adhesion of cells⁶ and, most importantly, they can be readily synthesized on a variety of substrates, including metallic and non-metallic surfaces.⁹

Rühe et al.¹⁰ and Matsuda et al.^{11,12} have reported that “grafting from” approaches represent an extraordinarily powerful means for synthesizing quasi 3D films based on polymer brushes. This technique was used to fabricate polymer films presenting tunable morphologies, like in the case of mixed brush systems, or characterized by tailorable chemical properties which can be obtained, for example, by polymerization-biofunctionalization.

As it was described in Chapter 2, interfaces featuring adjustable characteristics can be synthesized by exploiting the intrinsic versatility of controlled, surface-initiated polymerization methods (such as atom transfer radical¹³ or *iniferter*-mediated polymerization¹⁴). Furthermore, these synthetic methods allow one to tether polymer chains, thus maintaining active chemical functionalities at the

chain ends. These groups have the capability of reinitiating the polymerization mechanism in subsequent stages. Consequently, this feature can be employed for an in-depth chemical structuring of the polymer film, i.e. growing a first layer of brushes, modifying them and later adding a subsequent grafted layer using the existing brushes as tethered macroinitiators (see Scheme 5.1).

In this study, this stepwise “grafting from” method was used to synthesize bio-adhesive platforms based on poly(methacrylic acid) (PMAA) brushes functionalized with an arginine-glycine-aspartic acid (RGD) peptide sequence.⁴ This amino acid sequence is found within most extracellular matrix proteins (ECM), and is known to enhance cell adhesion via interactions with the recognition domains of the transmembrane proteins known as integrins.^{3,15,16}

PMAA, a weak polyelectrolyte inherent of pH-responsive properties,¹⁷⁻¹⁹ is a polymer of special interest in molecular biology and biomaterials with applications in the synthesis of platforms for protein adsorption, in cell adhesion studies and in developing biosensors.^{20,21} Furthermore, PMAA has been used to improve surface hydrophilicity in tissue engineering scaffolds, as well as in drug delivery devices, among other applications.^{22,23}

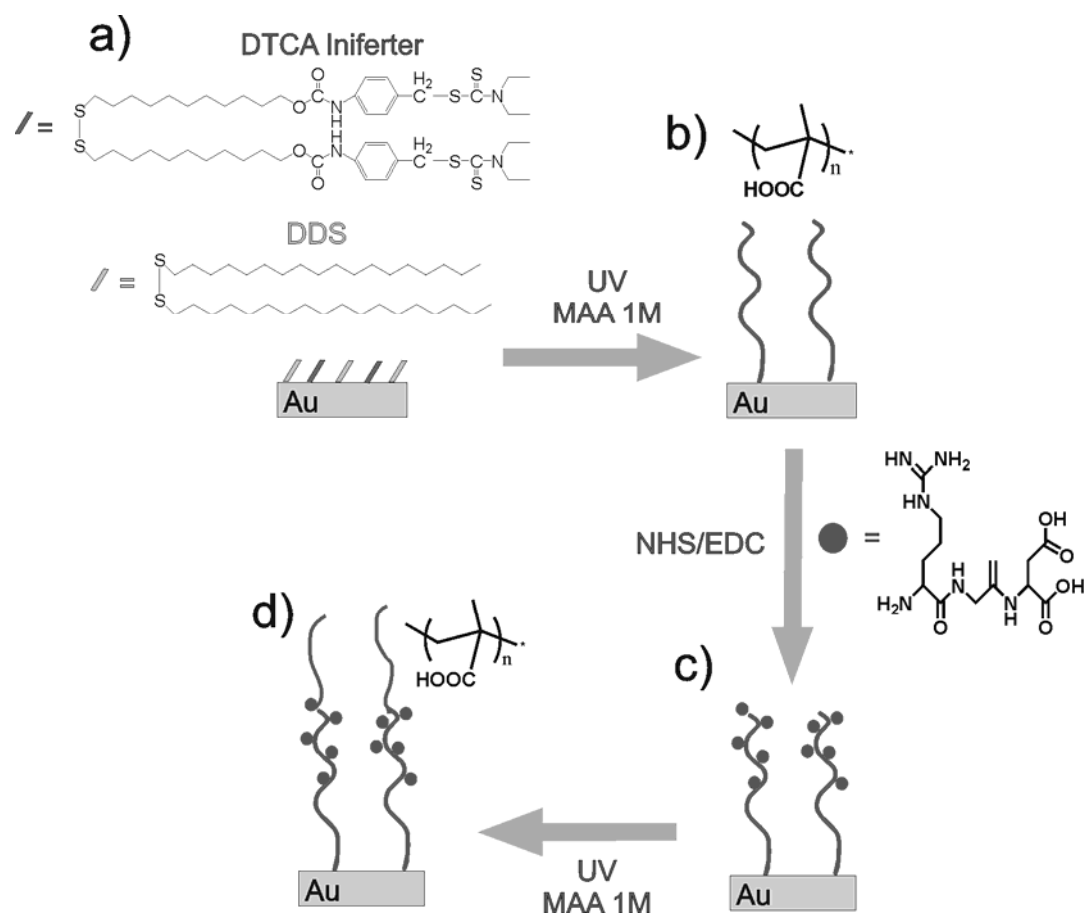
In the present study PMAA brushes were synthesized by photopolymerization of disulfide *iniferters* (DTCA initiators introduced in the previous Chapters) immobilized on Au substrates. Subsequently, human osteoblastic bone cells were used to evaluate the effect of the chemical composition of these brushes on the cell response, specifically focusing on the role of the brush structure on the variation of the cell morphology.

5.2 Results and discussion

5.2.1 Surface Characterization

The objective of this study was to engineer polymeric interfaces using PMAA brushes in order to control the cell adhesion process. PMAA brushes were grafted from Au substrates and subsequently functionalized with RGD. As the diethyldithiocarbamyl groups were still present at the chain ends, the modified grafts

could eventually be extended through an additional polymerization step as it was demonstrated in Chapter 4. In the present study, this fabrication strategy lead to peptide sequences being positioned at various positions along the brush structure (Scheme 5.1). The chemistry and characterization of the obtained platforms are first discussed.



Scheme 5.1. Preparation of RGD-modified polymer brushes grafted from immobilized precursors on gold by photopolymerization: a) and b) photografting of PMAA brushes from immobilized photoiniferter DTCA/ODT SAMs; c) immobilization of RGD peptides; d) chain extension via photografting of a top PMAA brush layer.

Following the procedure already reported in Chapter 4, polymer brushes were synthesized from precursor SAMs presenting the initiator adsorbed mixed with inert thiol species. In the present study mixed feeding solutions with DTCA:ODT molar ratio equal to 50:50 were used for the SAMs deposition. In order to monitor

the chemical properties of the synthesized polymer layers following every synthetic step, the surfaces were analyzed with a number of characterization techniques.

Contact angle measurements were performed in order to prove the effective grafting of PMAA from the initiating self-assembled monolayers. Following the immersion in the ODT/iniferter mixture, the water contact angle on the substrates' surface increased from $40 \pm 3^\circ$ (corresponding to bare gold) to $109 \pm 1^\circ$. The subsequent grafting of poly(methacrylic acid) resulted in a considerable decrease in the water contact angle, which dropped to $48 \pm 4^\circ$.

Depending on the functional groups that were exposed at the platform surfaces, the water contact angle values varied, thus indicating modifications/changes in the surface chemistry. After immersion of the gold substrates in a mixed solution of DTCA-ODT in chloroform, the contact angle values were found to increase markedly, confirming the formation of hydrophobic self-assembled monolayers of the two components. Following the photo-grafting of the PMAA brushes, the contact angle values dropped, proving the successful growth of a hydrophilic layer of PMAA that covered the substrate.

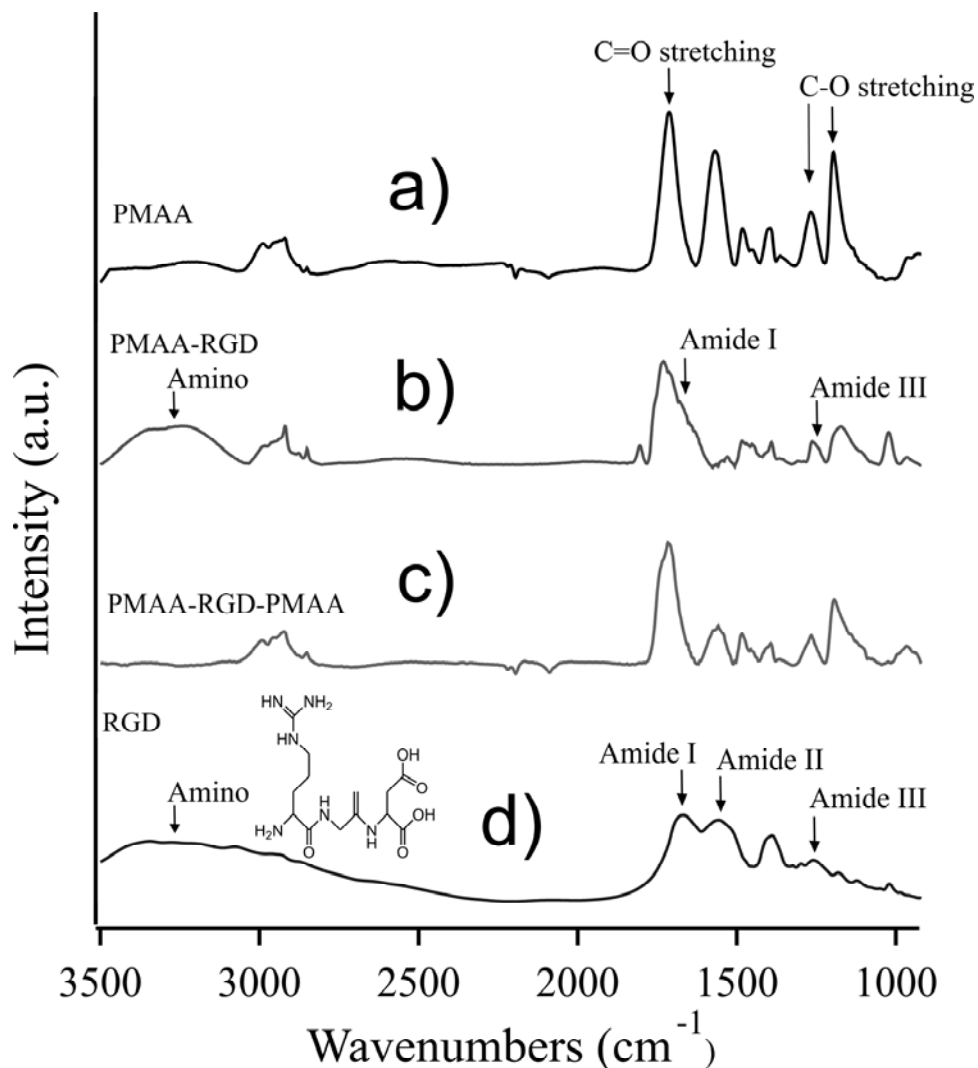


Figure 5.1. FTIR spectra of the gold surface after grafting PMAA brushes (a), RGD coupling (b) and further extension of the PMAA brushes (c). The FTIR spectrum (d) and the chemical structure of RGD is also included.

FTIR analysis confirmed the presence of PMAA immobilized on the samples' surface. In Figure 5.1a, the intense peak around 1700 cm^{-1} was assigned to the C=O stretching vibration in the carboxylic acid groups of the polymer. In addition, C-O stretching characteristics to PMAA were observed at 1203 and 1269 cm^{-1} . The PMAA layer was then successfully functionalized with RGD peptides through the reaction of the activated COOH groups (NHS esters) and the amine moieties of the arginine constituent.

In Figure 5.1b a clear broadening of the peak at 1712 cm^{-1} was recognized as a result of the partial overlapping of the amide I signal of RGD, usually placed at 1660

cm⁻¹.^{24,25} In addition, a broad shoulder corresponding to amine groups appeared around 3300 cm⁻¹ as well as a signal at 1260 cm⁻¹ representing amide III. The presence of the latter peak was accompanied by the weakening of the C-O stretching vibrations relative to the free carboxylic acids of the polymer.²⁶

As it has been already mentioned, the polymerization of PMAA could be reinitiated in a second stage, exploiting the already functionalized brushes which could act as immobilized macroinitiators, when the substrates were immersed in a new solution of monomer. After brush extension by further photopolymerization, a weakening of the amide signals and a simultaneous increase of the intensity of the bands that corresponded to COOH groups were observed. Figure 5.1c displays the FTIR spectrum of samples with an additional layer of PMAA grown on top of the pre-existing polymer film. A sharpening of the peak at 1712 cm⁻¹ as well as an increasing intensity of the two C-O stretching peaks at 1203 and 1269 cm⁻¹, characteristic of PMAA, were observed.

The latter results confirmed the formation of an additional superficial brush layer of PMAA that buried the peptide sequences inside the polymeric structure.

In order to estimate the height of the brushes following various polymerization times, AFM and ellipsometry were employed. The increase of the brush height as a function of the UV-irradiation time was evaluated from TM-AFM experiments in both air and liquid on patterned substrates (see Table 5.1). Regular patterns of PMAA brushes were prepared by depositing DTCA-ODT molecules via an “inked” PDMS stamp, thus giving rise to patterns consisting of 10 μm wide regular monolayer stripes on gold, exhibiting gaps of 5 μm. These gaps were subsequently back-filled by a solution deposition of self-assembled monolayers of ODT. The polymerization of PMAA was performed using these patterned substrates in 1 M solutions of MAA and was carried out for 5, 10 and 20 min. The values obtained in dry conditions were compared with AFM experiments performed in water at pH 7.4, as well as with the corresponding dry thicknesses measured by ellipsometry on continuous PMAA films synthesized following the same experimental conditions (see Sample Preparation section). In all cases the measured values increased remarkably with the photopolymerization time. After 20 min of UV irradiation, an ellipsometric thickness of 60 ± 9 nm was measured and the height of the patterns from TM-AFM was evaluated as 66 ± 10 nm.

Table 5.1. PMAA brush patterns' height measured with TM-AFM and dry ellipsometric thickness of brush films following different polymerization times (nm \pm SD)

Polymerization time	5 min	10 min	20 min	5min+RGD	5min+RGD+5min
AFM in air (nm)	6 \pm 1	16 \pm 3	66 \pm 10	12 \pm 3	24 \pm 2
AFM in water pH7.4 (nm)	10 \pm 3	22 \pm 4	100 \pm 9		
Dry thickness by ellipsometry (nm)	14 \pm 1	20 \pm 1	60 \pm 9		

The results obtained with ellipsometry were in good agreement with the height increments recorded with AFM in air. The same measurements performed in an aqueous medium at pH 7.4 displayed higher values for the height patterns, as could be expected for weak polyacids. At the physiological pH of 7.4 in an aqueous environment, the carboxylic acid moieties along the polymer backbone were partially deprotonated, thus causing negative charges to accumulate along the brush structure. These charges created an electrostatic repulsion between neighboring chains thereby extending the brush.²⁶ The height of the PMAA patterns, as measured with TM-AFM, thus increased by 40-60% when immersed in water (Table 5.1). The comparison between dry and swollen thickness (or swelling ratio) for polymer films grafted from flat surfaces can be used to evaluate the density of the tethered chains. This procedure was systematically applied for neutral polymer brushes immersed in good solvents, like poly(hydroxyethyl methacrylate)²⁷ and poly(oligoethyleneglycol methacrylate)⁷ in water, in order to calculate the grafting density. In the present case, considering weak polyacids grafts immersed in neutral medium, the same quantitative analysis (initially introduced by Jordan et al.²⁸) would lead to incorrect results because of the necessary modeling required (which goes beyond our purposes). Nevertheless the swelling ratio measured here was much lower than the one reported for PMAA in neutral water grafted with free radical polymerization techniques²⁶ and was in good agreement with the values, calculated in the same conditions, recently reported for PMAA brushes.²⁹ Thus a good indication of relatively high density of grafted chains in the present case can be derived.

The RGD sequence was chosen as the molecular modifier for the so-formed polymeric platforms since it is a very well-known peptide sequence that has been widely used for cell adhesion applications.³⁰ The effectiveness of the RGD sequence as a unit that promotes cell adhesion depends on several parameters. For instance, it is known that a lateral spacing of the ECM adhesion motifs is very important in regulating interactions between cell and ECM.³¹ Parameters such as the length of the spacer between the exposed surface and the RGD motif may also play important roles in cell adhesion processes. In addition, the positioning of the adhesive motif inside the polymer layers, as opposed to exposing it at the surface, represents an interesting platform for cell adhesion studies.

Following RGD functionalization, the height of the PMAA patterns was shown to increase remarkably with respect to the height of the precursor PMAA brushes, doubling its value as measured by TM-AFM in air (Table 5.1, sample indicated as 5min+RGD). The latter phenomenon was presumably due to the increase in volume of the grafted PMAA chains after functionalization with the tri-peptides. Following the second polymerization step, PMAA chains were extended above the functionalized layer thus increasing the height of the patterns which reached 24 ± 2 nm (Table 1, sample indicated as 5min+RGD+5min).

TOF-SIMS analysis was performed in order to obtain a depth profile with regard to the concentration of RGD units within the brush. This technique has in recent years been used to investigate the morphology of block copolymer-based films^{32,33} as well as to characterize biomaterials and protein-functionalized surfaces.³⁴⁻³⁷

In this study, TOF-SIMS analysis was used in order to detect the nitrogen containing fragments characteristics of the RGD peptide units, getting an indication of the concentration profiles of such motifs before and after re-initiation of the polymerization of PMMA (which leads to PMAA-RGD-PMMA samples) from the already functionalized polymer films (PMAA-RGD). Figure 5.2 shows the intensity profiles recorded for a) PMAA brushes functionalized with RGD, and b) PMAA brushes first functionalized with RGD and subsequently extended by a further photopolymerization step.

The intensity of the signals related to the ionic fragments containing nitrogen (indicative of the presence of peptides units) was recorded as a function of the

etching time and compared with the Au signal produced by the surface of the underlying substrate. In order to simplify and better illustrate the etching time-concentration profiles for the peptides in the polymer matrix, the concentration intensities of only $C_4H_8N^+$, which was reported as characteristic of RGD units,³⁸ are illustrated in Figure 5.2 as a function of the bombardment time. Thus, the obtained plots give a qualitative estimation of the depth profile relative to the concentration of RGD units in the polymer layer.^{39,40}

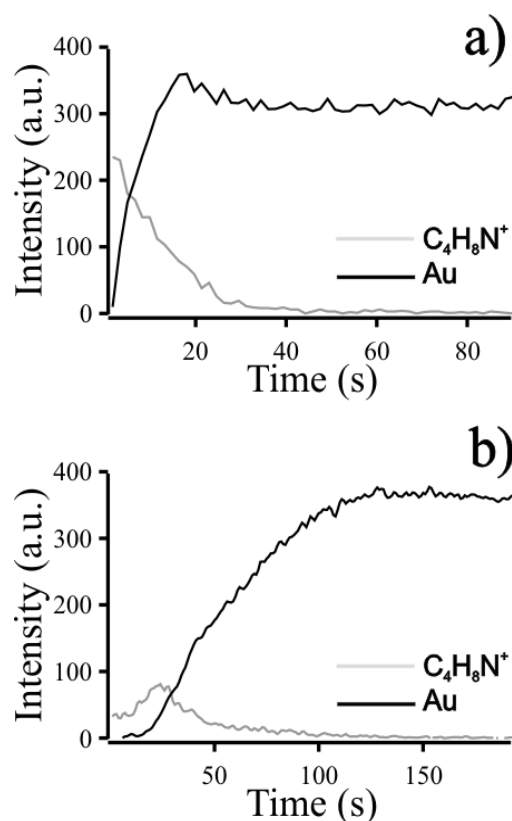


Figure 5.2. TOF-SIMS spectra showing the integrated intensity at molecular ions with $C_4H_8N^+$ fragment and Au as a function of ion bombardment time (related to depth into the brush layer) of the studied surfaces; a) PMAA brushes with RGD peptides; b) PMAA brushes with RGD peptides and an extra layer of PMAA.

In both spectra reported in Figure 5.2a and b, initially, the intensity profiles showed the presence of the organic fragment. With increasing etching time, however,

Au ions from the underlying substrate increased their intensity and reached a steady state following removal of the brush layer.

For peptides covalently bound to the grafted PMAA chains, and prior to additional growth of PMAA, the intensity of the nitrogen fragments slowly decreased from very high values to zero as the sputtering time was increased. Following the extension of the polymer chains grown on the prefunctionalized brushes, the intensity profile of the nitrogen-containing ions demonstrated a maximum at an etching time of approx. 24 s, followed by a constant decrease for higher times. The ionic intensities of the $C_4H_8N^+$ fragments thus displayed clear differences when the RGD groups were coupled on top of the polymer layer or as opposed to being buried under additional grafted PMAA chains. In the first case, the intensity of the signal decreased from very high values as the etching time increased. At the same time, the intensity profile related to the gold signal reached a plateau at approximately 20 s. This suggested that the gold surface was reached after around 10 s of etching, taking into account the atomic mixing effect at the interface between the PMAA layer and gold. The concentration of the N-fragments underwent a gradual decrease until becoming irrelevant. It was also expected that the RGD groups would react, not only on the exposed brush interface, but also inside the brush layer. Due to steric hindrance, the RGD concentration was relatively high at the surface as compared to in the internal part of the film closer to the gold substrate.

In the second case, where the RGD groups were buried within the PMAA brushes, TOF-SIMS analysis demonstrated the presence of an intensity maximum for the concentration of N-fragments between 10 and 40 s of etching time. When comparing this trend to the position of the plateau with regard to the Au-ions, the presence of a superimposed film of PMAA brushes without RGD, which covered an internal layer with a relevant concentration of peptides, could be confirmed.

5.2.2 Cell Adhesion Studies

The cell adhesion was assessed from two different points of view. The viability of the cells was evaluated using the LDH assay and the cell morphology was

monitored using immunofluorescence staining. Figure 5.3 displays the absorbance values after 2, 6 and 20 h of adhesion as measured by the LDH assay.

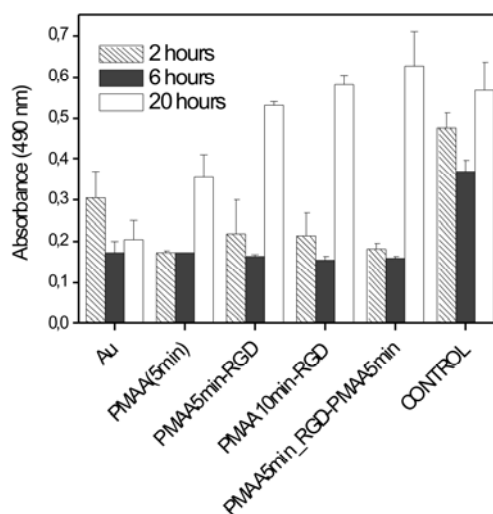


Figure 5.3. LDH results of the effect of the different surfaces on MG63 cells alter 2, 6 and 20 hours of contact. Vertical lines represent \pm SD.

After 2 h of contact with the studied surfaces, the polystyrene control plate showed the highest absorbance values and the gold substrates values significantly higher than the substrates functionalized with PMAA and PMAA-RGD-PMAA. No significant differences ($p < 0.05$) were observed between the samples containing the RGD sequence directly exposed or buried under an additional layer of brushes. After 6 h of culture, no significant differences were observed between the functionalized samples and the bare gold. However, once again, the polystyrene plate showed the highest absorbance values. After 20 h of adhesion, the surfaces functionalized with RGD presented absorbance values similar to those of the polystyrene control plate, and significantly higher than those obtained for the bare gold surface or for the substrates grafted with only PMAA. No significant differences were observed between substrates with RGD in direct contact at the interface or buried.

The substrates featuring PMAA polymerized for either 5 or 10 min displayed equivalent absorbance values. According to the LDH assay, after 20 h of culture, the samples with RGD either at the interface or buried by brush extensions did not present statistically significant differences ($p < 0.05$).

Despite the fact that, after 6 h, the LDH assay did not display any important difference ($p < 0.05$) for the surfaces functionalized with the RGD sequence, the immunofluorescence study demonstrated very clear variations in the morphology of the cells. Figure 5.4 shows images of the MG-63 cells adhering to the various substrates after 6 h of contact.

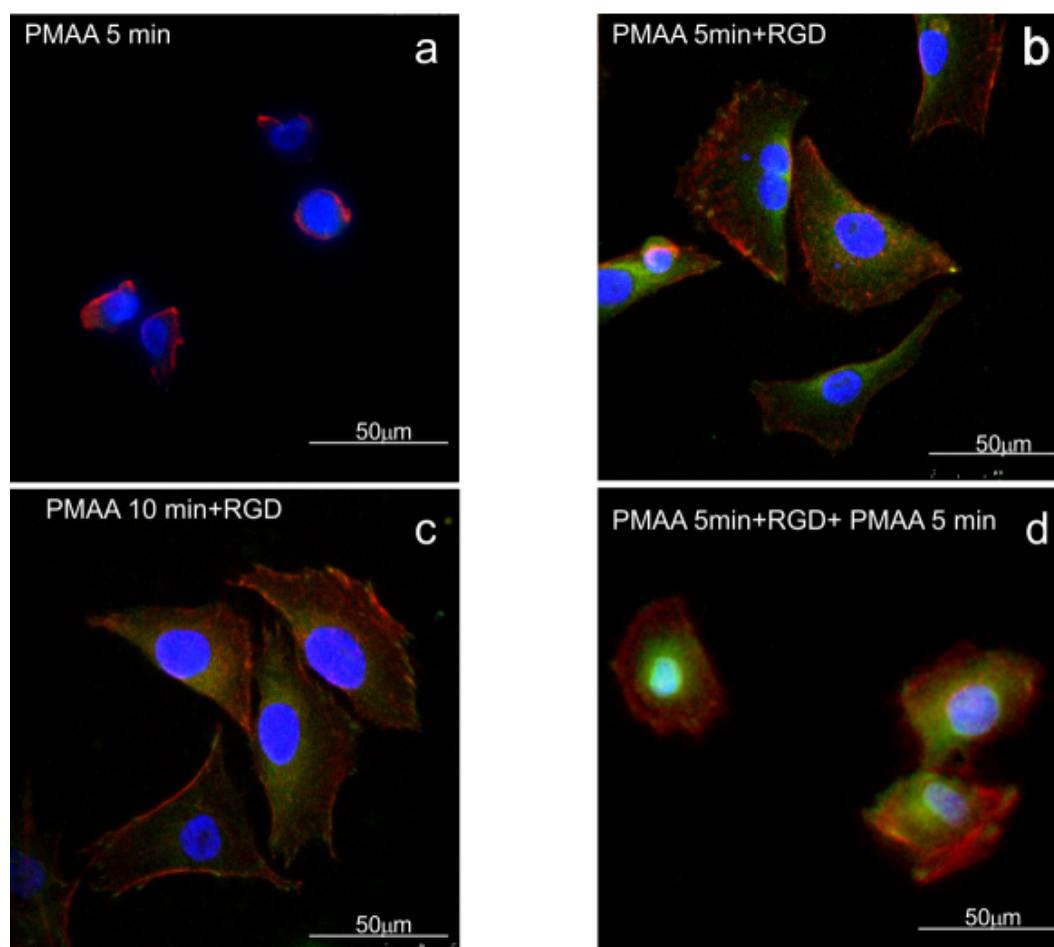


Figure 5.4. Immunofluorescence images of MG63 cells on the studied surfaces: a) PMAA, b) and c) PMAA-RGD and d) PMAA-RGD-PMAA after 6 hours of contact.

The cells adhering to the substrate functionalized with PMAA brushes showed rounded shapes, were scarcely spread on the surface and displayed almost no signs of vinculin. In the case where the RGD motif was coupled on the top of the PMAA brushes, the cells showed a very well-spread morphology with highlighted focal

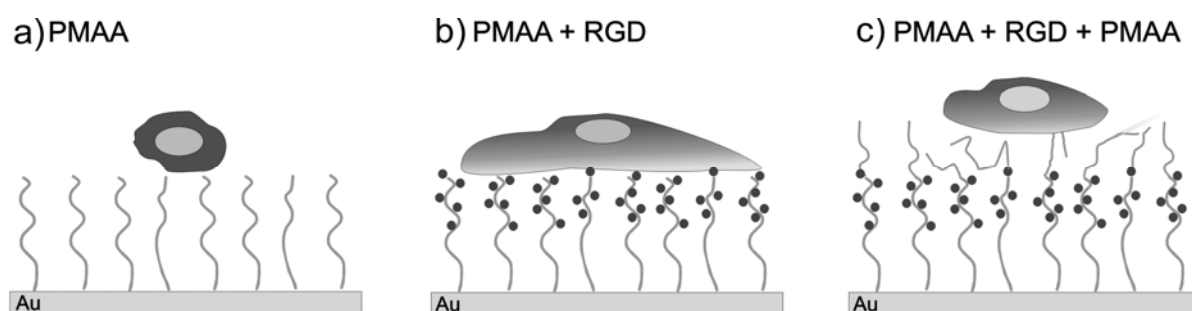
points. A different cellular morphology was recognized when the RGD sequence was capped within the brush structure. The cells displayed a spread and more rounded morphology, and moreover, the vinculin staining was only observed in the cytosol of the cell and not at its borders where the focal points were mainly supposed to be formed.

The cell adhesion results, in combination with the images obtained from the immunofluorescence study, showed an interesting picture of the cells' behavior in contact with the studied surfaces after short periods of time. The immobilization of the RGD motif on the surface of the samples profoundly influenced the cell response in terms of absorbance values as compared to those of the PMAA and bare gold samples, and also in terms of the cell morphology. According to the LDH assay, the number of cells cultured on the surfaces underwent a general diminution after 6 h of contact. After this period of time, the cells that were not properly attached to the surface as well as those that were not viable were removed, leaving only those that were well attached. In all cases, the remaining cells proliferated after 20 h of culture. The main differences between the surfaces with and without RGD could be observed after 20 h when cell proliferation took place. The surfaces where RGD was either directly exposed or buried inside the brush displayed higher, statistically significant ($p < 0.05$) absorbance values as compared to the surfaces without the RGD motif. The cells that were cultured on the samples with RGD showed values similar to those of the polystyrene control plate.

No significant differences were observed with respect to the LDH assay at 2 and 6 hours when comparing brush layers onto which RGD was directly coupled with brushes in which the RGD sequences were buried. This fact demonstrated that the number of viable cells adhered was unaffected by the difference in accessibility of the anchoring points. However, in spite of the LDH results obtained after 6 hours, remarkable differences were observed in the cells' morphology when comparing differently structured platforms.⁴¹ After 6 h of adhesion, immunofluorescence images showed clear variations in the morphology of the cells depending on what substrate had been used (see Figure 5.4). Varying the thicknesses of the functionalized brushes, on the other hand, did not lead to any variations in the cell's morphology. The cells spread very well, with a clear cytoskeleton and focal points marked at the borders of the cytoplasm on samples with RGD units coupled on the surface, independently of the thickness of the underlying brush structure (PMAA5min-RGD and PMAA10min-

RGD in Figure 5.4). However, in the case of the samples with the buried RGD, the cells showed an extended but rounded morphology, also with a very clear cytoskeleton, but in this case the vinculin staining was concentrated towards the nucleus, and the focal points at the cells' borders were rather unclear.

In order to explain the differences in cell morphology, Scheme 5.2 depicts a schematic of both situations, i.e. RGD directly exposed or buried within the PMAA brushes.



Scheme 5.2. A schematic representing the morphological changes of MG-63 cells on a pmaa brush without RGD (a) and with RGD at different depths in the brush layer (b and c).

In the first case, the adhesive units were highly concentrated at the exposed surface of the polymer layer and the cells could adhere and spread on the functionalized surface. When RGD was not directly accessible but buried beneath a thin but uniform layer of non-functionalized PMAA brushes, the cells adopted a different morphology. The cytoskeleton still appeared clear and the contrast produced by the staining of the focal adhesion could be clearly recognized. These indications confirmed the anchoring of the cells to the surface through an attachment on the adhesive units even if they were incorporated inside the brush structure. In the present model, the cells and the brushes underwent a mutual morphological rearrangement: on the one hand, the cellular morphology was tuned in order to reach the RGD motifs, on the other hand, the intrinsic flexibility of the grafted chains allowed an internal reorganization inside the fluid mass of the brush.

The evidences of the immunofluorescence study, together with the proposed representation, showed how surfaces modified with well defined, bio-chemically

nanostructured polymer brushes can represent model platforms for the study of changes in the cellular morphology.

5.3 Conclusions

Iniferter-mediated surface-initiated photopolymerization was used to graft poly(methacrylic acid) brushes from self-assembled monolayers on gold surfaces. The PMAA chains were subsequently functionalized with the RGD cell-adhesive peptide sequence. RGD units were covalently immobilized both at the top of the brushes and within the brushes layer after extension of the polymer chains by further polymerization step. The stepwise fabrication/chemical modification of the brush-like platforms was monitored by FTIR spectroscopy and the position of the cell adhesive units within the polymer layers was evaluated via TOF-SIMS measurements.

MG63 osteoblastic cells were used to evaluate the effect of RGD positioning within the brush. No significant differences were observed with the LDH-based adhesion study. However, there were noteworthy differences with respect to cells' morphology. Cells spread well with marked focal adhesion points at the periphery of the cytoplasm on samples with RGD motifs coupled on the surface, whereas in the case of the samples where RGD was buried, cells were found to adopt a rounded morphology and focal adhesions concentrated toward the internal part of the cell.

The findings reported in this Chapter indicate that there is a direct correlation between the vertical position of the RGD motif and cell morphology. The evidences reported in this work, showed how surfaces modified with well defined, bio-chemically nano-structured polymer brushes can represent model platforms for the study of changes in the cellular morphology.

5.4 Experimental

Photopolymerization. A mixture of a disulfite-containing photo-*iniferter* dithiodiundecane-11,11-diylbis[4-((diethylamino)carbonothioyl)thioethyl]phenyl]carbamate} (DTCA) (50 mol %) and octadecylthiol (ODT) (50 mol %) was used to form the initial self-

assembled monolayers (SAMs). Gold substrates with areas of 1 cm² (40 nm thick Au layer, Ssens BV, Hengelo, The Netherlands) were cleaned with a “piranha” (30% H₂O₂ / 70% H₂SO₄) solution and subsequently immersed in a DTCA-ODT solution overnight at room temperature. In order to obtain brush height, the ODT/DTCA mixtures were deposited on Au substrates with a polydimethylsiloxane (PDMS) stamp and the gaps between the patterned areas were functionalized with an ODT monolayer via deposition from a 1 mM ethanolic solution. Both un-patterned and patterned samples were then placed in quartz flasks containing a 1.0 M aqueous solution of MAA, after which they were extensively purged with N₂ and finally irradiated through a 280 nm cut-off filter for the necessary polymerization time by an array of six UV-B lamps (15W, G15T8E, Ushio, Japan, sample-to-lamp distance: 20 cm). After carrying out the photopolymerization for the desired time, the substrates were extensively rinsed with water.

Immobilization of RGD groups at the surface. Carboxylic acid groups of surface-immobilized PMAA were activated using a solution of 38 mg/ml N-(3-dimethylaminopropyl)-N'-ethylcarbodiimide (EDC, Aldrich) and 6 mg/ml N-hydroxysuccinimide (NHS, Aldrich) in 0,1 M phosphate buffer solution (PBS) at pH 7.4. The PMAA-functionalized gold substrates were immersed in the EDC/NHS solution for 1 h at room temperature. Subsequently, RGD peptide sequences were chemically conjugated by immersing the samples in a 2 mM RGD solution in PBS at pH 7.4 overnight at room temperature. In order to assure the complete removal of physically adsorbed peptides, after the functionalization step, all the samples were rinsed overnight in PBS solution and afterwards extensively with Milli-Q water.

Chain extension experiments. Following the RGD coupling, the substrates were placed back in the quartz flasks that had been used for the photopolymerization, now containing a freshly prepared 1.0 M aqueous solution of MAA. The polymerization and rinsing procedures were continued over a predetermined time period.

Surface characterization. Contact angle measurements were performed on the functionalized surfaces to study the changes in wettability following the various steps of the functionalization process. Static contact angle measurements with water were performed by the sessile drop technique using an optical contact angle device equipped with an electronic syringe unit (OCA15, Dataphysics, Germany). This set-up

was then connected to a charge-coupled device (CCD) video camera. The sessile drop was deposited onto the polished surface of the materials with the syringe, and the drop contour was fitted by the Young-Laplace method. Twenty measurements of each specimen were performed.

Grazing incidence FTIR-spectra (spectral resolution of 8 cm⁻¹, 2048 scans) were obtained using a BIO-RAD FTS575C FTIR spectrometer equipped with a nitrogen-cooled cryogenic mercury telluride detector. Background spectra were obtained by scanning a clean gold substrate functionalized with deuterated octadecylthiol.

Time of flight-secondary ion mass spectroscopy (TOF-SIMS) measurements were performed in order to study at what depth the RGD sequence was buried within the polymer brushes. An IONTOF IV instrument equipped with a dual source column for high current sputtering, including O₂ and Bi, was utilized. The operating conditions included the use of a primary beam of Bi³⁺⁺ at 25 keV with a cycle time of 100 μs, and an O₂ sputtering beam at 500V, 50 nA covering a 300×300 μm² sputtered area. The study was based on the detection of the N-containing fragments.

AFM was used to estimate the height of the brushes in both air and water at pH 7.4. The AFM measurements were carried out in tapping mode using a Dimension D3100 instrument (AFM, Digital Instruments, Veeco, Santa Barbara, CA, USA) equipped with a liquid cell.

The dry thickness of the PMAA brushes was measured using a computer-controlled null ellipsometer (Philips Plasmon) working with a He-Ne laser ($\lambda = 632.8$ nm) at an incidence angle of 70°. The measurements were formed at 22°C and 30% relative humidity. The data were averaged over 100 points at the surface of each sample. For the grafted PMAA layers, a refractive index of 1.475 was used.⁴²

Cell cultures. A human osteoblastic cell line, MG63, was employed for cell culture studies. Cells were plated in culture flasks with Dubelcco's Modified Eagle Medium (DMEM) (Gibco) supplemented with 10% fetal bovine serum, 1% penicillin/streptomycin, 1% L-glutamine and 1% pyruvate (all supplements from Gibco) at 37°C in a humidified atmosphere of 5% CO₂ in air. The culture medium was changed every 2 days. At the fourth passage, cells were rinsed with phosphate buffered saline (PBS) and trypsinized with Trypsin-EDTA (0.25%) in an incubator during 5 min at 37°C. The cells were replated according to the conditions for the lactate dehydrogenase (LDH) test.

Adhesion and proliferation tests. The cell adhesion was investigated by LDH assays (Roche, Germany), which quantified the LDH activity released from the cytosol of cell into the supernatant.⁴³ The LDH activity was determined by means of an enzymatic reaction where the tetrazolium salt was reduced to formazan. The increase in the supernatant LDH activity was directly correlated to the amount of formazan obtained. A polystyrene microplate and bare gold substrates were used as control samples. The functionalized gold substrates were located in a 48-well polystyrene standard culture plate with 300 μ l of medium per well, and an amount of $1 \cdot 10^4$ cells were cultured on the gold substrates in each well. Supplemented DMEM with 1% penicillin/streptomycin, 1% L-glutamine but without pyruvate was used for the LDH essays, and the cell adhesion was studied at 2, 6 and 20 h. Subsequently, the cells were washed with PBS and frozen in 500 μ l of medium. The cells were thawed and frozen three times to guarantee the rupture of the cell membrane. For the assay, 100 μ l of sample were added to 100 μ l of freshly prepared working reagent on a 96-well plate. The plate was incubated at room temperature for 30 min, and absorbance values were read in the spectroscopic microplate reader at 490 nm using a Power-Wave X, Bio-Tek spectrophotometer. The results are expressed as the averaged absorbance levels of three replicates.

A one-way analysis of variance between groups (ANOVA) test was performed to determine the statistical significance ($p < 0.05$) of the differences in the absorbance values.

Immunofluorescence studies. In order to observe the morphology and the distribution of focal points in the cells attached to the studied surfaces, an immunofluorescence study was performed. After 6 h of culturing, the cells were fixed by immersion in 3% paraformaldehyde in 10 mM PBS at room temperature for 15 min. The cells were rinsed with a mixture of 10 mM PBS and 20 mM glycine. Subsequently, the cells were permeabilized with a solution of 0.05% saponine in 10 mM PBS/20 mM glycine. After 10 min, the cells were blocked with a 1% BSA solution in 10 mM PBS/20 mM glycine for 20 min and then incubated with various specific antibodies and dyes (anti-vinculin 1:400; phalloidin-TRITC 1:2000 and Hoechst 1:500) during 1h at 37°C. The anti-vinculin was used to stain focal points, the phalloidin-TRITC was used to stain actin filaments of the cytoskeleton, and Hoechst

was used to dye the cells' nuclei. The samples were rinsed and secondary antibodies were allowed to react during 1 h at 37°C. After rinsing, the samples were mounted on slides with Mowiol mounting media (Calbiochem), and observed in a Leica TCS40 confocal microscope.

5.5 References

- (1) Aota, S.; Nomizu, M.; Yamada, K. M. *J. Biol. Chem.* **1994**, *269*, 24756.
- (2) Petrie, T. A.; Capadona, J. R.; Reyes, C. D.; Garcia, A. J. *Biomaterials* **2006**, *27*, 5459.
- (3) Pierschbacher, M. D.; Ruoslahti, E. *Nature* **1984**, *309*, 30.
- (4) Hersel, U.; Dahmen, C.; Kessler, H. *Biomaterials* **2003**, *24*, 4385.
- (5) Yamada, K. M.; Geiger, B. *Curr. Opin. Cell Biol.* **1997**, *9*, 76.
- (6) Tugulu, S.; Silacci, P.; Stergiopoulos, N.; Klok, H. A. *Biomaterials* **2007**, *28*, 2536.
- (7) Singh, N.; Cui, X. F.; Boland, T.; Husson, S. M. *Biomaterials* **2007**, *28*, 763.
- (8) Li, X.; Wei, X. L.; Husson, S. M. *Biomacromolecules* **2004**, *5*, 869.
- (9) Zhao, B.; Brittain, W. J. *Prog. Polym. Sci.* **2000**, *25*, 677.
- (10) Santer, S.; Kopyshov, A.; Donges, J.; Yang, H. K.; R uhe, J. *Adv. Mater.* **2006**, *18*, 2359.
- (11) Matsuda, T.; Ohya, S. *Langmuir* **2005**, *21*, 9660.
- (12) Magoshi, T.; Ziani-Cherif, H.; Ohya, S.; Nakayama, Y.; Matsuda, T. *Langmuir* **2002**, *18*, 4862.
- (13) Patten, T. E.; Matyjaszewski, K. *Adv. Mater.* **1998**, *10*, 901.
- (14) Otsu, T.; Matsumoto, A. *Microencapsulation - Microgels - Iniferters* **1998**, *136*, 75.
- (15) Ruoslahti, E.; Pierschbacher, M. D. *Cell* **1986**, *44*, 517.
- (16) Giancotti, F. G.; Ruoslahti, E. *Science* **1999**, *285*, 1028.
- (17) Israels, R.; Gersappe, D.; Fasolka, M.; Roberts, V. A.; Balazs, A. C. *Macromolecules* **1994**, *27*, 6679.
- (18) Israels, R.; Leermakers, F. A. M.; Fleer, G. J. *Macromolecules* **1994**, *27*, 3087.
- (19) Israels, R.; Leermakers, F. A. M.; Fleer, G. J.; Zhulina, E. B. *Macromolecules* **1994**, *27*, 3249.
- (20) Mei, Y.; Wu, T.; Xu, C.; Langenbach, K. J.; Elliott, J. T.; Vogt, B. D.; Beers, K. L.; Amis, E. J.; Washburn, N. R. *Langmuir* **2005**, *21*, 12309.
- (21) Harris, B. P.; Kutty, J. K.; Fritz, E. W.; Webb, C. K.; Burg, K. J. L.; Metters, A. T. *Langmuir* **2006**, *22*, 4467.

- (22) Zhu, Y. B.; Gao, C. Y.; Guan, J. J.; Shen, J. C. *J. Biomed. Mater. Res. A* **2003**, *67A*, 1367.
- (23) Guan, J. J.; Gao, C. Y.; Feng, L. X.; Shen, J. C. *J. Appl. Polym. Sci.* **2000**, *77*, 2505.
- (24) Lin, Y. S.; Wang, S. S.; Chung, T. W.; Wang, Y. H.; Chiou, S. H.; Hsu, J. J.; Chou, N. K.; Hsieh, T. H.; Chu, S. H. *Artificial Organs* **2001**, *25*, 617.
- (25) Gumusderelioglu, M.; Muftuoglu, O. E.; Karakecili, A. E. G. *React. Funct. Polym.* **2004**, *58*, 149.
- (26) Biesalski, M.; Johannsmann, D.; Rühle, J. *J. Chem. Phys.* **2002**, *117*, 4988.
- (27) Bao, Z. Y.; Bruening, M. L.; Baker, G. L. *Macromolecules* **2006**, *39*, 5251.
- (28) Jordan, R.; Ulman, A.; Kang, J. F.; Rafailovich, M. H.; Sokolov, J. *J. Am. Chem. Soc.* **1999**, *121*, 1016.
- (29) Rahane, S. B. F., A.; Metters, A.T.; Kibley, S. M. II *Adv. Funct. Mater.* **2008**, *18*, 1232.
- (30) Hern, D. L.; Hubbell, J. A. *J. Biomed. Mater. Res.* **1998**, *39*, 266.
- (31) Cavalcanti-Adam, E. A.; Micoulet, A.; Blummel, J.; Auernheimer, J.; Kessler, H.; Spatz, J. P. *Eur. J. Cell. Biol.* **2006**, *85*, 219.
- (32) Yokoyama, H.; Kramer, E. J.; Rafailovich, M. H.; Sokolov, J.; Schwarz, S. A. *Macromolecules* **1998**, *31*, 8826.
- (33) Yokoyama, H.; Mates, T. E.; Kramer, E. J. *Macromolecules* **2000**, *33*, 1888.
- (34) Belu, A. M.; Graham, D. J.; Castner, D. G. *Biomaterials* **2003**, *24*, 3635.
- (35) Poulin, S.; Durrieu, M. C.; Polizu, S.; Yahia, L. H. *Appl. Surf. Sci.* **2006**, *252*, 6738.
- (36) Michel, R.; Castner, D. G. *Surf. Interface. Anal.* **2006**, *38*, 1386.
- (37) Mahoney, C. M.; Yu, J. X.; Fahey, A.; Gardella, J. A. *Appl. Surf. Sci.* **2006**, *252*, 6609.
- (38) Zhang, Z. P.; Yoo, R.; Wells, M.; Beebe, T. P.; Biran, R.; Tresco, P. *Biomaterials* **2005**, *26*, 47.
- (39) Zalm, P. C. *Mikrochim. Acta* **2000**, *132*, 243.
- (40) van Duren, J. K. J.; Yang, X. N.; Loos, J.; Bulle-Lieuwma, C. W. T.; Sieval, A. B.; Hummelen, J. C.; Janssen, R. A. J. *Adv. Funct. Mater.* **2004**, *14*, 425.
- (41) In this study the presence of dithiocarbamate-based chains ends was not taken into consideration even if it could have some influence on the composition of the polymer-liquid interface and subsequently on cell-adhesion.
- (42) Anon, J. *Spe Journal* **1966**, *22*, 343.
- (43) Macnair, R.; Rodgers, E. H.; Macdonald, C.; Wykman, A.; Goldie, I.; Grant, M. H. *J. Mater. Sci.-Mater. Med.* **1997**, *8*, 105.

Chapter 6

Poly(hydroxyethyl methacrylate)-Based Brush Gels: Synthesis, Characterization and Use for the Fabrication of Polymer/Metal Nano-Particles Hybrid Films*

In this Chapter the preparation of new functional brush-gel platforms is described. Poly(hydroxyethyl methacrylate)(PHEMA)-based (PHEMA) freely grafted and crosslinked brushes were grown from self-assembled monolayers (SAMs) of initiator to gold substrates using surface-initiated atom-transfer radical polymerization (ATRP). Following their preparation, the brush structures were functionalized with succinic anhydride in order to introduce ionizable acidic functionalities, which made these layers respond to external pH by varying their swelling properties. Freely grafted brushes and brush-gels were characterized with Fourier-transform infrared spectroscopy (FTIR) in order to monitor the composition of the films following every preparation step.

In order to study the influence of crosslinking on morphology, swelling and mechanical properties of the prepared brush layers, atomic force microscopy (AFM) imaging and AFM-based mechanical compression analysis were performed. The results obtained show a clear relationship between the relative amount of crosslinking agent used during the preparation of the films, their degree of swelling at equilibrium and their resistance to compression. In addition, also the surface morphology of the brush layers was influenced by the presence of a brush network if compared to a freely grafted brush.

* Part of this Chapter was reported in: Benetti, E.M.; Sui, X.F.; Zapotoczny, S.; Vancso, G.J. submitted

In the second part of this Chapter the prepared brush layers are shown to act as effective matrixes for the controlled synthesis of silver nano-particles. Also in this case, the amount of crosslinking is demonstrated to influence the growth of the metallic clusters inside the brushes. AFM, UV-absorption spectroscopy and high-resolution scanning electron microscopy (HR-SEM) were used to characterize the hybrid films. The results obtained from these techniques demonstrate how the size, the size distribution and the shape of the metallic nano-particles was controlled as a function of the type of brush structure employed as support.

6.1 Introduction

As it was demonstrated in the previous Chapters, surface-initiated controlled radical polymerization (CR-SIP) represents a powerful tool for the preparation of “smart” polymeric platforms. The capability to control the film thickness, to tune the composition and possibly to pattern functional polymer grafts across the length-scales demonstrated the versatility of this method and opened the way for a vast variety of applications.

As an example, surface fabrication by SIP was successfully employed for the synthesis of bio-interfaces with tunable characteristics^{1,2} or, alternatively, for the preparation of polymer/metal hybrid systems.³⁻⁶ In both these cases functional polymer brushes were used as starting material for the subsequent functionalization/modification of the precursor films.

Either in the designing of new polymeric coatings as biomaterials or as hybrid layers for electronic and optical applications, the use of brush-films in the form of gels would open new avenues for applications. Polymeric gels are characterized by mechanical and swelling properties which depend on the chemical composition of the polymers as well as on the relative amount of crosslinks (e.g. crosslink density).⁷ These materials can be deposited on surfaces in form of thin layers but, unfortunately, the stability of the so-formed films might be affected by the weak interaction with the underlying substrate and several properties such as thickness and morphology could not be a-priori determined by employing the usual physical deposition protocols.^{8,9} These relevant drawbacks could indeed be easily overcome

by using densely and robustly grafted polymer brushes as constituents for the synthesis of surface-immobilized gels.

The in-situ synthesis of brush-based gels by SIP with controlled characteristics has represented up to now a quite unexplored synthetic path. As a first attempt, crosslinked grafted systems were synthesized by Baker et al. using controlled surface-initiated atom transfer radical polymerization (ATRP).^{10,11} These films showed high density of crosslinks confirmed by a marked decrease in the swelling ratio when the films were immersed in a good solvent if compared to the corresponding freely grafted brush. It should be mentioned that in the preparation of these brush-gels only bi-functional monomers were used during the polymerization process (e.g. dimethacrylates), thus control over the characteristics of the network was not accomplished.

In a second report by Huck et al.¹² poly(methyl methacrylate) (PMMA) was grafted by ATRP in the presence of a very little amount of ethylene glycol dimethacrylate (EGDMA) (MMA:EGDMA = 1000:1) thus forming a grafted polymer network. The use of higher amounts of crosslinking agents in this case was reported as unfeasible due to very high surface roughening following polymerization.¹²

Thus, the controlled synthesis of brush gels, in-situ (not considering post-polymerization crosslinking^{13,14}), represents a challenging task. Not only the problems due to physisorption of insoluble material formed in solution during the grafting process must be considered, but also the very high mechanical stress introduced in the structure of the films by increasing the crosslink density should be taken into account.¹⁵

The successful preparation of brush gels accomplished by finely tuning the properties of the layers and by varying the characteristics of the network, would allow one to obtain polymeric coatings which possess the peculiar characteristics of polymer brushes (high density of chains/functionalities), and in addition feature tunable swelling and mechanical properties.

In this Chapter we report on the synthesis and characterization of poly(hydroxyethyl methacrylate) (PHEMA)-based brush gels, synthesized by surface-initiated ATRP.^{16,17} Poly(ethylene glycol) dimethacrylate (PEGDMA) was used as crosslinking agent and its concentration was varied in the polymerization process in order to tune the characteristics of the grafted network. Following SIP, the so prepared films were functionalized with succinic anhydride, which, by reacting with

the hydroxyethyl units of the polymer, introduced ionizable carboxylic acid moieties inside the brush structure.

The morphological, the mechanical (mechanical compression) and the swelling properties of the brush films synthesized were studied by atomic force microscopy (AFM) and they were shown to be dependent on the relative amount of PEGDMA used during the preparation. These characteristics were in every case compared to the corresponding freely grafted PHEMA-based brush.

Due to the presence of carboxylic acid moieties in the brush architecture, these grafted gels were demonstrated to behave similarly to grafted weak polyacid brushes.^{18,19} Thus, the swelling properties of all the prepared films were also analyzed in aqueous solutions presenting different pH, demonstrating a sharp pH-response across a narrow range of values.

In the second part of this Chapter the use of PHEMA-based brush-gels as nano-reactors for the controlled synthesis of silver nano-particles (Ag-NPs) is reported.

Polymeric materials such as layer-by-layer assemblies^{20,21} or micro-gels²² were widely used for the controlled synthesis of metallic nano-structures. In these instances, the size-related characteristics of the nano-clusters could be adjusted by either varying the experimental conditions during the reduction processes²³ or by previously tuning the properties of the polymeric supports.²⁴ The present study represents a first successful attempt to control the formation of metallic nano-particles by changing the inner structure of a flat brush film.

Ag-NPs were synthesized inside the brush structures by chemical reduction from the corresponding metallic salts using diluted NaBH₄ aqueous solutions as reducing agent. The size, the morphology and the optical properties of Ag-NPs were respectively characterized with AFM and UV-absorption spectroscopy. The mentioned properties exhibited, in all cases, marked differences as a function of the type of brush structure used as starting support material.

In summary, the novel brush-gel structures reported in this Chapter were proven as very promising starting materials for the fabrication of functional platforms with tunable properties. They were characterized by a relatively easy preparation procedure and, in addition, they presented pH-responsive behavior. Their use as nano-reactors for the synthesis of Ag-NPs allowed the size and the

properties of the metallic clusters to be precisely tuned as a function of the characteristics of the brush platform employed.

We believe that the synthetic methods proposed here could open several possible fabrication paths in order to obtain a new class of brush based films which could find a wide range of applications in biology and electronics. In addition, the intrinsic versatility peculiar of the SIP processes could easily allow the synthesis of such hybrid layers to be carried out inside micro-fluidic devices, thus allowing the preparation of new catalytic nano-systems.

6.2 Results and Discussion

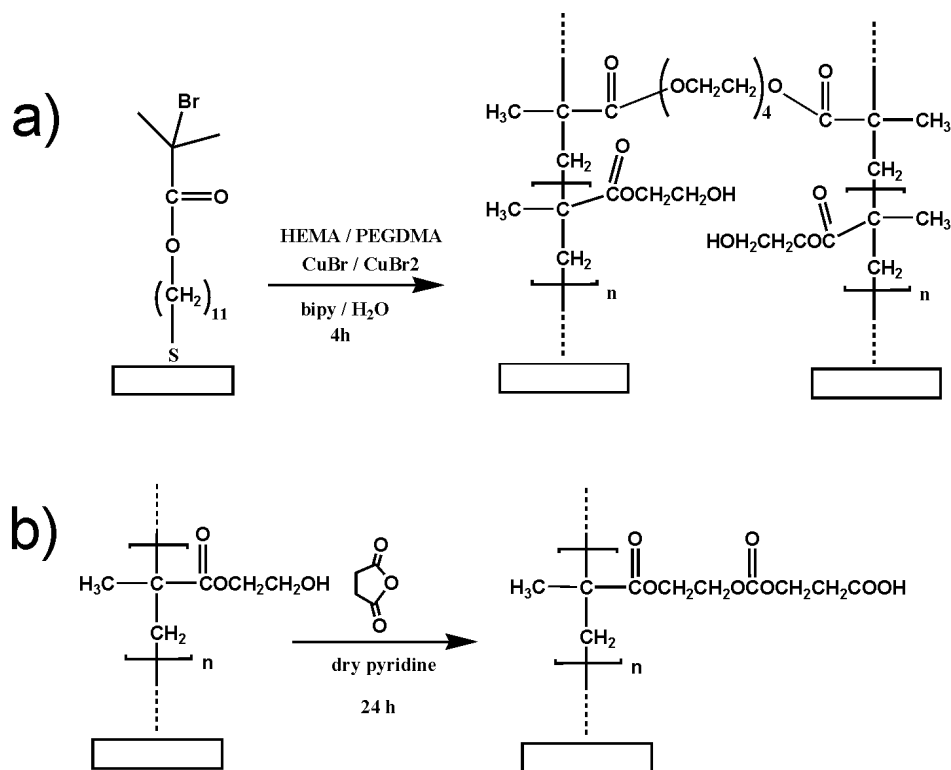
6.2.1 PHEMA-Based Gels: Preparation and Characterization

PHEMA brushes and PHEMA-based brush-gels were grafted using aqueous ATRP from self-assembled monolayers of thiol initiators deposited on gold surfaces (see Scheme 6.1a and experimental section for details). The use of surface-initiated ATRP in water was previously shown to allow the growth of relatively thick films during a short reaction time.²⁵ In this report three different films were grown, namely PHEMA brush (named PHEMA), PHEMA brush-gel grafted in the presence of 1% in volume of PEGDMA (named as PHEMA1%) and finally PHEMA brush-gel grafted with 2% PEGDMA (PHEMA2%).

The thickening rate following the polymerization was measured by ellipsometry and it was reported in Figure 6.1 for all the three samples prepared. As it can be seen, the thickness of the films initially increases very fast, reaching, after 1 hour of reaction, a maximum value between 60 and 70 nm. Following this expected accelerated behavior, the polymerization slowed down, presumably because of termination reactions.^{25,26} It should further be mentioned that the growth rates showed very similar trends for all the films synthesized demonstrating that the presence of PEGDMA did not influence the kinetics of the grafting process.¹²

The chemical composition of the grafted films was first characterized by FTIR. In Figure 6.2a the spectrum recorded for PHEMA brush presents the characteristic C=O stretching band at 1730 cm⁻¹ and a broad shoulder between 3000 and 3500 cm⁻¹ corroborating the presence of the HO- groups of the hydroxyethyl methacrylate

monomer units. The FTIR spectra recorded for PHEMA1% and PHEMA2% show no relevant differences if compared to the spectra of PHEMA and thus they were not reported in Figure 6.2 for clarity.



Scheme 6.1. Step-wise preparation of PHEMA-based brush and brush-gels. a) Surface-initiated ATRP from SAMs of thiol initiators on gold; b) post-functionalization of the PHEMA-based brush layers by reaction with succinic anhydride.

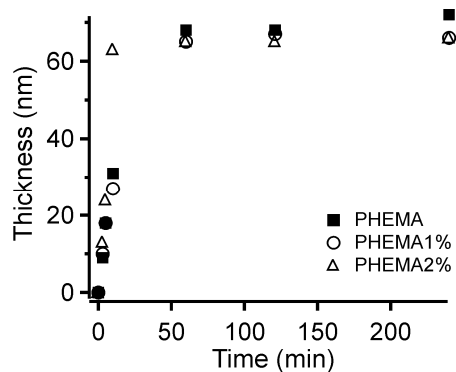


Figure 6.1. Ellipsometric thickness of PHEMA brushes (squares), PHEMA1% brush-gels (circles) and PHEMA2% brush-gels (triangles) measured as a function of polymerization time.

Representative samples for the three different brush structures were subsequently reacted with succinic anhydride in order to introduce carboxylic acid moieties along the polymer backbones. PHEMA, PHEMA1% and PHEMA2% layers presenting ellipsometric thicknesses of 65 ± 4 , 63 ± 2 and 59 ± 5 nm, respectively, were incubated for 20 hours in a dry pyridine solution of succinic anhydride. Following the reaction, the thickness (measured by ellipsometry) was shown to increase by $30 \pm 4\%$ for all the analyzed films due to the expected volume increase of the monomer units constituting the brushes¹⁸ (following reaction the samples were named as PHEMA-SUC.ANHY, PHEMA1%-SUC.ANHY and PHEMA2%-SUC.ANHY, respectively).

FTIR spectroscopy was used to prove the presence of COOH groups inside the brush architectures following the reaction. As it can be seen in Figure 6.2b, in the case of PHEMA brushes, following succinic anhydride functionalization the HO-band completely disappeared and a clear signal related to the stretching of the COO- functionalities appeared at 1580 cm^{-1} .

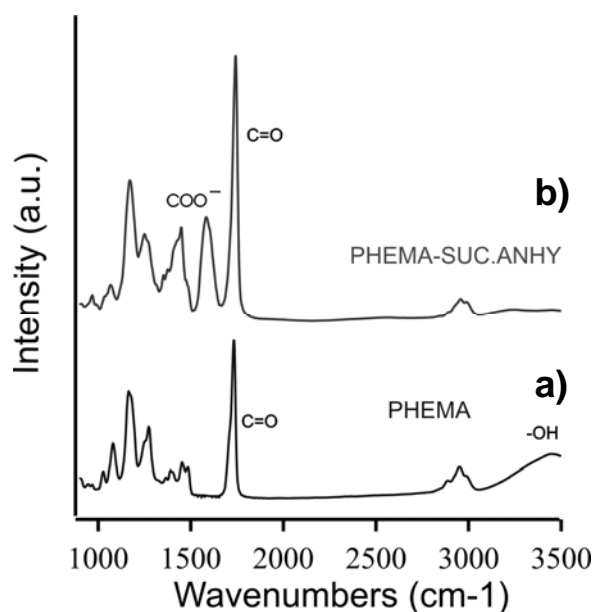


Figure 6.2. FTIR spectra of a) PHEMA brush film and b) PHEMA-SUC.ANHY film following the reaction with succinic anhydride.

In order to confirm the presence of a polymeric network in the case of PHEMA1%-SUC.ANHY and PHEMA2%-SUC.ANHY, swelling experiments were performed and compared to the results obtained for the freely grafted brush PHEMA-SUC.ANHY.

Measuring the swelling equilibrium in a good solvent and deriving, via conventional gravimetric analysis, the solvent uptake with respect to the dry gel represent a standard procedure to evaluate the crosslink density and other characteristics of a network.²⁷⁻³⁰ In the case of nano-thin brush films this procedure was unfeasible due to the lack of sufficiently precise analytical methods. Thus, in order to estimate the degree of swelling for the brush structures studied, contact mode AFM (CM-AFM) was performed on micro-patterned films prepared following the same synthetic paths used to synthesize the continuous layers (see experimental section). Following this procedure, the volume occupied by a brush grafted form an area of 25 μm^2 was measured in the dry state by bearing analysis of the AFM images and subsequently compared to the volume of the same polymeric pattern swollen in a good solvent at equilibrium.

Due to the presence of ionizable COOH groups, ethanol was chosen as a solvent for these experiments instead of water thus avoiding pH-related changes in the swelling of the grafted films (*vide infra*).

PHEMA-SUC.ANHY showed an increase in volume by 53% when immersed in ethanol as expected inferring the good solubility of the brush in such solvent. Interestingly, for the brush films prepared by adding 1 and 2% of PEGDMA the degree of swelling markedly decreased. In fact, PHEMA1%-SUC.ANHY and PHEMA2%-SUC.ANHY exhibited a volume increase by 36% and 29%, respectively, when immersed in ethanol. This result confirmed the formation of networks inside the brush structure which could not swell profusely as a free brush due to the presence of crosslinks.

Due to the presence of physical constraints like crosslinkings inside the brush structure, also the mechanical properties of the brush-gels should differ from the corresponding free brushes. To evaluate this, the same micro-patterned samples immersed in ethanol were analyzed by CM-AFM recording the volume occupied by the polymeric structures by scanning the features at different loads (see also Chapter 3). The compression values obtained exhibit a decrease of volume (%) of the brushes

as a function of the load applied and they were compared for the three different samples in Figure 6.3.

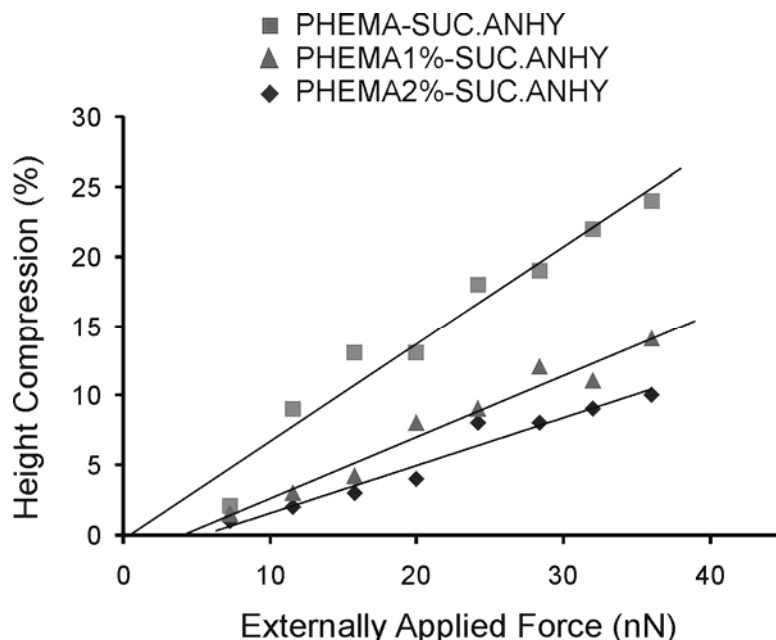


Figure 6.3. Height compression (%) values expressed as the decrease in volume of brush patterns measured with CM-AFM as a function of the externally applied load (nN). The graph depicts the data calculated for PHEMA-SUC.ANHY (squares), PHEMA1%-SUC.ANHY (triangles) and PHEMA2%-SUC.ANHY (rhombs).

The compression values for these systems were fitted by a linear relationship to estimate trends in the brush compressibilities. As expected, the PHEMA-SUC.ANHY brush showed the highest slope (e.g. highest compressibility) and PHEMA2%-SUC.ANHY (the lowest compressibility).

It is thus possible to calculate the compressibility³¹ (k) for each brush structure which results 0.7, 0.4 and 0.3 nN^{-1} for PHEMA-, PHEMA1%- and PHEMA2%-SUC.ANHY, respectively. This observed trend can be interpreted by the decrease of compressibility with increasing network density.

We finally note that the linear fits yielded positive intercept values for the measured vertical force. This we tentatively interpret by assuming an entropy repulsion contribution by the free chains resulting in a force component which decreases the effective normal force at the externally applied load experimented by the brush

(compare also the repulsion towards compression by swollen PNIPAM brushes determined by AFM force measurements described in Chapter 4).

Both swelling and mechanical properties of the brush layers were thus shown to be dependent on the amount of crosslinking agent used during their preparation.

In order to evaluate whether the presence of a network influenced the morphology of the exposed air-brush interfaces we imaged the three different films by TM-AFM in air (Figure 6.4).

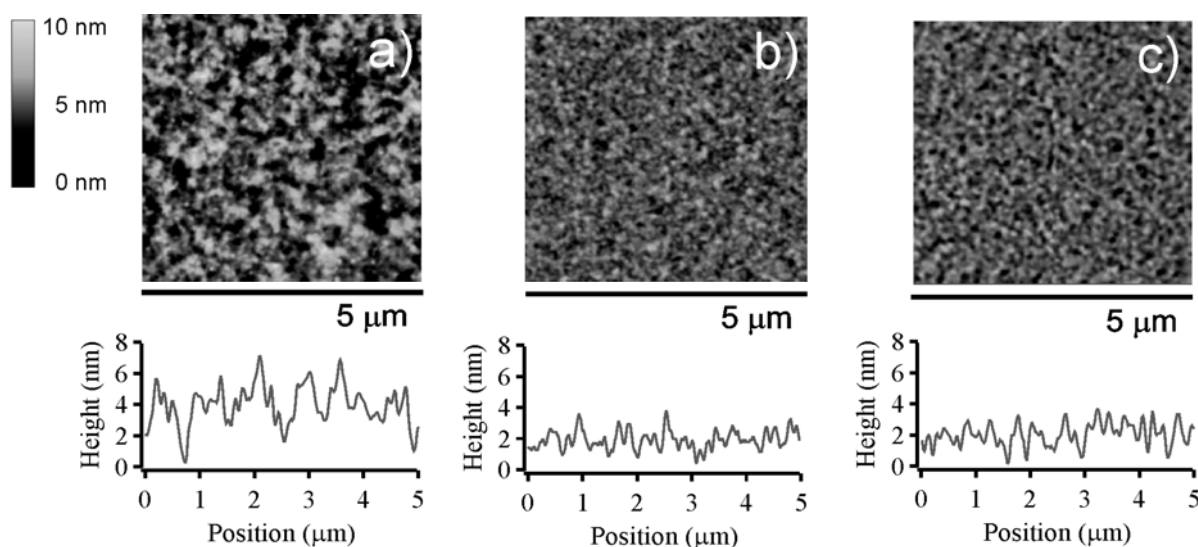


Figure 6.4. TM-AFM micrographs depicting height images of representative brush surfaces recorded for a) PHEMA-SUC.ANHY, b) PHEMA1%-SUC.ANHY and c) PHEMA2%-SUC.ANHY .

By comparing Figure 6.4a with 6.4b and c it can be seen that PHEMA-SUC.ANHY brushes exhibited higher surface roughness if compared to the brush-gels. The average root-mean-square roughness values (RMS measured over $5 \times 5 \mu\text{m}^2$ areas) were found 1.1 ± 0.3 nm for PHEMA-SUC.ANHY while 0.6 ± 0.1 nm and 0.6 ± 0.2 nm in the cases of PHEMA1%- and PHEMA2%-SUC.ANHY respectively.

Not only the RMS roughness values presented differences when the free brush was compared with the brush-gels but also the nano-morphological characteristics were influenced by the networking of the grafted chains. These differences are highlighted in Figure 6.5 and 6.6, where high-resolution TM-AFM micrographs are

displayed for PHEMA- and PHEMA2%-SUC.ANHY, respectively. By observing the two different brush surface morphologies and by comparing the cross sectional profiles the presence of polymer aggregates which extended out of the film surface can be noticed for the free brush while they are much less pronounced for the brush-gel.

We believe these structures were due to polymer chain aggregates near the brush surface. Their presence is likely related to the very fast grafting process when the polymerization was carried out in fully aqueous environment. We further speculate that the absence of such morphology on the brush-gels' surfaces might be due to the physical constraints introduced between the polymer chains by the crosslinks allowing a more uniform growth of the film.

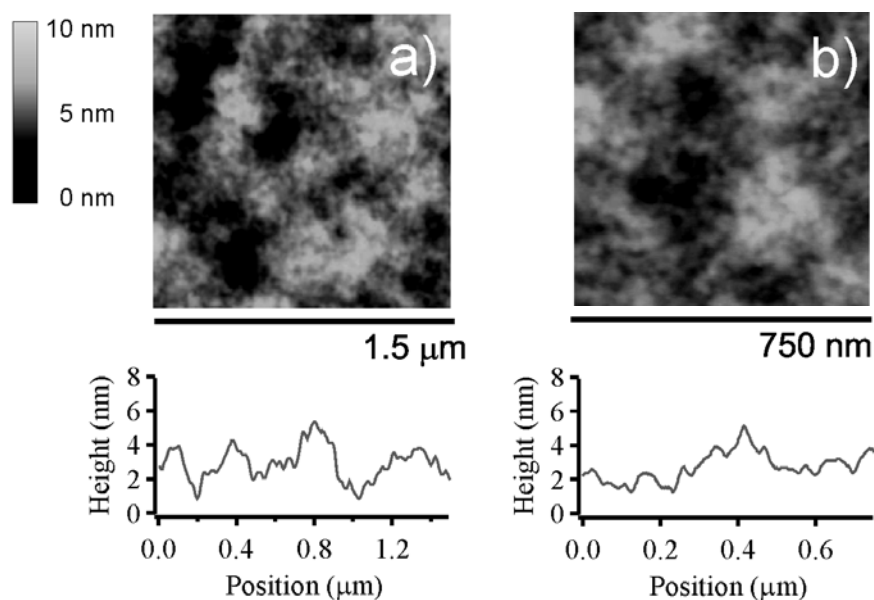


Figure 6.5. High-resolution TM-AFM micrographs displaying height images of brush surfaces of PHEMA-SUC.ANHY.

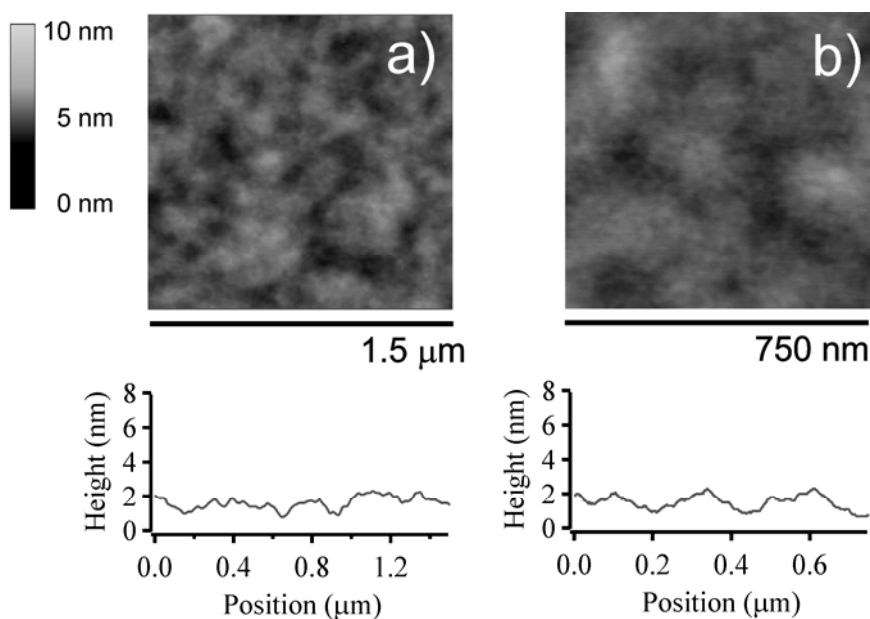


Figure 6.6. High-resolution TM-AFM micrographs displaying height images of brush surfaces of PHEMA2%-SUC.ANHY.

6.2.2 pH-Responsive Behavior of PHEMA-Based Gels

As it was already anticipated, the presence of carboxylic acid functionalities inside the brush structure made the swelling properties of these layers pH-dependent when they are immersed in aqueous media. This property is a direct consequence of the variation of charge density of weak polyacid brushes as a function of the external pH.¹⁹

In this study the pH-responsive behavior of the films was evaluated by recording the volume occupied by micro-patterned grafts immersed in water at different pH $[V(\text{pH})]$ with CM-AFM and by calculating the swelling ratio $[(V(\text{pH})/V(\text{dry}))]$ of the brushes at every measurement point with respect to their corresponding dry volume $[V(\text{dry})]$ (Figure 6.7).

As it was depicted in Figure 6.7 for both the free brush and the grafted gels no important swelling was recorded below pH 7.0. Between pH 7.0 and 9.0 a sharp transition took place and the volume of the polymer grafts increased markedly for all the samples studied as a consequence of the deprotonation of the COOH moieties. Thus swelling showed an effective pKa value around ~ 8 . We attributed the shift of

the expected pKa value (which has a value of around 5.5 for the bulk solution) to hydrogen bonding interactions between the COOH groups and the ester functionalities present in every monomer unit following functionalization with succinic anhydride and also partly due to confinement stabilizing effects. These interactions presumably affected the total driving force necessary to deprotonate the carboxylic acid moieties of the polymer and thus induced a shift of the pH values at which the brush accumulated charges and swelled.

In addition, the calculated swelling ratios at the highest pH measured reached values around 4 for the brush-gels while slightly higher values (up to 5) characterized the free brush films. It should be mentioned that this difference, even if not very important, is probably due to conformational rearrangements which take place in the case of stimuli-responsive (freely grafted) polymer brushes.

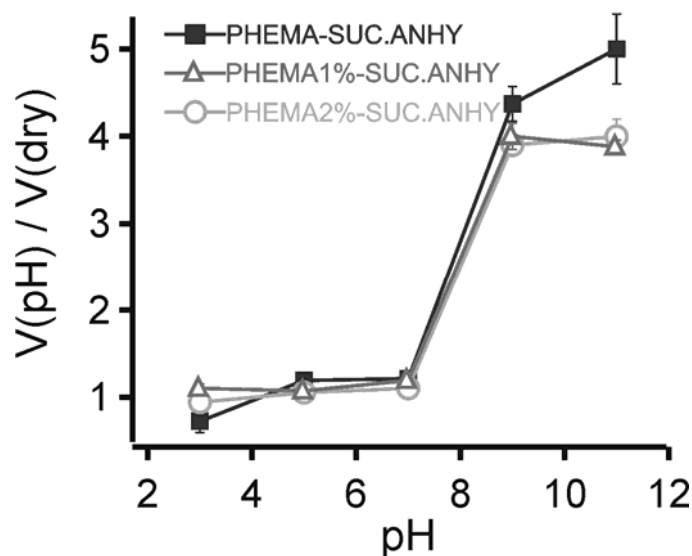


Figure 6.7. Swelling ratio calculated for PHEMA- (squares), PHEMA1%- (triangles) and PHEMA2%-SUC.ANHY (circles) expressed as a function of external pH.

These phenomena were observed to influence the sharpness of temperature- and pH-driven thermodynamical transitions across the lower critical solution temperatures (LCST) and the pKa values of the corresponding polymers respectively.^{19,32-34} In the present case, the water uptake for the free brush increased continuously over a wider range of pH values if compared to the corresponding gels demonstrating the influence of the brush architecture on the stimulus-response of the whole film.

6.2.3 Controlled Synthesis of Silver Nano-Particles Using PHEMA-Based Gels

The brush films prepared and characterized as previously described in this Chapter were subsequently used as nano-reactors for the synthesis of silver nanoparticles. The preparation of the metal/polymer brush hybrid films followed the well known procedure³⁵⁻³⁹ using AgNO_3 as a source of silver ions and NaBH_4 as reducing agent (see experimental section for details). Following overnight incubation in dilute aqueous solutions containing Ag(I) , PHEMA-, PHEMA1%- and PHEMA2%-SUC.ANHY films were immersed in the reducing solutions and finally extensively rinsed with milli-q water. The presence of carboxylate groups inside the brushes allowed the complexation of Ag(I) ions along the grafted chains, which were subsequently reduced to metallic silver by NaBH_4 .

FTIR spectra were recorded before and after the reduction in the case of PHEMA-SUC.ANHY samples and they were reported in Figure 6.7a and b respectively (no relevant differences were observed in the FTIR spectra of PHEMA1%- and PHEMA2%-SUC.ANHY). Following incubation in Ag(I) solution and before the reduction (Figure 6.7a) the stretching signal related to the Ag(I) /carboxylate complex was present at 1550 cm^{-1} . After the reaction with NaBH_4 (Figure 6.7b) this band disappeared due to the reduction of the COO^- groups to COOH and the concomitant formation of Ag(0) clusters inside the brush structure.

In order to confirm the presence of Ag NPs inside the brush films UV-absorption spectroscopy and TM-AFM analysis were performed on the three different types of samples studied.

Figure 6.8 displays the UV-absorption spectra for PHEMA-, PHEMA1%- and PHEMA2%-SUC.ANHY following the reaction with NaBH_4 . In all the three cases absorption bands typical of Ag NPs were found. In the case of PHEMA2%-SUC.ANHY an intense plasmon absorption band emerged with maximum at 410 nm. This peak was typical for Ag colloids and its almost symmetrical profile suggested the nano-particles are well-dispersed and spherical.^{40,41} For PHEMA- and PHEMA1%-SUC.ANHY, instead, the plasmon band showed a maximum at 450 nm. Such a red shift of this peak might indicate an increase of the particles' diameter or partial aggregation of the metallic clusters.^{42,43} At the same time, in the case of these two samples, an additional absorption band appeared at 350 nm. The latter signal

showed very high intensity for Ag nano-particles formed inside the PHEMA-SUCC.ANHY films and it was less evident in the case of PHEMA1%-SUCC.ANHY. The absorption profiles characteristic of the Ag colloids formed in these brush films thus suggested the presence of larger or partially aggregated particles which were also characterized by anisotropic shape which induced the appearance of multiple peaks in the recorded spectra.⁴⁴

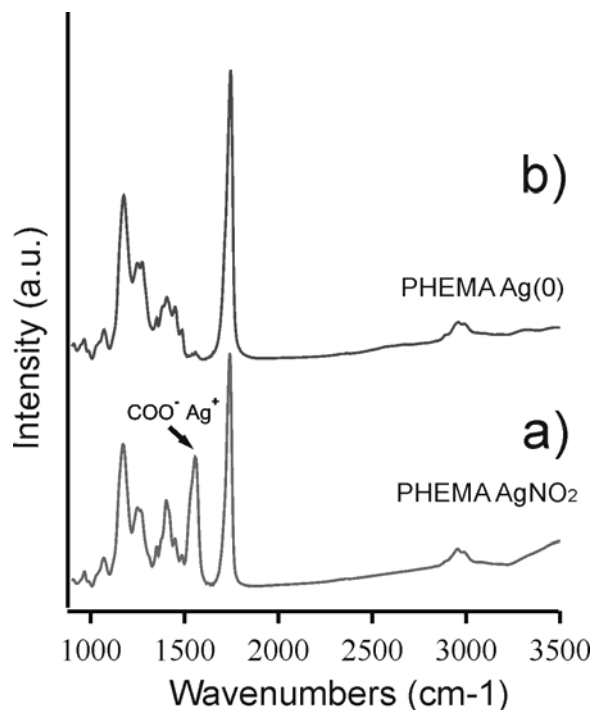


Figure 6.7. FTIR spectra recorded for PHEMA-SUC.ANHY brush films following incubation in AgNO₂ solution a) and after Ag-NPs formation b).

As it was anticipated, in order to better visualize the characteristics of the Ag-NPs formed in the brush films, high-resolution TM-AFM was used to analyze the films' surfaces. In Figure 6.9 TM-AFM micrographs for the three different films following the formation of Ag nano-particles are shown.

In the case of PHEMA2%-SUCC.ANHY well dispersed spherical particles with an average diameter of 13 ± 2 nm were observed (Figure 6.9c), thus confirming the results drawn from the UV-absorption spectrum obtained for this film. The Ag colloids formed in PHEMA- and PHEMA1%-SUC.ANHY showed bigger diameters, 15 ± 3 and 20 ± 4 nm respectively. In addition, very big metallic clusters with different

shapes can be recognized at the brush surfaces hence corroborating the observations derived from the UV-absorption spectra recorded for these two samples.

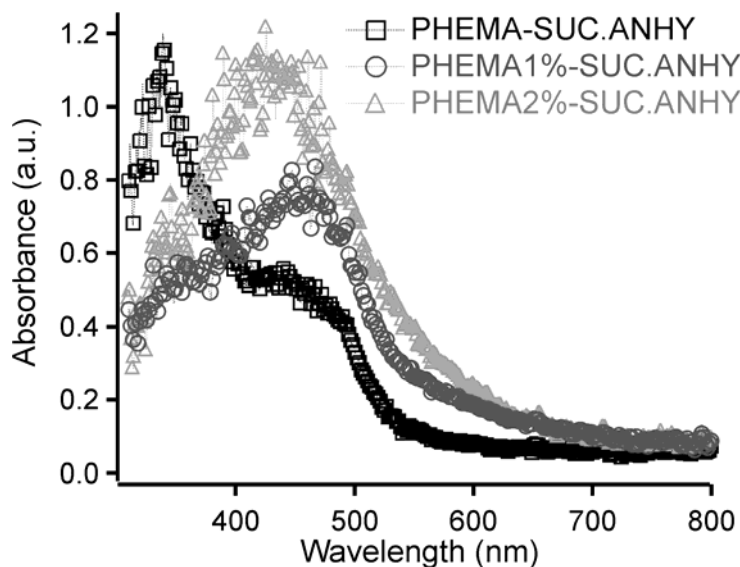


Figure 6.8. UV-absorption spectra recorded for PHEMA- (squares), PHEMA1%- (circles) and PHEMA2%-SUC.ANHY (triangles) following the reduction of Ag-NPs.

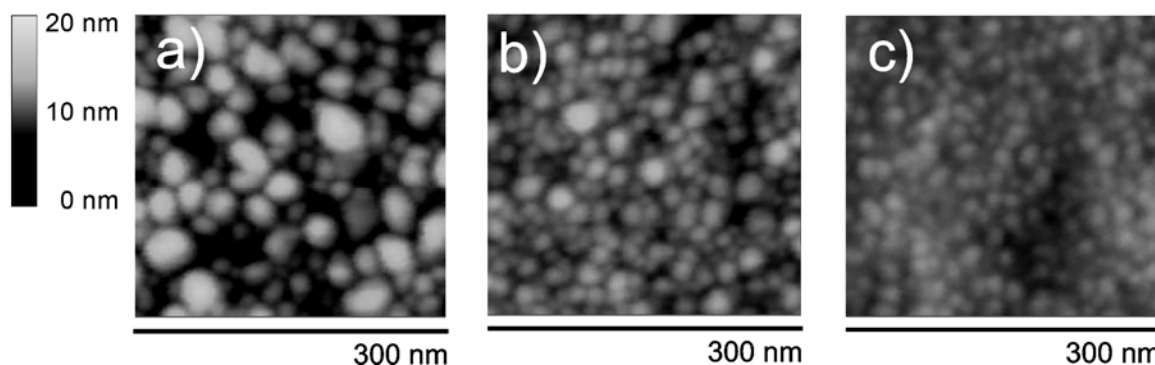


Figure 6.9. TM-AFM micrographs displaying brush and brush-gel surfaces following the formation of Ag-NPs. a) PHEMA-SUC.ANHY; b) PHEMA1%-SUC.ANHY; c) PHEMA2%-SUC.ANHY.

The size distribution calculated from the AFM micrographs showed also interesting aspects. As it can be seen in Figure 6.10, the size distribution presented a broad profile in the case of Ag-NPs formed in the free brush (Figure 6.10a) while it

became narrower when the brush gels were used as supports for the synthesis of the colloids (Figure 6.10b and c).

In order to evaluate the distribution of the particles inside the brush structure and to demonstrate their presence at the brush interface as well as inside the brush structure HR-SEM was used. In Figure 6.11 the HR-SEM picture depicts a cross sectioned PHEMA-SUC.ANHY film after the formation of Ag-NPs. The metallic nano-structures were uniformly dispersed across the film thus proving that the growth of the colloids took place inside the brush film.

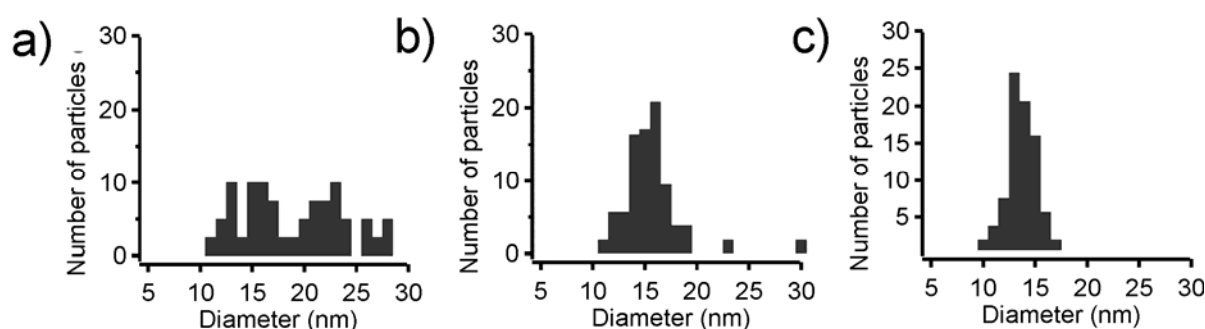


Figure 6.10. Size distribution calculated from TM-AFM images for Ag NPs-modified PHEMA-based brush layers. The histograms are reported for a) PHEMA-SUC.ANHY, b) PHEMA1%-SUC.ANHY and c) PHEMA2%-SUC.ANHY respectively.

In summary, the prepared brush layers were successfully used as supports for the synthesis of Ag-NPs. The procedure reported here allowed the preparation of uniform metal/polymer brush hybrid films with controlled properties. The characteristics of the precursor brush films were shown to influence the size, the shape and the size-distribution of the Ag-NPs formed. By increasing the relative amount of PEGDMA during the preparation of the brush-gels and thus their degree of crosslinking, smaller and more uniformly dispersed particles were formed. This phenomenon was presumably due to a gate effect which was already observed in the case of micro-gels²⁴ and which influenced nucleation and growth of the nano-particles.

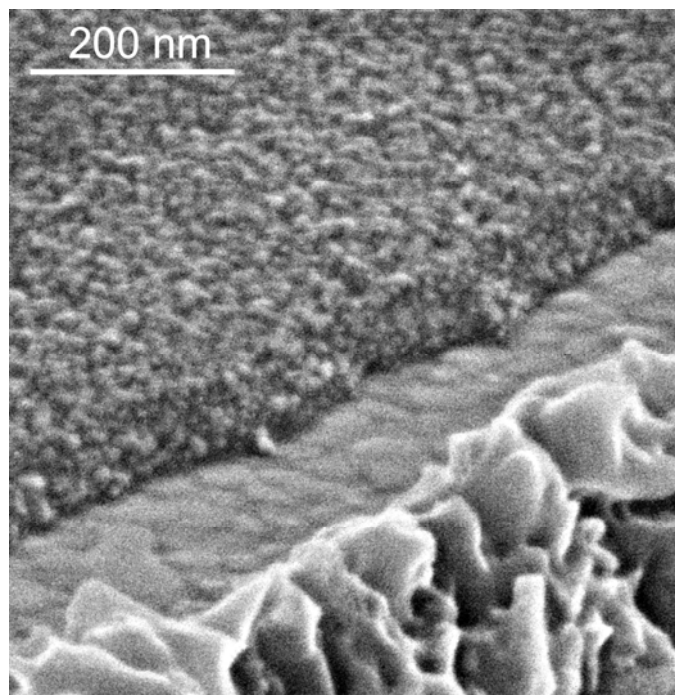


Figure 6.11. High-resolution scanning electron microscopy picture depicting the surface and the cross section of Ag NPs-modified PHEMA-SUC.ANHY brush film.

6.3 Conclusions

In this Chapter the preparation and characterization of PHEMA-based brush-gels and their application as successful supports for the controlled synthesis of silver nano-particles was reported.

The swelling behavior, the mechanical and the morphological properties of the prepared films were demonstrated to be dependent on the amount of crosslinking agent used for their preparation and they were compared to the case of the corresponding freely grafted brush. Namely, the solvent uptake at equilibrium markedly decreased for brush-gels if compared to the free brush. In addition, AFM compression tests demonstrated the grafted networks to show enhanced mechanical resistance towards compression with respect to the same brushes without lateral bindings. Also the surface morphology of the films was influenced by crosslinking. The latter phenomenon caused the brush gels' surface being more uniform if compared to the free brush.

The presence of ionizable carboxylic acid functionalities in the synthesized brush films made them respond to the external pH by varying their swelling properties. The swelling ratio was shown to undergo a sharp transition around pH 8 for all the samples.

In the second part of this Chapter the use brush and brush-gel films as supports for the controlled preparation of silver nano-particles was described. AFM measurements and UV-absorption spectroscopy showed the particles synthesized inside the brush gels being smaller, more narrowly distributed and with a more isotropic shape if compared to the case when the freely grafted brush was used as support.

6.4 Experimental

Preparation of the brush films. CuBr₂ was purchased from Sigma and used as received. CuBr was purified by washing with glacial acetic acid and, after filtration, by rinsing with ethanol and acetone. Hydroxyethyl methacrylate (HEMA) was purchased from Sigma and subsequently purified from inhibitors by high vacuum distillation and stored at -26°C before use. Bipyridine (bipy) and succinic anhydride were purchased from Fluka and used as received. Pyridine was purchased from Merck and distilled over calcium hydride before use. The thiol based ATRP initiator was synthesized according to the reported procedure.⁴⁵ In order to prepare the initiator SAMs-functionalized substrates gold samples with areas of 1 cm² (40 nm thick Au layer, Ssens BV, Hengelo, The Netherlands) were cleaned with a “piranha” (30% H₂O₂ / 70% H₂SO₄) solution and subsequently immersed in a 10 mM ethanolic solution of ATRP initiator overnight at room temperature. The samples used for the swelling experiments were prepared by depositing the ATRP initiator solution on Au substrates with a polydimethylsiloxane (PDMS) stamp and the gaps between the patterned areas were functionalized with an octadecylthiol (ODT, Sigma) monolayer via deposition from a 1 mM ethanolic solution.

For both patterned and unpatterned samples surface-initiated ATRP was performed following the same experimental procedures. Namely, 20 ml of 25% water solution of purified HEMA containing 0.35 g of bipyridine were degassed by three freeze-thaw-pump cycles and they were subsequently transferred, through a

degassed syringe, into a glass balloon purged with argon and containing 53 mg of CuBr and 6 mg of CuBr₂ (final reactants ratio: HEMA : CuBr : CuBr₂ : bipy = 100 : 1 : 0.1 : 5). The mixture was left under stirring at ambient temperature for roughly 30 minutes, until complete formation of a dark-red colored complex. Subsequently the reaction solution was transferred, via a degassed syringe, into an argon purged flask containing the SAMs functionalized samples and the surface-initiated polymerization was left proceeding for the necessary time. Following this reaction time, the samples were extracted from the solution and rinsed overnight in ethanol. PHEMA-based brush films were derivatized with succinic anhydride by overnight reaction in 30 mg/ml dry pyridine solution.

For the preparation of Ag nano-particles/brush films hybrid layers all the samples studied were first incubated overnight in a 5 mM aqueous solution of AgNO₂ (purchased by Merck). Subsequently the films were rinsed with milliq water and immersed for 10 seconds in a 1 mM energetically stirred solution of NaBH₄ in order to reduce the Ag(I) ions in the brush structure to Ag(0).

Characterization. Topography images of the fabricated brush and brush-gel films were recorded by tapping mode atomic force microscopy (TM-AFM). Contact mode AFM (CM-AFM) was performed inside a liquid cell setup in order to evaluate the swelling and mechanical properties of the grafts immersed both in ethanol and in aqueous solutions at different pH values. The pH was adjusted by adding 0.1 M HCl or 0.1 M NaOH to the aqueous solutions used for the measurements.

FTIR-spectra (spectral resolution of 8 cm⁻¹, 2048 scans) were obtained using a BIO-RAD FTS575C FTIR spectrometer equipped with a nitrogen-cooled cryogenic cadmium mercury telluride detector. Background spectra were obtained by scanning a clean gold substrate.

The dry thickness of the synthesized films was measured using a computer-controlled null ellipsometer (Philips Plasmon) working with a He-Ne laser ($\lambda = 632.8$ nm) at an incidence angle of 70°. The measurements were formed at 22°C and 30% relative humidity. The data were averaged over 100 points at the surface of each sample.

UV-absorption spectroscopy was performed on brush and brush-gel samples following the formation of Ag NPs by using a USB200 spectrophotometer (Ocean Optics, U.S.A.) equipped with integrating sphere of 30mm internal diameter (AvaSphere-30-Refl, Avantes, U.S.A.).

HR-SEM measurements on the same samples were obtained with a HR-LEO 1550 FEF SEM. The samples were not coated with a conducting layer.

6.5 References

- (1) Kaholek, M.; Lee, W. K.; Ahn, S. J.; Ma, H. W.; Caster, K. C.; LaMattina, B.; Zauscher, S. *Chem. Mater.* **2004**, *16*, 3688.
- (2) Tugulu, S.; Silacci, P.; Stergiopoulos, N.; Klok, H. A. *Biomaterials* **2007**, *28*, 2536.
- (3) Gupta, S.; Uhlmann, P.; Agrawal, M.; Lesnyak, V.; Gaponik, N.; Simon, F.; Stamm, M.; Eychmuller, A. *J. Mater. Chem.* **2008**, *18*, 214.
- (4) Gupta, S.; Uhlmann, P.; Agrawal, M.; Chapuis, S.; Oertel, U.; Stamm, M. *Macromolecules* **2008**, *41*, 2874.
- (5) Boyes, S. G.; Akgun, B.; Brittain, W. J.; Foster, M. D. *Macromolecules* **2003**, *36*, 9539.
- (6) Azzaroni, O.; Brown, A. A.; Cheng, N.; Wei, A.; Jonas, A. M.; Huck, W. T. S. *J. Mater. Chem.* **2007**, *17*, 3433.
- (7) Mark, J. E.; Erman, B. *Elastomeric Polymer Networks*; Prentice Hall: Englewood Cliffs, 1992.
- (8) Harmon, M. E.; Kuckling, D.; Pareek, P.; Frank, C. W. *Langmuir* **2003**, *19*, 10947.
- (9) Harmon, M. E.; Kuckling, D.; Frank, C. W. *Langmuir* **2003**, *19*, 10660.
- (10) Huang, W. X.; Baker, G. L.; Bruening, M. L. *Angew. Chem. Int. Ed.* **2001**, *40*, 1510.
- (11) Bruening, M. L.; Huang, W. X.; Baker, G. L. *Abs. Pap. Am. Chem. Soc.* **2001**, *221*, U432.
- (12) Pinto, J. C.; Whiting, G. L.; Khodabakhsh, S.; Torre, L.; Rodriguez, A. B.; Dalgliesh, R. M.; Higgins, A. M.; Andreasen, J. W.; Nielsen, M. M.; Geoghegan, M.; Huck, W. T. S.; Siringhaus, H. *Adv. Funct. Mater.* **2008**, *18*, 36.
- (13) Comrie, J. E.; Huck, W. T. S. *Langmuir* **2007**, *23*, 1569.
- (14) Edmondson, S.; Huck, W. T. S. *Adv. Mater.* **2004**, *16*, 1327.
- (15) Edmondson, S.; Frieda, K.; Comrie, J. E.; Onck, P. R.; Huck, W. T. S. *Adv. Mater.* **2006**, *18*, 724.
- (16) Matyjaszewski, K.; Xia, J. H. *Chem. Rev.* **2001**, *101*, 2921.
- (17) Shah, R. R.; Merrezeys, D.; Husemann, M.; Rees, I.; Abbott, N. L.; Hawker, C. J.; Hedrick, J. L. *Macromolecules* **2000**, *33*, 597.
- (18) Wang, X.; Xiao, X.; Wang, X. H.; Zhou, J. J.; Li, L.; Xu, J. *Macromol. Rapid Commun.* **2007**, *28*, 828.

- (19) Biesalski, M.; Johannsmann, D.; Rühle, J. *J. Chem. Phys.* **2002**, *117*, 4988.
- (20) Zhang, L. Q.; Dutta, A. K.; Jarero, G.; Stroeve, P. *Langmuir* **2000**, *16*, 7095.
- (21) Dante, S.; Hou, Z. Z.; Risbud, S.; Stroeve, P. *Langmuir* **1999**, *15*, 2176.
- (22) Zhang, J. G.; Xu, S. Q.; Kumacheva, E. *J. Am. Chem. Soc.* **2004**, *126*, 7908.
- (23) Logar, M.; Jancar, B.; Suvorov, D.; Kostanjsek, R. *Nanotechnol.* **2007**, *18*.
- (24) Biffis, A.; Orlandi, N.; Corain, B. *Adv. Mater.* **2003**, *15*, 1551.
- (25) Huang, W. X.; Kim, J. B.; Bruening, M. L.; Baker, G. L. *Macromolecules* **2002**, *35*, 1175.
- (26) Robinson, K. L.; Khan, M. A.; Banez, M. V. D.; Wang, X. S.; Armes, S. P. *Macromolecules* **2001**, *34*, 3155.
- (27) Flory, P. J. *Principles of Polymer Chemistry*; Cornell University Press: Ithaca, 1953.
- (28) Tan, Z. J.; Jaeger, R.; Vancso, G. J. *Polymer* **1994**, *35*, 3230.
- (29) Baker, J. P.; Hong, L. H.; Blanch, H. W.; Prausnitz, J. M. *Macromolecules* **1994**, *27*, 1446.
- (30) Baker, J. P.; Blanch, H. W.; Prausnitz, J. M. *J. Appl. Pol. Sci.* **1994**, *52*, 783.
- (31) Atkins, P. W. *Physical Chemistry*; Oxford University Press: Oxford, 1998.
- (32) Plunkett, K. N.; Zhu, X.; Moore, J. S.; Leckband, D. E. *Langmuir* **2006**, *22*, 4259.
- (33) Yim, H.; Kent, M. S.; Mendez, S.; Balamurugan, S. S.; Balamurugan, S.; Lopez, G. P.; Satija, S. *Macromolecules* **2004**, *37*, 1994.
- (34) Mendez, S.; Subramanian, B.; Balamurugan, S. S.; O'Brien, M. J.; Lopez, G. P. *Abs. Pap. Am. Chem. Soc.* **2003**, *225*, U617.
- (35) Creighton, J. A.; Blatchford, C. G.; Albrecht, M. G. *J. Chem. Soc. Farad. Transact.* **1979**, *75*, 790.
- (36) Sager, W.; Eicke, H. F. *Colloids Surf.* **1991**, *57*, 343.
- (37) Zhai, X.; Efrima, S. *J. Phys. Chem.* **1996**, *100*, 11019.
- (38) Silvert, P. Y.; HerreraUrbina, R.; Duvauchelle, N.; Vijayakrishnan, V.; Elhsissen, K. T. *J. Mater. Chem.* **1996**, *6*, 573.
- (39) Jolivet, J. P.; Gzara, M.; Mazieres, J.; Lefebvre, J. *J. Colloid Interface Sci.* **1985**, *107*, 429.
- (40) Petit, C.; Lixon, P.; Pileni, M. P. *J. Phys. Chem.* **1993**, *97*, 12974.
- (41) Henglein, A.; Giersig, M. *J. Phys. Chem. B* **1999**, *103*, 9533.
- (42) Zheng, J.; Stevenson, M. S.; Hikida, R. S.; Van Patten, P. G. *J. Phys. Chem. B* **2002**, *106*, 1252.
- (43) Kuo, P. L.; Chen, W. F. *J. Phys. Chem. B* **2003**, *107*, 11267.
- (44) Mock, J. J.; Barbic, M.; Smith, D. R.; Schultz, D. A.; Schultz, S. *J. Chem. Phys.* **2002**, *116*, 6755.

- (45) Matyjaszewski, K.; Miller, P. J.; Shukla, N.; Immaraporn, B.; Gelman, A.; Luokala, B. B.; Siclovan, T. M.; Kickelbick, G.; Vallant, T.; Hoffmann, H.; Pakula, T. *Macromolecules* **1999**, *32*, 8716.

Chapter 7

Controlled Fabrication of Polymer “Hedge” and “Dot” Brushes by AFM-Assisted Lithography and Surface-Initiated Polymerization*

In this Chapter the combination of AFM-assisted nanolithographic techniques and controlled surface-initiated polymerization (SIP) for the preparation of grafted polymeric nano-structures is described. Fabrication of polymer grafts characterized by lateral dimensions ranging from hundred to few tens of nanometers was accomplished. These brush nano-structures were named polymer “hedge” and “dot” brushes, when the grafts were patterned in the form of lines or dots, respectively.

In the first part of the Chapter the preparation of polymer “hedge” brushes of poly(methacrylic acid) (PMAA), exhibiting a width from several hundreds to sub-40 nm and a controllable height is reported. These nano-structures were grafted from designer substrates by photopolymerization using the already introduced DTCA iniferters assembled on Au nano-wires. The Au nano-wires were obtained using H-terminated silicon as substrate for AFM tip-assisted (“dip-pen”) nanolithography of H₂AuCl₄ which yielded Au continuous structures upon reduction in contact with the surface. The polymer “hedge” structures were characterized by AFM.

In the second part of this Chapter the fabrication of pH-responsive PHEMA-based polymeric nano-structures is described. In this case polymer “hedge” and “dot” brushes were grown in a controlled manner by ATRP-based SIP. Initiator-functionalized nano-patterns were obtained on silicon wafers covered

* Part of this Chapter was published in: (a) Zapotoczny, S.; Benetti, E.M.; Vancso, G.J. *J. Mater. Chem.* **2007**, *17*, 3293. Benetti, E.M.; (b) Chung, H.J.; Vancso, G.J. *Macromol. Rapid Commun.* **2009**, in press

with organic resists by AFM scanning probe oxidation lithography (SPOL). AFM images confirmed isolated grafting of stimuli-responsive “hedges” and “dot” brush structures exhibiting dimensions corresponding to a few tens of chains.

7.1 Introduction

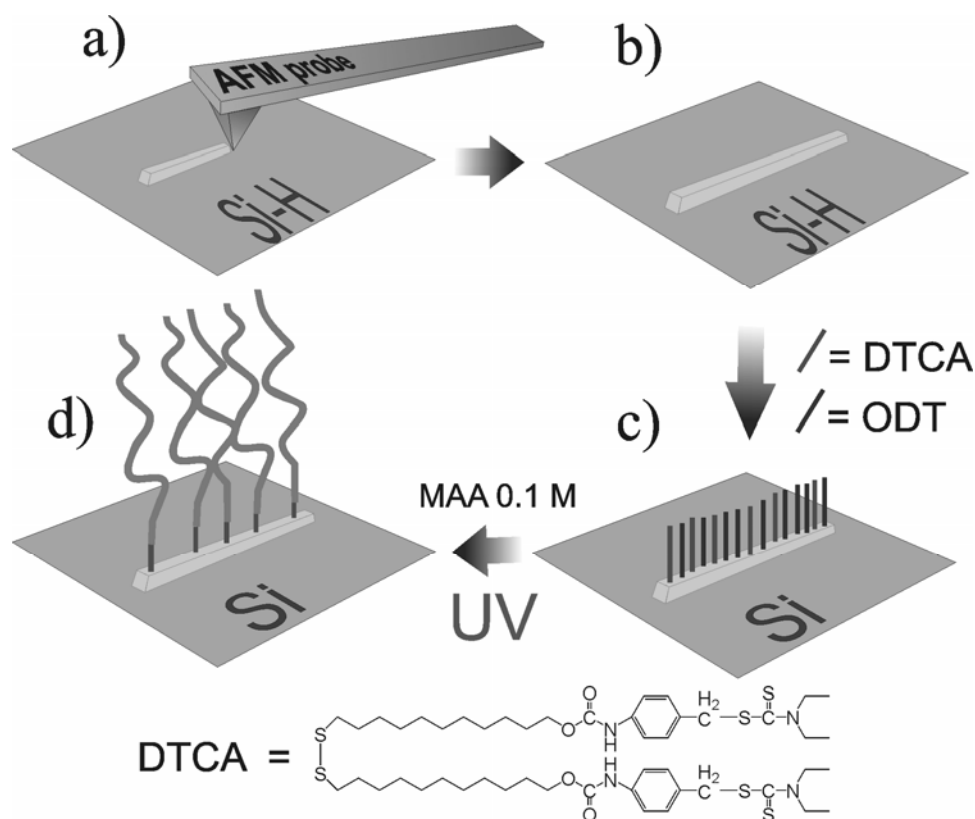
“Grafting-from” approaches combining micro-contact printing of initiators and subsequent controlled polymerization, to obtain stimulus responsive, patterned polymer brushes represent a well known fabrication method.¹ However, these approaches still do not allow one to obtain full single chain control of surface tethered macromolecules. Control of the overall dimensions and the exact position of single polymer graft chains on multiple lengthscales and in 1, 2 and 3 dimensions at various substrates is an issue of central importance in macromolecular nanotechnology. For example, locally patterned biopolymers, such as proteins, have been shown to act as building blocks for the synthesis of complex biomolecular architectures which can function as selective recognition sites for other specific biomolecules.²⁻⁷ In addition, for organic nanoelectronic devices, synthetic macromolecules have been used as well to form nano-patterns, whereby the synthesis of polyconjugated chains was scaled down towards single molecule devices.⁸⁻¹¹ In both cases, AFM tip-assisted methods have been employed to deposit macromolecules either in a “grafting to” fashion,^{12,13} or to promote the direct growth of polymers in locally defined areas on the nano-scale.^{8,9,14,15}

The combination of tip-assisted nanolithography to control initiator positions at the surfaces with “grafting-from” methods would allow one to form polymeric nano-structures keeping the control over the properties and the morphology of the macromolecular components. Moreover, this approach, if successful, would represent a first step towards controlled growth of single macromolecules from pre-functionalized sites.

In this Chapter the coupling of AFM-assisted nanolithography with controlled SIP methods for the successful fabrication of polymer “hedge” and “dot” brushes is described. These polymeric nano-structures possess typical dimensions down to few tens of nanometers and they are thus constituted by a limited number of grafted chains.

Two different AFM-assisted fabrication approaches for surface-modification and immobilization of initiators for SIP on the nano-scale are introduced.

In the first part of this Chapter we report on the preparation of long, linear brush structures possessing typical width values down to sub-40 nm (polymer “hedge” brushes). In our approach we followed a stepwise method as summarized in Scheme 7.1. First gold nano-wires were deposited on silicon substrates by AFM tip (“dip-pen” nanolithography, DPN), which acted as selective platform for the immobilization of disulfide-based DTCA initiators (compare Chapters 3, 4 and 5). These *iniferters* were used to initiate the controlled growth of poly(methacrylic acid) (PMAA) brushes by photopolymerization. Height and width of the polymer “hedge” brushes were controlled by the preparation conditions.



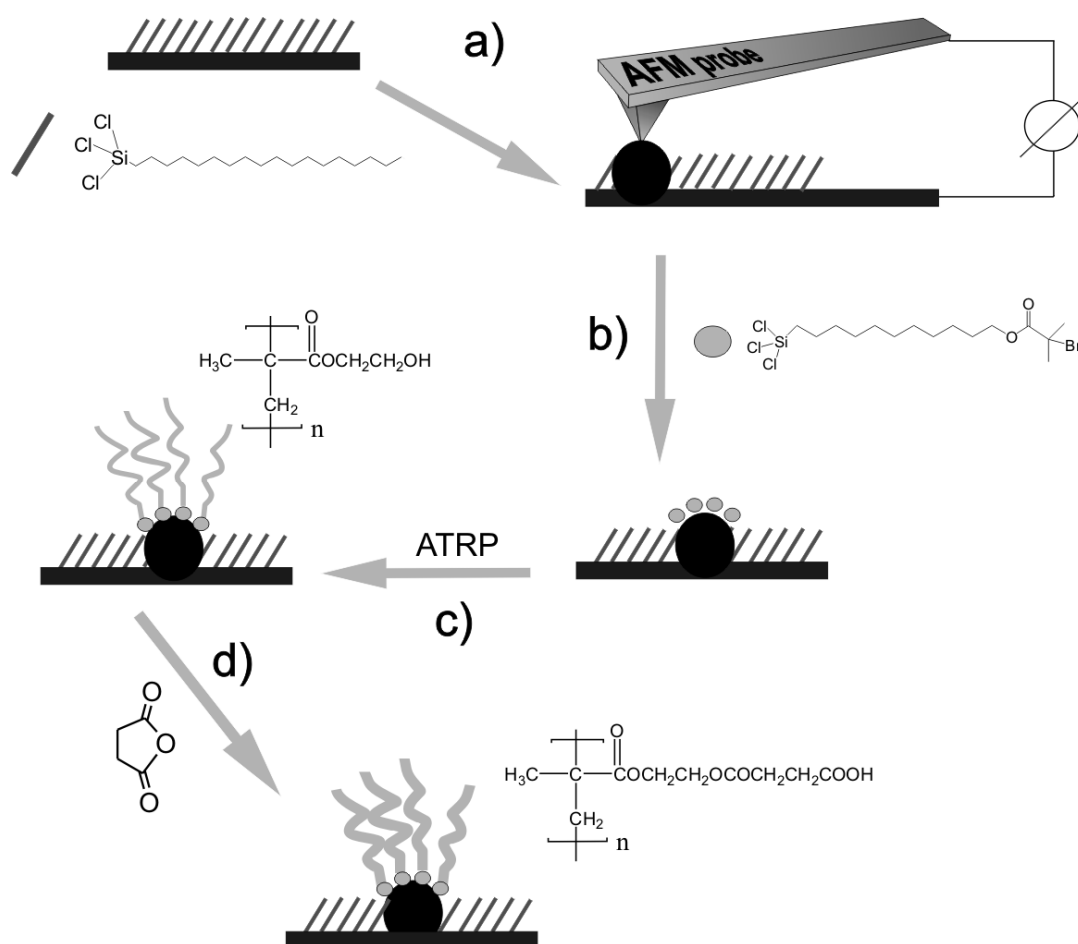
Scheme 7.1. Preparation of polymer “hedge” brushes grafted from immobilized precursors on gold nano-wires. a) and b) tip-assisted deposition of gold nanowires on hydride-terminated silicon; c) selective immobilization of functional adsorbates on the gold structures; d) UV-initiated grafting of PMAA brushes using the functionalized nanowires as platforms.

AFM DPN has been used to create nano-sized features by delivering chemically different adsorbates (so called ink molecules) on metallic and non metallic substrates.¹⁶⁻¹⁹ These chemical adsorbates, because of the unselective affinity for the surrounding, tend to diffuse on the substrate's surface once they are locally delivered²⁰⁻²³ thus affecting the resolution, stability and the lateral size of the features created. If the molecules deposited by DPN would be attached to the substrate in a robust way, then the pattern stability problem could be circumvented. By DPN, as we show here, it is possible to locally deliver reactive ink molecules, which get anchored due to the formation of strong local binding. One example constitutes using Au salts as reactive ink, which can yield in contact with hydrogenated silicon Au deposits. The binary system gold nanostructures-silicon, acts in this sense as selective substrate in the presence of thiol\disulfide species which adsorb preferentially on gold.²⁴ The influence of the environmental and operational conditions on the width of the gold features drawn was studied, demonstrating the capability to synthesize sub-20nm wide gold lines from which polymer "hedges" were eventually grown.

In the second part of this Chapter, silane-based organic resists on silicon substrate were used as starting surfaces for the localized formation of silicon oxide nano-patterns by AFM-assisted SPOL,²⁵⁻²⁷ thus forming precursor platforms for the subsequent grafting of pH-responsive polymer brush nano-structures (Scheme 7.2). Although previous studies revealed the robustness, high resolution (up to sub-10 nm resolution) and implementability of SPOL to fabricate nano-structured resist-covered surfaces,²⁸⁻³¹ our aim here is to demonstrate the potentials of the combined SPOL-SIP based technique to fabricate highly controllable, and ultimately, single macromolecular stimulus-responsive systems. The optimization of the preparation method allowed the controlled synthesis of few grafted macromolecules forming sub-40 nanometers stimulus-responsive circular structures ("dot" brushes) or grafted line structures ("hedge" brushes) possessing a width in the order of several tens of nanometers.

The resists used for the SPOL experiments were based on octadecyltrichlorosilane (OTS) monolayers deposited on silicon oxide surfaces. By applying negative bias voltages to a gold coated AFM-tip in contact with the substrates, silicon oxide nano-patterns of different sizes and shapes were grown. The so-formed patterns were subsequently functionalized with silane-based initiators for

ATRP, selectively delivered from solution onto the exposed silicon oxide areas. Poly(hydroxyethyl methacrylate) (PHEMA) “dot” and “hedge” brushes were grafted from the functionalized patterns, with typical dimensions ranging from few tens to several hundreds of nanometers (in dot diameter or hedge width).



Scheme 7.2. Preparation of pH-responsive polymer brushes (here “dot” brush) from functionalized silicon oxide patterns. (a) SPOL of OTS monolayers and formation of silicon oxide nano-patterns; (b) selective functionalization of silicon oxide nano-patterns with ATRP initiator; (c) surface-initiated ATRP of HEMA and formation of PHEMA “dot” brushes; (d) functionalization of PHEMA “dot” brushes with succinic anhydride.

The magnitude of the bias voltage applied to the AFM probe during SPOL influenced the size of the precursor oxide lines and thus, indirectly, the number of macromolecules subsequently grafted and the width of the polymer “hedge” brush

structures. The height and the width of the polymer grafts were also tuned by varying the incubation time of the locally oxidized substrates in the initiator solution. With increasing incubation time the surface coverage of initiators on the silicon oxide surface was increased. Following the grafting step, PHEMA brushes were functionalized with succinic anhydride in order to derivatize chain backbone with carboxylic acid (Scheme 7.2d). The so-modified brushes presented pH dependent charge density when immersed in aqueous environment and their swelling properties were observed to remarkably change when immersed into solutions of different pH (see also Chapter 6).

7.2 Results and Discussion

7.2.1 Preparation and Characterization of Polymer “Hedges” Grafted from Gold Nano-Wires

As mentioned earlier, in the first part of this Chapter we describe the preparation of polymer “hedges” grafted via controlled *iniferter*-mediated SIP from Au nano-wires. These metallic nanostructures were deposited on silicon-hydride by DPN-mediated chemical reduction of Au salts. In the DPN experiments an AFM contact tip inked with a 1% aqueous solution of HAuCl_4 was brought in contact with silicon hydride surfaces thus inducing the reduction of Au(III) to Au(0) in the contacted areas. In addition, the DPN process was carried out at different relative humidity in order to tune the size of the Au features obtained.

Representative examples of Au nano-wires (hexagons and/or lines) thus obtained are shown in Figure 7.1a (AFM tapping mode height image of nanowires obtained at 40% relative humidity) and in Figure 7.2a (AFM tapping mode height image of nanowires obtained at 30% relative humidity). As one can see, under humid deposition conditions, the Au line width is significantly larger (240 ± 30 nm) as compared with the Au line thickness obtained at 30% relative humidity (20 ± 5 nm) taking tip convolution effects into account. In both cases the height of the Au features varied between 0,5 and 1,0 nm. The influence of relative humidity on the line characteristics has already been reported for organic-based inks in DPN.²⁰ Ink transfer and line width/height are related to capillary forces which play a crucial role

in the ink deposition. In our case, the humidity effect is even stronger, since the ink used is water soluble.

While previously achieved gold lines were reported to have sub-100 nm width,²⁴ we could obtain even ultrathin (<1 nm high by AFM) sub-20 nm wide lines by decreasing the relative humidity (RH) to 30%.

Writing speed of the AFM tip was also crucial for obtaining continuous lines at low humidity condition. Best results were obtained at 30 nm/s writing speed while at 100 nm/s practically no writing was observed. Thus, a careful optimization/balancing of humidity and writing speed, which primarily govern the mass transfer from the tip to the surface, enables tuning of the deposited line width.

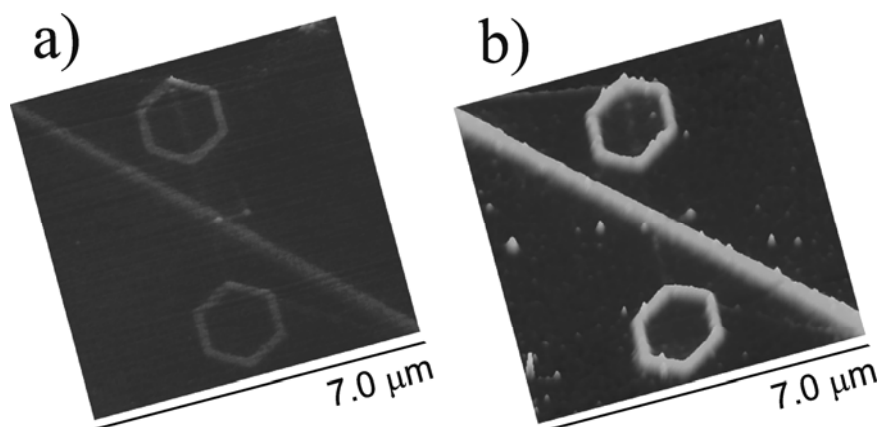


Figure 7.1. Height images (vertical scale from black to white 10 nm) from tapping-mode AFM measurements illustrating 240 (+/-30) nm wide gold wires deposited on hydride terminated silicon a) and the subsequently grafted PMAA brushes b).

The so formed gold nano-wires can be used to immobilize thiols or disulfides with functional groups which initiate *iniferter*-based controlled photopolymerization (see experimental section for details). We exploited here, for the first time, the confined growth of polymeric nano-structures based on polymer brushes from these initiators attached to the previously fabricated Au nano-wires.

We specifically focused on the synthesis of PMAA brushes using the disulfide DTCA initiator depicted in Scheme 7.1.

Representative AFM images using Au wires of 240 ± 30 nm wide (Figure 7.1a) and the polymer “hedge” brush obtained after the photopolymerization (Figure 7.1b) capture the starting and ending point of the process. The polymer “hedges” height reached a value of 5 ± 1 nm.

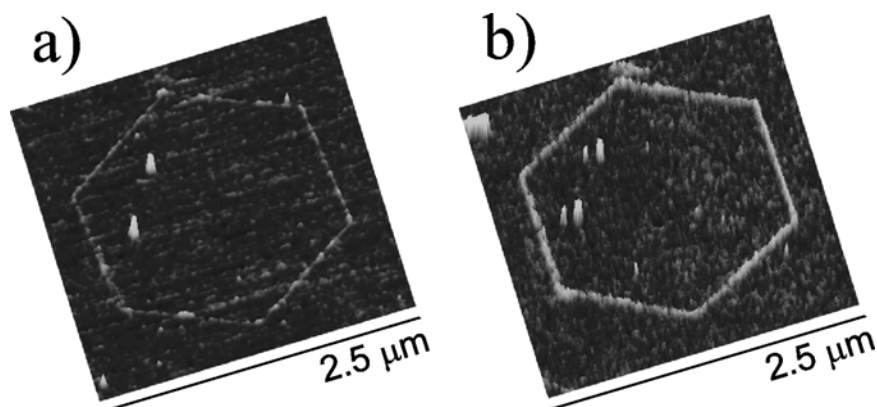


Figure 7.2. Height images (vertical scale from black to white 2 nm) from AFM tapping-mode measurements of 20 nm wide gold nanowires deposited on hydride terminated silicon a) and the subsequently grafted PMAA brushes b).

The surface-initiated polymerization of PMAA was performed also on very narrow, 20 nm wide, functionalized gold wires. Corresponding images prior to and following 15 minutes of UV irradiation, showing the Au lines and the polymer “hedges”, respectively, are depicted in Figure 7.2. Surprisingly, in this case, the height observed after the same polymerization time was much less than the value observed for thicker features. At the same time the width of the polymer “hedges” was doubled (the same tip was used for capturing both images). This observation can be explained if one takes into account the extension of the polymer chains beyond the edges of the grafting region. This effect was recently theoretically described by Patra et al.³² who studied the conformation of polymer brushes grafted from patterns with variable width. The relevant widening of the patterns after the polymer grafting is a consequence of the release of osmotic pressure inside the brush system. Such relative widening effect, due to chain flattening, is obviously much more pronounced with diminishing of the “hedge” width.

The surface properties of the polymer “hedges” with 240 nm width immersed in water were monitored by AFM in force-volume (FV) mode (capturing adherence

images) as well. Figure 7.3a illustrates the topographic image of the PMAA brushes taken simultaneously with the corresponding FV image depicted in Figure 7.3b. In aqueous environment the PMAA brushes swells profusely owing to their hydrophilic character. This makes high fidelity AFM topography (height) imaging a challenging task (see Figure 7.3a). However, the corresponding FV micrograph (Figure 7.3b) clearly shows that the adhesion properties sharply change between the polymeric nano-structures and the surrounding substrate. The clear contrast enhancement in Figure 7.3b is, in fact, a result of the repulsive forces which dominate the tip-PMAA brushes interaction.

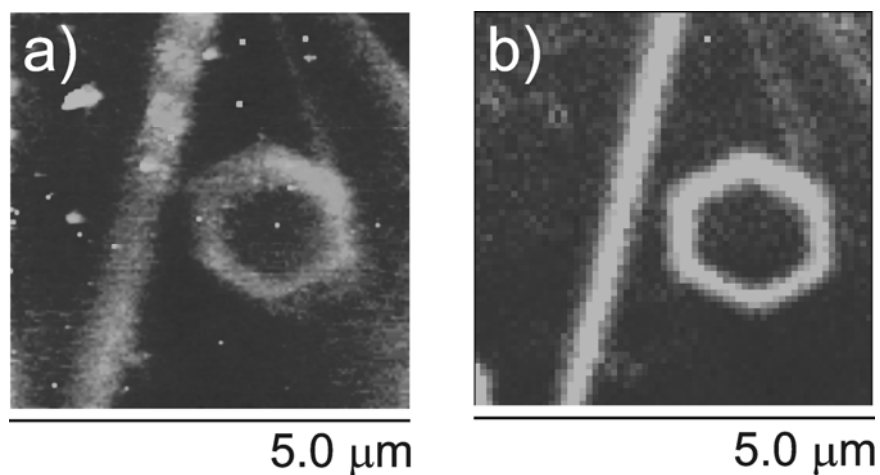


Figure 7.3. AFM height image a) (vertical scale from black to white 15 nm) and force-volume image b) of the grafted PMAA brushes immersed in water at pH 7.0. The contrast in image b) is given by areas of high (black) and low (white) adherence between the AFM tip and the surface.

7.2.2 Preparation and Characterization of pH-Responsive “Hedge” and “Dot” Brushes by Scanning Probe Oxidation and Surface-Initiated Polymerization

In this section the preparation and characterization of pH-responsive PHEMA-based “hedges” and “dot” brushes are reported.

In a typical experiment to obtain “hedge” brushes, silicon oxide lines with an average width of 50 ± 3 nm were first prepared by applying a constant negative tip bias of -7.0 V at 0.5 $\mu\text{m}/\text{sec}$ lithography rate (Figures 7.4a and cross sectional profile

in Figure 7.4d). Selective chemisorption of the ATRP initiator only onto the oxide features was then achieved by overnight incubation of the substrate in a toluene solution of the initiator. Subsequent SIP was performed in 25% aqueous solutions of HEMA, presenting CuBr/CuBr₂-bipyridine as catalytic system (see experimental section for details). In order to monitor the chemical composition of the polymer grafts, SIP was also performed on a flat silicon oxide substrate functionalized with a continuous monolayer of the same ATRP initiator. Fourier transform infrared spectroscopy (FTIR) was used to analyze the films obtained (Figure 7.5). The corresponding FTIR spectrum for the continuous films showed the stretching at 1740 cm⁻¹ characteristic of the carboxyl groups of the polymer and also a broad band between 3000 and 3500 cm⁻¹ corresponding to the hydroxyl groups of the monomer units. Following a surface grafting step, 79 ± 10 nm high and 180 ± 20 nm wide PHEMA “hedge” brushes were grown from functionalized silicon oxide lines (Figure 7.4b).

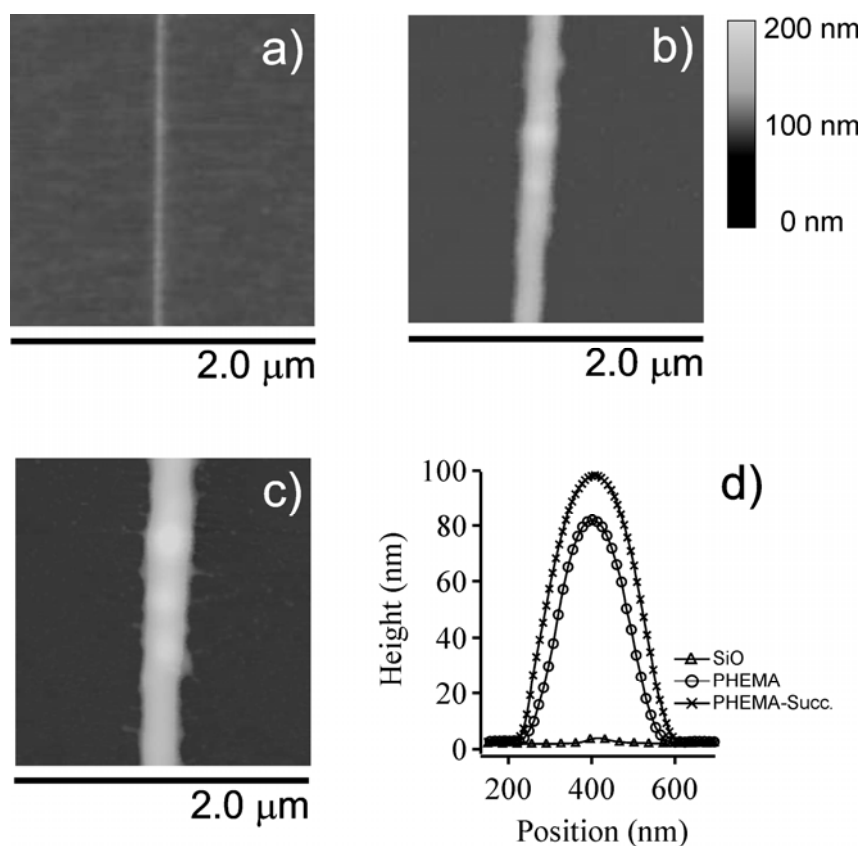


Figure 7.4. AFM tapping-mode height images of a) 50 nm wide silicon oxide nano-patterns deposited on OTS resist by SPOL; b) the subsequently grafted PHEMA “hedge” brushes; and c)

PHEMA “hedge” brushes after succinic anhydride functionalization c). Cross sectional profiles recorded following every fabrication step are shown in d). The images were taken in air.

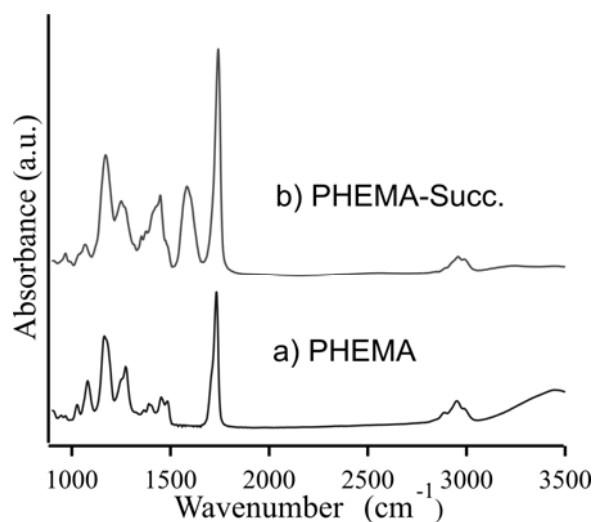


Figure 7.5. FTIR spectra of a) PHEMA film grafted from silicon oxide surface; and b) following functionalization with succinic anhydride.

In order to transform the PHEMA brushes into pH-responsive weak polyacids, substrates exhibiting PHEMA grafts were reacted with succinic anhydride (see experimental section), thus introducing COOH functionalities along the polymer chains by reaction of the OH- moieties of the hydroxyethyl groups with the anhydride. Following polymer functionalization the FTIR spectrum of the films showed the disappearance of the –OH band around 3400 cm⁻¹, a clear increase in the absorbance of the C=O stretching and the appearance of the signal corresponding to the carboxylate ion at 1580 cm⁻¹. Furthermore, as it was already observed for PHEMA brushes grafted from flat surfaces, the functionalization with the bulky anhydride molecules induced an increase of the volume occupied by the polymer chains.³³ In the present case, after the reaction with succinic anhydride, the polymeric patterns increased their overall dimensions reaching 96 ± 15 nm in height and 240 ± 20 nm in width (Figure 7.4c and cross sectional profile in Figure 7.4d). All these observations thus corroborated the successful functionalization and the introduction of the succinic acid derivatives along the PHEMA chains (defined as PHEMA-Succ. after derivatization).

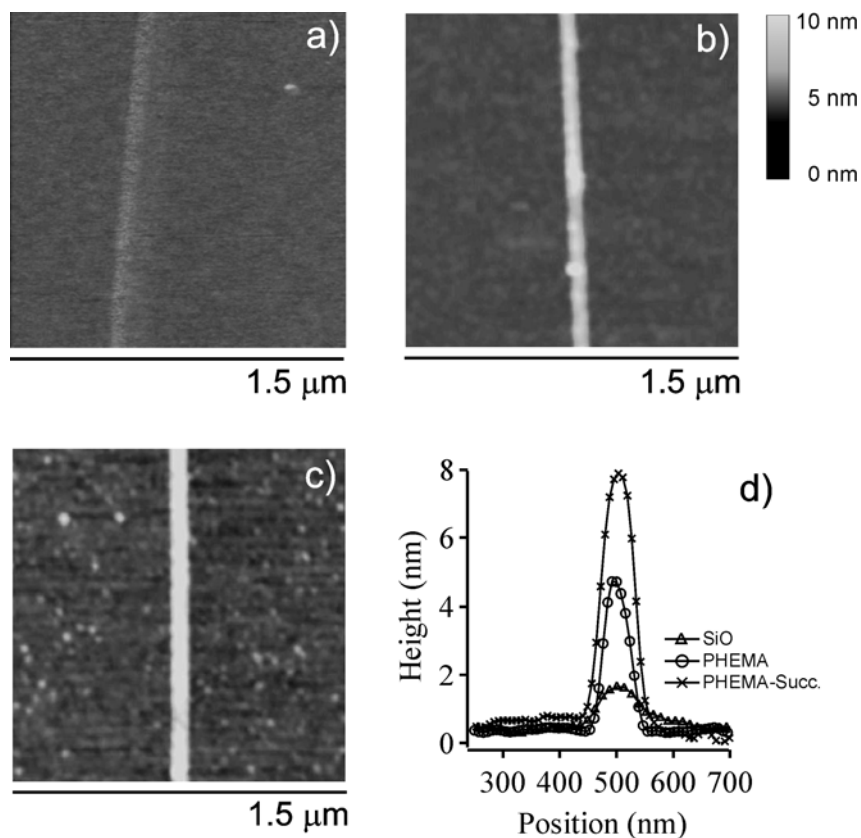


Figure 7.6. AFM tapping-mode height images of a) 50 nm wide silicon oxide nano-patterns deposited on OTS resist by SPOL; b) the subsequently grafted PHEMA “hedge” brushes; and c) PHEMA “hedge” brushes after succinic anhydride functionalization. Cross sectional profiles recorded following every fabrication step are shown in d). The images were taken in air.

Control of aqueous surface-initiated ATRP is usually a challenging task.^{33,34} Thus precise control of the dimensions of the PHEMA brushes by varying the polymerization time is also difficult to achieve. Specifically, the polymerization rate (and thus the thickening) proceeds extremely fast in the first minutes of the reaction and subsequently decreases until an irreversible leveling off of the film growth after long reaction times is reached.³⁵ In order to control both the width and height of the “hedge” brush structures, precursor patterned substrates were incubated for shorter time in the solution of trichlorosilane-based ATRP initiator, resulting in less adsorption of initiator molecules on the silicon oxide lines. By dipping the substrates for 4 hours in initiator solution instead of 13 hours (as for the samples reported in Figure 7.4), following 1 hour of polymerization, PHEMA “hedge” brushes with height of 4 ± 2 nm and width of 55 ± 5 nm were grown from 50 ± 10 nm wide silicon oxide

lines (Figures 7.6a, 7.6b and corresponding cross sectional profiles in Figure 7.6d). The reaction with succinic anhydride then doubled the average height of the brushes to 8 ± 1 nm and increased the width to 65 ± 5 nm (Figure 7.6c and cross sectional profiles in Figure 7.6d).

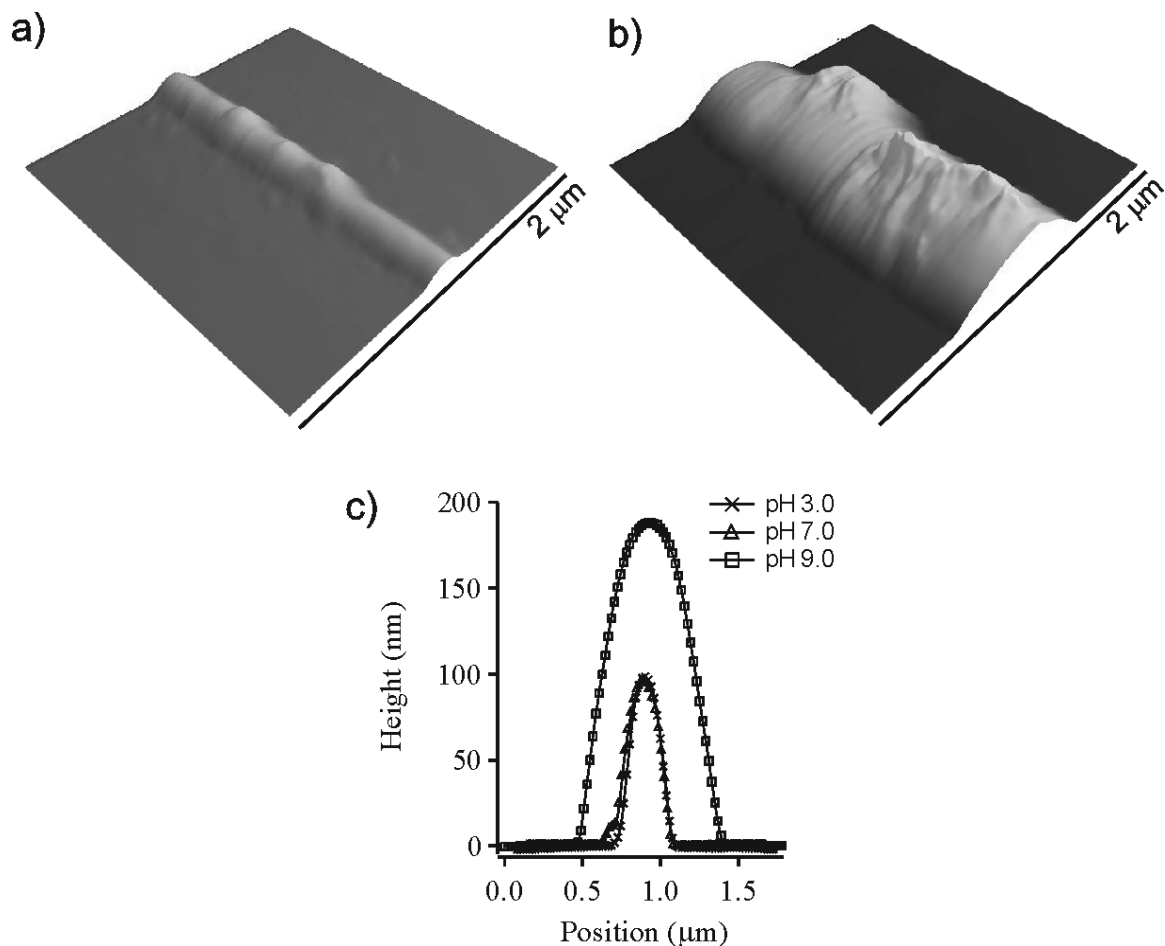


Figure 7.7. AFM contact-mode height images of PHEMA brushes immersed in water a) at pH 3.0 and b) at pH 9.0. Cross sectional profiles of PHEMA “hedge” brush structures immersed in water at different pH values are shown in c).

In order to explore the pH responsive properties of the PHEMA-Succ. grafts, “hedge” brush structure with a height of 96 ± 15 nm and a width of 240 ± 20 nm were immersed in water solutions of different pH values and AFM topographic images were recorded (Figure 7.7a and 7.7b). As it can be seen in Figure 7.7a and by comparing the cross sectional profiles in Figure 7.7c, in acid and neutral

environments (pH 3.0 and 7.0, respectively) the polymer chains did not swell remarkably, presenting an average height of 100 ± 10 nm and a width of 242 ± 20 nm for the hedge, which are close to the values reported in Figure 7.4c and 7.4d for the same PHEMA-Succ. “hedge” brushes in the dry state. However, by rising the pH to 9.0 the polymer chains swell profusely (Figure 7.7b). Correspondingly, the cross sectional profile (in Figure 7.7c) shows an increase of the average height by 90% (reaching 190 ± 30 nm) and the average width by 230% (reaching 800 ± 40 nm).³⁶ Such dramatic change of the swelling properties is a direct consequence of the deprotonation of COOH, i.e. the increase in density of the COO⁻ groups, typical for polycarboxylic acids immersed in basic environments.³⁷ We tentatively attribute the significantly higher value of pKa observed in the PHEMA-Succ. brush if compared with free aliphatic carboxylic acids (pKa~5.5) to hydrogen bonding formation and related stabilizing effects (see also Chapter 6). It is also worth mentioning that the PHEMA-Succ. “hedge” brushes showed pH-induced size variations comparable to the film height values of PHEMA-Succ. continuous films immersed in aqueous solutions at various pHs (compare also Chapter 6).

Aiming at the development of site-specific individual stimulus responsive systems, silicon oxide dots with variable size were also obtained by applying different bias voltages varying from -6 to -9 V on locally selected positions (Figure 7.8). The influence of the size of the precursor silicon oxide patterns on the subsequent grafting of PHEMA nano-brushes was thus investigated. Observing the AFM images in Figure 7.8a and comparing the cross sectional profiles reported in Figures 7.8d and 7.8e it can be seen that oxide dots with average width ranging from 20 ± 3 nm to 80 ± 5 nm could be grown on the resist surface by varying the applied bias between -6 and -9V.

The silicon oxide dots were subsequently incubated over 4 hours in ATRP initiator solution, followed by SIP of HEMA. PHEMA grafts (“dot” brushes) grown from the broadest functionalized oxide dot (~80 nm in width) reached an average height of 5 ± 2 nm, not showing significant widening when compared to the lateral dimension of the starting oxide pattern (Figure 7.8a, 7.8b and cross sectional profile in Figure 7.8d). On the contrary, grafting PHEMA from the smallest, 20 nm wide dot, produced “dot” brushes which doubled the average width of the underlying silicon oxide feature, reaching 40 ± 2 nm in lateral size and 3 ± 1 nm in height. This phenomenon was previously observed in the case of polymer “hedges” grafted from

sub-20 nm Au nano-wires (see section 7.2.1) and it was theoretically described as a consequence of the release of osmotic pressure inside the brush structure.^{32,38} Similar to the polymer “hedges” structures, the reaction with succinic anhydride also induced a significant increase in the height of the “dot” brushes. In fact, going from the smallest to the largest “dot” brush structures, following derivatization, the height was shown to increase by 30 to 45% depending on the feature size.

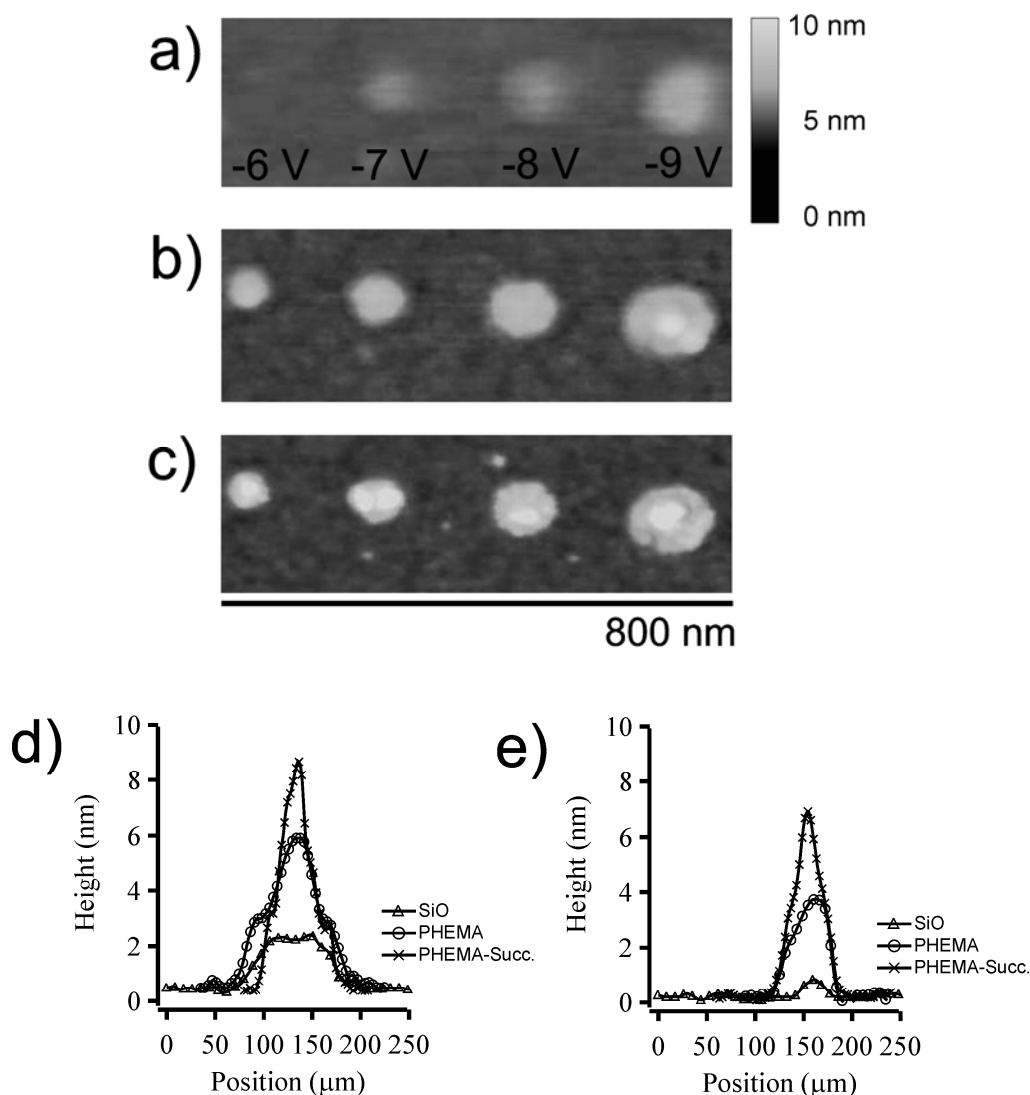


Figure 7.8. AFM tapping-mode height images of a) silicon oxide nano-dots with variable lateral size deposited on OTS resist by SPOL at different voltages; b) following surface-initiated ATRP of PHEMA; and c) after succinic anhydride functionalization. Cross sectional profiles relative to d) the largest and e) the thinnest silicon oxide dot recorded following every fabrication step are reported.

7.3 Conclusions

In summary, we have reported in this Chapter two examples of fabrication of grafted polymeric nano-structures (“hedges” and “dot” brushes) exploiting AFM-assisted lithography and controlled SIP.

In the first part of the Chapter a new approach which couples AFM DPN-assisted deposition of Au nano-wires with the controlled grafting of polymer brushes was described. DPN has been successfully used to deposit gold wires with width values down to 20 nm on silicon substrates. PMAA macromolecular “hedges” have been subsequently grafted from the functionalized nano-patterns using controlled *iniferter*-based photopolymerization. This nano-fabrication method thus represents an easy stepwise “bottom-up” technique to synthesize polymeric nano-features ranging from hundreds of nanometers down to sizes comparable with only few arrays of grafted macromolecules.

In the second part of this Chapter we have reported the SPO-assisted, stepwise synthesis of pH-responsive PHEMA nano-brushes grafted via ATRP-based SIP from passivated silicon substrates. Precursor silicon oxide lines and dots were fabricated through SPOL and served as site-specific anchoring platforms for the immobilization of initiators and subsequent grafting of HEMA. Simple post-functionalization procedures allowed the chemical modification of the PHEMA grafts, thus creating ionizable brush nano-structures, which responded to pH stimuli with tunable swelling properties. This fabrication technique was successfully used for the synthesis of stimulus-responsive polymeric grafts reaching sub-40 nanometers in dimensions.

The lateral resolutions obtained in both the studies reported confirmed the accomplishment of the isolated grafting of a few tens of macromolecules in preselected positions at the substrate surface. We believe that further technical improvements could easily lead to the controlled grafting of stimuli-responsive single macromolecules, and contribute to the realization of single chain molecular scale sensors and smart systems, thus opening new possibilities in macromolecular (bio)nanotechnology.

7.4 Experimental

DPN-assisted formation of Au nano-wires. In the DPN experiments an AFM contact tip (spring constant: 0.6 N m^{-1}) was dipped in 1% aqueous solution of HAuCl_4 (Sigma) for 30 seconds and afterwards the liquid droplet was thinned down by a gentle stream of nitrogen. The silicon substrate was hydrogenated by immersion of a clean silicon wafer with native oxide layer in 2.5% aqueous solution of HF (Aldrich) for 1 minute.

In order to minimize deactivation of the surface by oxidation at ambient conditions, the HF-treated silicon substrate was used within 5 minutes after the treatment. DPN was performed using a Dimension D3100 Atomic Force Microscope (AFM, Digital Instruments Veeco, Santa Barbara, CA, U.S.A.) equipped with an X-Y closed loop scanner and the dedicated nanolithography software, NanoMan (Digital Instruments Veeco, Santa Barbara, CA, U.S.A.). All the lithographic experiments were carried out at room temperature while DPN was performed also at controlled humidity.

Photopolymerization. Poly(methacrylic acid) brushes were subsequently grafted from the prepared Au nano-wires using the photo $iniferter$ DTCA as initiating system (the synthesis of DTCA is reported in Chapter 3).

Prior to adsorption of DTCA the sample with the gold features was left overnight at $60 \text{ }^\circ\text{C}$ in air to ensure the passivation of the surrounding hydrogenated silicon surface by thermal oxidation. Then, the substrates were immersed overnight in a 1 mM ethanolic solution of a mixture of DTCA and inert octadecylthiol (ODT) in 50:50 molar ratio. The so-prepared substrates were immersed in a quartz flask filled with 0.1 M aqueous solution of methacrylic acid (MAA) and, after extensive N_2 purging, they were irradiated for 15 minutes with UV lamps (6x15 W, max emission at 300 nm wavelength, sample-lamps distance 20 cm).

Preparation of samples for SPOL. Silicon substrates with native silicon oxide layer, prior to deposition of the organic monolayers, were cleaned with *piranha* solution (30% H_2O_2 and 70% H_2SO_4 , caution must be paid in handling *piranha* solutions since they may detonate unexpectedly in contact with organic materials) and later on extensively rinsed with milli-q water and ethanol. The cleaned substrates were subsequently immersed overnight in 0.2 mM toluene solutions of OTS (Sigma). Following SPO lithography, the patterned samples were incubated for a

specified period of time in 0.2 mM toluene solutions of ATRP initiator (synthesized in following the procedure already reported³⁹) and successively rinsed with toluene and ethanol.

For surface-initiated ATRP the procedure reported in Chapter 6 was followed. PHEMA brushes were subsequently derivatized with succinic anhydride (Fluka) by overnight reaction in 30 mg/ml dry pyridine solution.

SPOLE and sample characterization methods. Scanning probe oxidation was performed by a Dimension 3100 (Digital Instruments, Veeco, Santa Barbara, CA, USA) closed loop AFM with Nanoman™ lithography (Digital Instruments Veeco, Santa Barbara, CA, USA). Gold coated contact tips (0.12N/m) were used in the bias-induced local oxidation with negative tip bias in the range of -7V to -10V. Topography images of the fabricated patterns, after every preparation step, were recorded by tapping mode atomic force microscopy (TM-AFM). Contact mode AFM (CM-AFM) was performed inside a liquid cell setup in order to evaluate the swelling properties of the PHEMA-based polymer grafts immersed in aqueous solutions at different pH values. The pH was adjusted by adding 0.1 M HCl or 0.1 M NaOH to the aqueous solutions used for the measurements.

Fourier Transmission Infrared Spectroscopy. Transmission FTIR-spectra (spectral resolution of 8 cm⁻¹, 2048 scans) were obtained using a BIO-RAD FTS575C FTIR spectrometer equipped with a nitrogen-cooled cryogenic cadmium mercury telluride detector. Background spectra were obtained by scanning a clean silicon substrate.

7.5 References

- (1) Jones, D. M.; Huck, W. T. S. *Adv. Mater.* **2001**, *13*, 1256.
- (2) Case, M. A.; McLendon, G. L.; Hu, Y.; Vanderlick, T. K.; Scoles, G. *Nano Lett.* **2003**, *3*, 425.
- (3) Lee, K. B.; Park, S. J.; Mirkin, C. A.; Smith, J. C.; Mrksich, M. *Science* **2002**, *295*, 1702.
- (4) Hyun, J.; Ahn, S. J.; Lee, W. K.; Chilkoti, A.; Zauscher, S. *Nano Lett.* **2002**, *2*, 1203.
- (5) Liu, M. Z.; Amro, N. A.; Chow, C. S.; Liu, G. Y. *Nano Lett.* **2002**, *2*, 863.
- (6) Kenseth, J. R.; Harnisch, J. A.; Jones, V. W.; Porter, M. D. *Langmuir* **2001**, *17*, 4105.

- (7) Wadu-Mesthrige, K.; Amro, N. A.; Garno, J. C.; Xu, S.; Liu, G. Y. *Biophys. J.* **2001**, *80*, 1891.
- (8) Lee, W. K.; Caster, K. C.; Kim, J.; Zauscher, S. *Small* **2006**, *2*, 848.
- (9) Woodson, M.; Liu, J. *J. Am. Chem. Soc.* **2006**, *128*, 3760.
- (10) Zhang, H.; Li, Z.; Mirkin, C. A. *Adv. Mater.* **2002**, *14*, 1472.
- (11) Maynor, B. W.; Filocamo, S. F.; Grinstaff, M. W.; Liu, J. *J. Am. Chem. Soc.* **2002**, *124*, 522.
- (12) Lee, S. W.; Sanedrin, R. G.; Oh, B. K.; Mirkin, C. A. *Adv. Mater.* **2005**, *17*, 2749.
- (13) Yu, M.; Nyamjav, D.; Ivanisevic, A. *J. Mater. Chem.* **2005**, *15*, 649.
- (14) Kaholek, M.; Lee, W. K.; LaMattina, B.; Caster, K. C.; Zauscher, S. *Nano Lett.* **2004**, *4*, 373.
- (15) Liu, X. G.; Guo, S. W.; Mirkin, C. A. *Angew. Chem. Int. Ed.* **2003**, *42*, 4785.
- (16) Kooi, S. E.; Baker, L. A.; Sheehan, P. E.; Whitman, L. J. *Adv. Mater.* **2004**, *16*, 1013.
- (17) Ginger, D. S.; Zhang, H.; Mirkin, C. A. *Angew. Chem. Int. Ed.* **2004**, *43*, 30.
- (18) Liu, G. Y.; Xu, S.; Qian, Y. L. *Acc. Chem. Res.* **2000**, *33*, 457.
- (19) Piner, R. D.; Zhu, J.; Xu, F.; Hong, S. H.; Mirkin, C. A. *Science* **1999**, *283*, 661.
- (20) Sheehan, P. E.; Whitman, L. J. *Phys. Rev. Lett.* **2002**, *88*.
- (21) Weeks, B. L.; Noy, A.; Miller, A. E.; De Yoreo, J. J. *Phys. Rev. Lett.* **2002**, *88*.
- (22) Rozhok, S.; Piner, R.; Mirkin, C. A. *J. Phys. Chem. B* **2003**, *107*, 751.
- (23) Manandhar, P.; Jang, J.; Schatz, G. C.; Ratner, M. A.; Hong, S. *Phys. Rev. Lett.* **2003**, *90*.
- (24) Maynor, B. W.; Li, Y.; Liu, J. *Langmuir* **2001**, *17*, 2575.
- (25) Avouris, P.; Hertel, T.; Martel, R. *Appl. Phys. Lett.* **1997**, *71*, 285.
- (26) M. Yang; Z. Zheng; Y. Liu; Zhang, B. *J. Phys. Chem. B* **2006**, *110*, 10365.
- (27) Wouters, D.; Willems, R.; Hoepfener, S.; Flipse, C. F. J.; Schubert, U. S. *Adv. Funct. Mater.* **2005**, *15*, 938.
- (28) Garcia, R.; Tello, M. *Nano Lett.* **2004**, *4*, 1115.
- (29) Wouters, D.; Schubert, U. S. *Nanotechnol.* **2007**, *18*.
- (30) Martinez, R. V.; Garcia, F.; Garcia, R.; Coronado, E.; Forment-Aliaga, A.; Romero, F. M.; Tatay, S. *Adv. Mater.* **2007**, *19*, 291.
- (31) Martinez, R. V.; Losilla, N. S.; Martinez, J.; Huttel, Y.; Garcia, R. *Nano Lett.* **2007**, *7*, 1846.
- (32) Patra, M.; Linse, P. *Nano Lett.* **2006**, *6*, 133.
- (33) Huang, W. X.; Kim, J. B.; Bruening, M. L.; Baker, G. L. *Macromolecules* **2002**, *35*, 1175.
- (34) Robinson, K. L.; Khan, M. A.; Banez, M. V. D.; Wang, X. S.; Armes, S. P. *Macromolecules* **2001**, *34*, 3155.

- (35) Brown, A. A.; Khan, N. S.; Steinbock, L.; Huck, W. T. S. *Eur. Polym. J.* **2005**, *41*, 1757.
- (36) It has to be mentioned that correspondent PHEMA films before functionalization with succinic anhydride present a swelling ratio of 20% in water. The swelling properties were not shown to depend on the pH of the medium.
- (37) Biesalski, M.; Johannsmann, D.; Rühle, J. *J. Chem. Phys.* **2002**, *117*, 4988.
- (38) Lee, W. K.; Patra, M.; Linse, P.; Zauscher, S. *Small* **2007**, *3*, 63.
- (39) Matyjaszewski, K.; Miller, P. J.; Shukla, N.; Immaraporn, B.; Gelman, A.; Luokala, B. B.; Siclovan, T. M.; Kickelbick, G.; Vallant, T.; Hoffmann, H.; Pakula, T. *Macromolecules* **1999**, *32*, 8716.

Summary and Outlook

The aim of the work described in this Thesis was to develop new fabrication techniques based on surface-initiated controlled polymerization (SIP) for the preparation of functional polymeric platforms across the lengthscales. Several synthetic processes based on controlled radical SIP were employed for the preparation of polymer brush platforms which presented tunable characteristics and, in some instances, a stimulus-responsive behavior. The SIP methods employed were furthermore coupled with atomic force microscopy (AFM)-assisted nanolithographic approaches in order to accomplish the preparation of polymer grafts constituted by a limited number of macromolecules grown on pre-determined positions on surfaces.

In Chapter 2, a broad overview of the most advanced methods for the structuring of surfaces using SIP was given. Representative examples of surface fabrication using SIP were reported highlighting the cases when the prepared grafted films presented tunable properties.

In Chapter 3, the SIP method based on initiator-transfer-terminator (*iniferter*) was introduced focusing on its kinetic aspects. Photografting of poly(methacrylic acid) (PMAA) using mixed initiating systems based on SAMs was investigated, demonstrating how the fine tuning of the composition of the starting layers (initiator surface coverage) could influence the morphology and the properties of the grafted films.

The growth rate of the PMAA films did not show a significant dependence on the composition of the starting self-assembled monolayers (SAMs), implying that radical recombination reactions played a substantial role in the surface grafting process. Comparing the extreme cases of PMAA grafts from full SAMs of initiators and from highly diluted SAMs, important morphological differences,

different swelling and mechanical properties were found. In addition, in situ quartz crystal microbalance with dissipation (QCM-D) measurements confirmed the different grafting kinetics for the two samples. The differences observed in morphology, swelling and mechanical properties were attributed to different graft structure originating from the reaction kinetics. Comparing the initial film mass growth and the viscoelastic properties for diluted and concentrated initiating systems more chains are initially grown in the case of concentrated SAMs of initiators. Nevertheless, due to termination reactions, this potential grafting efficiency did not turn into a higher thickening rate during the course of the polymerization with respect to films grown from diluted SAMs.

An example of the use of iniferter-based SIP for the synthesis of tunable brush platforms was given in Chapter 4. In this case DTCA photo-*iniferter* was used for the controlled surface grafting of micro-patterned temperature-responsive Poly-N(isopropylacrylamide) (PNIPAM) brushes. The brush height was easily controlled by the irradiation time through multiple subsequent irradiation stages. Temperature-induced changes in surface morphology and adhesion properties of the prepared PNIPAM brushes were monitored, for the first time, by in-situ AFM measurements. In addition, the inherent features of this SIP method were demonstrated to allow control of chain end functionalities as it was proven by a radical exchange test.

A further application of *iniferter*-mediated SIP was described in Chapter 5. Here the synthesis of RGD-functionalized PMAA brush films with variable structural characteristics was reported. PMAA brushes were first grafted from SAMs of initiators on gold surfaces and subsequently functionalized with the RGD cell-adhesive peptide sequence. These peptides were covalently immobilized both at the top of the brushes and within the brush layers following extension of the polymer chains by further polymerization step. After the preparation and characterization of the films, MG63 osteoblast cells were used to evaluate the effect of RGD positioning within the brush on cell adhesion. The results obtained demonstrated a good spread of cells with marked focal adhesion points at the periphery of the cytoplasm on samples with RGD motifs coupled on the surface, whereas in the case of the samples where RGD was buried, cells were found to

adopt a rounded morphology and focal adhesions concentrated toward the internal part of the cell. A direct correlation between the vertical position of the RGD motif inside the brush architecture and cell morphology was consequently found.

Atom transfer radical polymerization (ATRP) was introduced in the following Chapters. SIP-based fabrication using ATRP allowed the synthesis of thick brush films in relatively short time and it was exploited to prepare new brush architectures such as brush-gels and polymer nano-brushes.

In Chapter 6 the preparation of pH-responsive PHEMA-based brush-gels by surface-initiated ATRP and their successful application as matrixes for the controlled synthesis of silver nano-particles (Ag-NPs) was reported.

The swelling, mechanical and morphological properties of these brush films were investigated by AFM and they were demonstrated to be dependent on the amount of crosslinking agent used during their preparation. The solvent uptake at equilibrium markedly decreased for brush-gels if compared to the corresponding free brushes confirming the presence of a brush-network structure. In addition, AFM compression analysis showed enhanced mechanical resistance towards compression by the brush-gels and also the surface morphology of the films was found to be influenced by the presence of crosslinks.

The pH responsive behavior of the prepared layers was furthermore studied with AFM showing that the brush structures undergo a sharp transition around pH 8.

In the second part of this Chapter the use PHEMA-based brushes and brush-gels as supports for the controlled preparation of Ag NPs was described. From the results of AFM and UV-absorption spectroscopy a direct correlation between the characteristics of the Ag colloids and the type of brush architecture used was found. In particular, Ag NPs synthesized inside the brush-gels were found smaller, narrower distributed and with a more isotropic shape if compared to the case when the freely grafted brush was used as support.

In Chapter 7 the fabrication of grafted polymeric nano-structures (“hedges” and “dot” brushes) by coupling AFM-assisted lithography and controlled SIP was reported.

The *iniferter*-mediated preparation of PMAA “hedge” brushes grafted from Au nano-wires fabricated by dip-pen nanolithography-assisted reduction of Au salts was described. Following this procedure Au nano-structures with lateral size down to 20 nm were successfully fabricated. After functionalization of the metallic nano-wires with DTCA-initiator controlled grafting of limited number of PMAA chains was achieved.

In the second part of the Chapter the preparation of pH-responsive PHEMA-based “hedge” and “dot” brushes by scanning-probe oxidation lithography (SPOL) and SIP was reported. Silicon oxide linear and dot-like nano-structures were fabricated through SPOL and served as site-specific anchoring platforms for the immobilization of initiators and the subsequent ATRP-based SIP of HEMA. Post-functionalization of the PHEMA grafts turned the grafted polymers into pH-responsive “hedge” and “dot” brushes with tunable swelling properties. The proposed step-wise fabrication technique was successfully used for the synthesis of stimulus-responsive polymeric grafts reaching sub-40 nanometers in dimensions.

Both these examples demonstrated the possibility of attaching few tens macromolecules placed in preselected positions at surfaces. The results reported inferred that further technical improvements of AFM lithography coupled with controlled SIP could lead to controlled grafting of stimuli-responsive single macromolecules. This achievement would eventually allow to scale down to the molecular level the dimensions of bio-sensors and stimuli-responsive systems based on polymer grafts.

The results presented in this Thesis illustrate that the fabrication of polymeric platforms using SIP-based methods represents a versatile and powerful surface engineering technique. Several examples of the preparation of chemically structured polymeric coatings aimed at a wide range of applications were given. Spanning from the synthesis of bio-interfaces to the preparation of polymer/metal hybrid surfaces, surface modification using grafted polymers has been revealed as a key enabling approach in materials science. In addition, our new approaches for the immobilization of macromolecules in predetermined

positions at surfaces highlighted the high potential of the techniques used for surface engineering at the single molecular level.

Several further developments of the reported studies could be carried out opening new possible routes for the fabrication of multifunctional polymeric films. In addition in depth studies of the phenomena described in some sections of this Thesis could allow an enhanced understanding of the physical behavior of brush platforms in certain conditions.

In Chapter 3, for instance, QCM-D revealed as powerful tool to investigate the swelling properties of polyacid brushes grafted from designer surfaces. The response of these films on a change of solution pH could thus be studied by QCM-D. Following this approach, not only mass variation upon swelling could be monitored, but also changes of viscoelastic properties of the grafts at different pH values could be inferred.

The control on the chain end functionalities for PNIPAM polymer brushes which was presented in Chapter 4 has been recently demonstrated an effective method for the immobilization of nano-objects at determined positions on responsive brush surfaces. In an upcoming work¹ this approach has been used for the covalent attachment of CdSe/ZnS nano-crystals at the brush chain ends. In this case, the optical properties of the nano-crystals were shown to depend on the temperature-induced morphological transition of the grafted chains.

Finally, the fabrication methods reported in Chapter 6 have recently been employed for the functionalization of silicon micro-channels in micro-fluidic devices. Ag NPs/brush-gels hybrid films were grown in this confined environment in order to investigate the catalytic activity of the metal nano-clusters in such micro-systems. This approach carries great promise in micro-fluidic catalytic systems.

References

- (1) Tagit, O.; Tomczak, N.; Benetti, E.M.; Cesa, Y.; Blum, C.; Subramanian, V.; Herek, J.L.; Vancso, G.J. *Nanotechnol.* **2009**, in press

Samenvatting en Vooruitblik

Het doel van het in dit proefschrift beschreven werk was het ontwikkelen van nieuwe technieken gebaseerd op gecontroleerde, oppervlakte-geïnitieerde polymerisaties (OGPs) voor de fabricage van functionele polymeer platformen op verschillende lengteschalen. Diverse gecontroleerde radicaal OGP's werden toegepast voor het fabriceren van polymeer brush substraten met verschillende te tunen eigenschappen, waaronder in sommige gevallen 'stimuli responsive' gedrag. De toegepaste OGP's werden daarnaast gecombineerd met op AFM gebaseerde nano-lithografische methoden met als doel een gelimiteerd aantal macromoleculen op vooraf bepaalde posities op het oppervlak te laten groeien.

In hoofdstuk 2 wordt een breed overzicht van de meest geavanceerde methoden voor het structureren van oppervlakken middels OGP's gegeven. Hierbij wordt extra aandacht geschonken aan 'grafted' polymeer platformen met aan te passen eigenschappen.

In hoofdstuk 3 wordt de OGP methode gebaseerd op iniferters geïntroduceerd waarbij wordt gefocussed op de reactiekinetiek. 'Photografting' van PMAA op gemixte initiator systemen, bestaande uit SAMs, werd onderzocht. Aangetoond werd hoe de samenstelling van de initiator oppervlakte bedekking invloed kan uitoefenen op de morfologie en eigenschappen van de 'grafted' PMAA films.

De groeisnelheid van de PMAA films was niet significant afhankelijk van de samenstelling van de initiële initiator SAMs, wat impliceert dat radicaal recombinitie reacties een substantiële rol spelen in het oppervlakte 'grafting' proces. Voor de twee extreme gevallen van PMAA 'grafts' gegroeid van 100%

initiator SAMs en sterk verdunde SAMs werden behoorlijke verschillen in morfologie, zwellings- en mechanische eigenschappen waargenomen. Daarnaast werd met in situ 'quartz crystal microbalance' met dissipatie (QCM-D) metingen de verschillende 'grafting' kinetiek bevestigd voor deze twee samples. De waargenomen verschillen in morfologie, zwellings- en mechanische eigenschappen werden toegekend aan verschillende 'graft' structuren welke afhankelijk zijn van de reactiekinetiek. Uit het vergelijken van de initiële film massa toename en de viscoelastische eigenschappen voor verdunde en geconcentreerde initiator oppervlakken bleek dat in het begin van de reactie meer ketens groeiden op de geconcentreerde initiator SAMs. Desalniettemin resulteerde dit niet in een grotere filmdikte toename in de loop van de reactie voor de geconcentreerde initiator SAM oppervlakken vergeleken met de verdunde initiator SAM oppervlakken, wat werd verklaard door aanwezigheid van terminatie reacties.

Een voorbeeld van het gebruik van iniferter gebaseerde OGP voor de synthese van te tunen 'brush' films wordt gegeven in hoofdstuk 4. In dit geval werd DTCA photo-iniferter gebruikt voor de gecontroleerde oppervlakte 'grafting' van temperatuur 'responsive' PNIPAM brushes met een micrometer schaal patroon. De brush hoogte werd gecontroleerd door de belichtingstijd te variëren via opeenvolgende belichtingssessies. Temperatuur geïnduceerde verschillen in oppervlakte morfologie en adhesie eigenschappen van de PNIPAM brushes werden voor het eerst waargenomen met in situ AFM metingen. Daarnaast werd door middel van een radicaal uitwisseling test aangetoond dat inherent aan deze OGP methode controle kan worden uitgeoefend op de keteneinde functionaliteit.

Een andere toepassing van iniferter gebaseerde OGP wordt beschreven in hoofdstuk 5. De synthese van RGD gefunctionaliseerde PMAA 'brush' films met variabele structurele eigenschappen wordt besproken. PMAA 'brushes' gegroeid van initiator SAMs op goud oppervlakken werden gefunctionaliseerd met een RGD cell-adhesie peptide sequentie. Deze peptides werden covalent geïmmobiliseerd op de top van een PMAA brush laag, waarna eventueel de polymeer ketens worden verlengd met een volgende polymerisatie reactie resulterende in peptide sequenties in de PMMA brush laag. Na karakterisatie van deze films werden MG63 osteoblast cellen gebruikt om het effect van de RGD

sequentie positie in de film op de cel adhesie te onderzoeken. De resultaten lieten een goede cel spreiding met gemarkeerde focale adhesie punten op de periferie van het cytoplasma zien voor samples met de RGD sequenties op de top van de brush laag. In het geval de RGD sequenties zich bevonden in de brush laag werd een meer ronde cel morfologie met focale adhesie geconcentreerd dichtbij het interne gedeelte van de cel waargenomen. Een directe samenhang tussen de verticale positie van de RGD sequenties in de polymeer laag en de cell morfologie werd consequent aangetoond.

'Atom transfer radical polymerization' (ATRP) werd geïntroduceerd in de volgende hoofdstukken. Dikke brush lagen werden in relatief korte polymerisatie tijden gerealiseerd met ATRP gebaseerde OGP's en werden dan ook als zeer geschikt beschouwd om dit systeem verder te verkennen voor de ontwikkeling van nieuwe brush architecturen zoals 'brush-gels' en polymeer 'nano-brushes'.

In hoofdstuk 6 worden de fabricage van pH 'responsive' 'brush-gels' bestaande uit PHEMA middels oppervlakte geïnitieerde ATRP en de succesvolle toepassing van deze films als matrix voor gecontroleerde synthese van zilver 'nano-particles' (AG NP) beschreven.

De zwellings, mechanische eigenschappen en morfologie van deze brush films werden met AFM onderzocht en bleken afhankelijk te zijn van de hoeveelheid crosslinker gebruikt tijdens de polymerisatie reactie. De evenwichts opname van oplosmiddel bleek voor 'brush-gels' significant lager te zijn dan voor de vrije brush lagen, wat de aanwezigheid van een brush-netwerk structuur bevestigt. Daarnaast bleek uit AFM compressie metingen dat de brush-gels een substantieel hogere weerstand tegen mechanische compressie hadden vergeleken met de vrije brush lagen als wel dat de morfologie van de brush gels afhankelijk was van de aanwezigheid van crosslinks.

Het pH responsive gedrag van de gemaakte lagen was ook onderzocht met AFM waarbij er een scherpe transitie in de brush structuur werd waargenomen bij een pH van 8.

In het tweede deel van dit hoofdstuk wordt het gebruik van films bestaande uit PHEMA brushes en brush-gels als matrix voor het gecontroleerd synthetiseren van AG NPs beschreven. De AFM en UV-absorptie spectroscopie

resultaten laten een directe correlatie tussen de eigenschappen van de Ag kolloïden en het type brush architectuur zien. AG NPs gesynthetiseerd in de brush-gels waren over het algemeen kleiner, nauwer verdeeld en meer isotropisch van vorm vergeleken met AG NPs in de vrije brush lagen als support.

In hoofdstuk 7 wordt de fabricage van 'grafted' polymeer nano-structuren ('hedges' en 'dot' brushes) via gecombineerde AFM gebaseerde lithografie en gecontroleerde OGP's besproken.

De iniferter gebaseerde synthese van PMAA 'hedge' brushes gegroeid vanaf Au nano-wires welke waren gedeponereerd via dip-pen nanolithography geassisteerde reductie van Au zouten werd beschreven. Met deze procedure werden succesvol Au nano-structuren met een laterale resolutie van 20 nm geschreven. Na functionalisatie van de metallische nano-wires met DTCA-initiator werd een gelimiteerd aantal PMAA ketens gecontroleerd gegroeid vanaf deze nano-wires.

In het tweede deel van dit hoofdstuk wordt de fabricage van pH-responsive PHEMA 'hedge' en 'dot' brushes via 'scanning probe oxidativ lithography' (SPOL) and OGP's beschreven. Silicon oxide lineaire en dot achtige nano-structuren werden geschreven met SPOL en dienden vervolgens als platforms voor de immobilisatie van initiatoren en de opeenvolgende ATRP gebaseerde OGP's van HEMA. Post-functionalisatie van de PHEMA 'grafts' veranderde het 'grafted' polymeer in pH responsive 'hedge' en 'dot' brush domeinen met minimale laterale dimensies van sub-40 nm.

Beide voorbeelden laten zien dat het mogelijk is enkele tientallen macromoleculen op vooraf geselecteerde posities op oppervlakken te plaatsen. De beschreven resultaten wijzen erop dat een verdere technische verbetering van de AFM lithografie gecombineerd met gecontroleerde OGP's eventueel kan leiden tot het gecontroleerd koppelen van één enkel stimuli-responsive macromolecuul. Dit zou het uiteindelijk mogelijk maken bio-sensoren en stimuli-responsive systemen gebaseerd op polymeer 'grafts' te ontwerpen op moleculair niveau.

De resultaten besproken in dit proefschrift laten zien dat methoden gebaseerd op OGP's een veelzijdige en krachtige oppervlakte engineering techniek omvatten voor het fabriceren van polymeer platformen. Enkele voorbeelden van

de fabricage van chemisch gestructureerde polymeer coatings gericht op een breed scala aan toepassingen werden gegeven. Uiteenlopend van de synthese van bio-interfaces voor cel adhesie studies tot de fabricage van polymeer/metaal hybride oppervlakken, de oppervlakte modificatie met 'grafted' polymeren als bouwstenen heeft zich gepresenteerd als een sleutel element in de materiaalkunde. Daarnaast hebben onze nieuwe benaderingen voor de immobilisatie van macromoculen op goed gedefinieerde posities op oppervlakken laten zien dat de gebruikte technieken een hoog potentieel hebben voor de mogelijke oppervlakte engineering op het niveau van één enkel molecuul.

Enkele verdere ontwikkelingen van de beschreven studies zouden kunnen worden uitgevoerd om nieuwe routes te openen voor de fabricage van multifunctionele polymeer films. Daarnaast zou het in meer detail bestuderen van fenomenen beschreven in meerdere delen van dit proefschrift een beter inzicht kunnen verschaffen in het fysische gedrag van brush gebaseerde platformen onder diverse omstandigheden.

In hoofdstuk 3 bijvoorbeeld wordt QCM-D beschreven als een krachtige techniek voor de analyse van zwellings eigenschappen van polyacid brushes op oppervlakken. De reactie van deze films op een verandering in pH zou dus kunnen worden onderzocht met QCM-D. Niet alleen massa veranderingen als gevolg van zwellen kunnen worden gevolgd, maar ook is het mogelijk visco-elastische eigenschappen als functie van de pH met deze techniek te bepalen.

Controle over keteneinde functionaliteiten voor PNIPAM polymeer brushes zoals besproken in hoofdstuk 4 is recent geïntroduceerd als een effectieve methode voor de immobilisatie van nano-objecten op goed gedefinieerde posities op responsive brush gemodificeerde oppervlakken. In een toekomstig werk ¹ wordt deze aanpak gebruikt voor de covalente immobilisatie van CdSe/ZnS nano-kristallen aan de brush keten einden. In dit geval bleken de optische eigenschappen van de nano-kristallen af te hangen van temperatuur geïnduceerde morfologie overgangen van de 'grafted' brushes.

Als laatste, de fabricage methode beschreven in hoofdstuk 6 is recentelijk toegepast voor de functionalisatie van silicon micro-channels in een micro-fluidisch apparaat. Ag Nps/brush-gels hybride films werden succesvol

gesynthetiseerd in deze micro-channels om de katalytische activiteit van de metalische nano-clusters te onderzoeken in dit soort micro-fluidische apparaten.

Referenties

- (1) Tagit, O.; Tomczak, N.; Benetti, E.M.; Cesa, Y.; Blum, C.; Subramanian, V.; Herek, J.L.; Vancso, G.J. *Nanotechnol.* **2009**, in press

Acknowledgments

This Thesis reports just a part of the huge work which has been carried out by me and my closer colleagues over four years. These people started a project from the scratch, acquired skills, and put all their efforts in understanding and developing theories, methods and, above all, learning from their mistakes. The most amazing satisfaction for me is now seeing the many colleagues carrying out their studies on the basis of the ideas, intuitions and methods experimented in this work.

None of the many successes which characterized these years could be accomplished without the guide and the supervision of Prof. Julius Vancso. He is the first person to be acknowledged, not only for his fundamental scientific contribution to this work, but mainly for his unconditional support in every single moment that any support was needed, for his friendship, for his humanity, for the example he gave me of professionalism. Julius I really hope we will keep on working together.

Special thanks go to Dr. Szczepan Zapotoczny (Univ. Cracow) who supported me and the project continuously and who was always at my side, dear Szczepan I really thank you.

I also would like to thank some bright scientists who joined me on different stages in this research and contributed with their expertise. Dr. Erik Reimhult (ETH Zurich) for his fantastic contribution to the QCM-D study reported in Chapter 3 and for the beautiful time I spent with him in Switzerland. Dr. Melba Navarro (Univ. Liverpool) for the fundamental contribution in the “biological” part of this thesis. Prof. Marcus Textor (ETH Zurich) for his kind scientific support. My beautiful friend Dr. Marina Gianotti (IBEC, Barcelona) for her revision work on this Thesis and her contribution to the AFM studies reported. Dr. In Yee Phang (MTP, Univ. Twente) for being the youngest master of AFM techniques worldwide, it was an honor for me to work at his side during these years (have a good trip to Singapore man). I wish to thank Prof. Holger Schonherr (Univ. Siegen) for the many scientific discussions and the constant support. Dr. “Miguelito” Angel Mateos Timoneda (IBEC Barcelona) for the wise and the many suggestions he offered on the synthetic parts of this work and for his fantastic support during these years. Thank you for the everlasting help, for the patience, for the understanding and for the sincere friendship of Clemens Clemente Padberg. I really want to thank Genevieve Rietveld for having been always

there providing any kind of assistance, till the end and even after. This Thesis could not be definitely completed without the help of Janet Acgikoz. Janet has been not only a friend, she assisted me during this last year in any possible way, bringing me hot meals during the many nights spent working, giving me a bed to sleep and, most of all, being able to stand my terrible character... I wish to thank Francesca Costantini, Joost Duvigneau for all the help you have never stopped giving me, thank you very much dear friends. I have to thank also all the friends and beautiful people I met here in the Netherlands, I will never forget you, you do not see your names here because you are definitely too many. I think shaking our hands and hugging each others will be much more meaningful.

As almost last my beautiful family comes, which I have to thank for having being always with me (and which I have to apologize with for having been always far away during the last ten years...); my mother, my fantastic sister Linda, Giorgio, Tommaso and Francesco (soon getting married...), my beautiful “women” Benedetta and Umberta.

My “parallel” family, all the people that shared with me terrific experiences, happiness, difficulties: my friends, always with me after many years: Mr. Dolly, Darietto, Diego (there will be always a bed for you in my flat), Nonno Carlo (there will be always a couch for me in his one), Mr. Fox, Carlo and Giorgia, Alessio and Laura, Andrea “Biondo”, Mr. Super Iccio, Mr. Frasson and General Sara, Irene and Ale, Davide (a monument for him), Moniconna (the nicest person ever...), Sarah (an outstanding mix between Croatia and Südtirol), Maria, Aiko, Maurizio and Manu (who keeps me always healthy), Jim Morrison, Stanley Kubrik, Wes Anderson, Jim Jarmush and Johannes Brahms. I probably forgot many of them, sorry.

In the moment I’m writing now I find myself a bit surprised, astonished. Looking back I see intense years during which I have never stopped thinking for a moment. I quote my boss saying “whatever happens in my life, when I’m confused I come back to my science” there everything has a sense and things become easy, more precisely become true. Indeed through the lens of science we all face our life, the way we understand it, the way we “design” it, concrete but never complete. There is always something else to reach, we are never fully satisfied and if on the one hand this makes us a bit “unhappier” if compared to the rest of the people, on the other hand we will have always a dream to follow.

Curriculum Vitae

Edmondo Maria Benetti was born in Triest, Italy on October 6th, 1980. He studied Industrial Chemistry at the University of Padova (Italy) where he received his degree in November 2004. During his studies he specialized in polymer physics and structural characterization of polymeric/composite materials under the supervision of Prof. Antonio Marigo and Dr. Giuseppe Ferrara (“G. Natta” research center, Basell-Lyondell Polyolefins, Ferrara, Italy). In May 2005 he joined the group of Materials Science and Technology of Polymers at the University of Twente (the Netherlands), carrying out his PhD project under the supervision of Prof. G. Julius Vancso. The results of his research are described in this thesis. Since March 1st 2009 he has been appointed as research assistant at the department of physics of the University of Padova (Italy).